



Norwegian University of  
Science and Technology

# Investigation of methods for speckle contrast reduction

**Kristine Welde**

Master of Science in Electronics

Submission date: July 2010

Supervisor: Astrid Aksnes, IET

Co-supervisor: Ulf Østerberg, IET  
Sigbjørn Vindenes Egge, IET



# Problem Description

poLight AS is developing an optical modulator chip for use in HDTV projection display based on laser sources. The technology uses a polymer thin film where the surface can be modulated by use of an electrical field. This effect is exploited when creating a tunable diffraction grating array that by the use of line-scan optics can project a high resolution 2 mega pixel image in rear projection TV.

Coherent laser illumination combined with a diffuse screen gives rise to unwanted speckle in the projected image, which creates noise in the form of a granular pattern and thereby reduces the image quality.

In this master thesis a general study of the speckle effect in laser based displays will be performed and different methods to measure and characterize the effect identified.

The main goals are to give a theoretical basis to understand speckle, build a setup for characterization of speckle in laser based displays, and perform practical measurements. It is necessary to identify important physical parameters that influence speckle phenomena and determine which quantitative measurements that can be performed (e.g. speckle contrast, speckle size and autocorrelation). Methods to perform the measurements will be evaluated and the setup realized. A main part of the setup will be based on a B/W digital video camera with imaging optics that is adapted to the detector geometry.

Speckle contrast and different methods to reduce the speckle contrast will be studied. A description of the physics behind the speckle will be attempted, as well as optical modeling. Measurements of speckle contrast will be made for different experimental configurations to reduce speckle contrast:

1. a diffuse screen
2. a rotated diffuse screen
3. a sinusoidal rotating grating implemented by means of a spatial light modulator

A Fourier Transform system will be built into the speckle contrast measurement setup to optimize the positioning of the speckle reduction device.

Tools that will be used are e.g.:

- MATLAB
- ZEMAX optical system design software
- Spatial light modulator (SLM)

An evaluation of the measurements will be made and based on these results a suggestion will be made for which speckle reduction technique to pursue.

Assignment given: 29. January 2010

Supervisor: Astrid Aksnes, IET



# Abstract

Speckle arises when coherent light is reflected from a rough screen and observed by an intensity detector with a finite aperture. Because speckle causes serious image degradation when lasers are used as light sources in e.g. projectors, methods for reducing the speckle contrast need to be developed. Different speckle contrast reduction methods are investigated in this thesis, such as a rotating diffuser and a sinusoidal rotating grating. In addition, speckle simulations with the optical system design software ZEMAX has been explored.

A setup consisting of a 4-f imaging system with a rotating diffuser in the Fourier plane was developed in order to decide whether or not it is advantageous to perform speckle reduction in the Fourier plane. Hence, measurement series were performed with the rotating diffuser placed at different positions in the 4-f imaging system for comparison. Measurement series were executed both with an empty object plane and with a lens in it to spread the light in the Fourier plane. Placing a rotating diffuser in the Fourier plane does not appear to be effective for speckle contrast reduction.

The last setup investigated was a transmissive spatial light modulator (SLM) placed in the beam path. Sinusoidal rotating gratings created by means of gray levels, to simulate a potential modulator based on a deformable polymer layer, were implemented on the SLM. The gratings were rotated around their centers, and in a spiral in order to reduce the speckle contrast. For the first method the modulator speckle contrast was 34 % for  $N = 18$  averaged images, and for the second method it was 31 % for  $N = 36$  averaged images, both with a grating period of 4 pixels. Due to the drawbacks of the SLM optimal results were not achieved, but the SLM is useful for a proof-of-concept. Further measurements should be performed for this promising, novel method based on a true sinusoidal grating.



# Preface

This thesis has been conducted during the last semester of my master degree at the Department of Electronics and Telecommunication of the Norwegian University of Science and Technology (NTNU). The work has been a part of the HICFODS project, which is a collaboration between poLight AS, Vestfold University College and NTNU. My supervisors have been Associate Professor Astrid Aksnes, Professor Ulf Österberg and PhD student Sigbjørn Vindenes Egge. I am very grateful for their guidance, and the advices and feedback they have provided.





# Contents

<b>1</b>	<b>Introduction</b>	<b>1</b>
<b>2</b>	<b>Theory</b>	<b>3</b>
2.1	Speckle statistics . . . . .	3
2.1.1	Random phasor sum . . . . .	3
2.1.2	Means, variances and correlation of the resultant phasor	5
2.1.3	Statistics of the length $A$ and the phase $\theta$ of the resultant phasor . . . . .	6
2.1.4	Statistics of the intensity and the phase . . . . .	7
2.1.5	Sums of speckle patterns . . . . .	10
2.2	Fourier optics . . . . .	13
2.2.1	Fourier transforms . . . . .	13
2.2.2	Linear shift-invariant systems . . . . .	14
2.2.3	Optical system . . . . .	15
2.2.4	Optical Fourier transform . . . . .	15
2.3	4-f imaging system . . . . .	16
2.4	Temporal and spatial coherence . . . . .	18
2.5	Speckle size . . . . .	19
<b>3</b>	<b>Optical simulations in ZEMAX</b>	<b>21</b>
3.1	Sequential mode . . . . .	21
3.2	Non-sequential mode . . . . .	25
<b>4</b>	<b>Instrumentation and methods</b>	<b>29</b>
4.1	Components used in the laboratory setups . . . . .	29
4.2	Rotating diffuser in the 4-f imaging system . . . . .	29
4.2.1	The general setup . . . . .	30
4.2.2	Speckle reduction methods . . . . .	32
4.2.3	Calibration of the setup . . . . .	35
4.3	Sinusoidal rotating grating . . . . .	37

---

4.3.1	The setup . . . . .	38
4.3.2	Speckle reduction methods . . . . .	41
4.4	Post-processing of the speckle patterns . . . . .	43
<b>5</b>	<b>Results</b>	<b>45</b>
5.1	Rotating diffuser in the 4-f imaging system . . . . .	45
5.1.1	Empty object plane . . . . .	45
5.1.2	A lens in the object plane . . . . .	49
5.1.3	Diffusers with different grit sizes . . . . .	52
5.2	Sinusoidal rotating grating . . . . .	58
5.2.1	Rotation around the center . . . . .	58
5.2.2	Rotation in a spiral . . . . .	60
<b>6</b>	<b>Discussion</b>	<b>63</b>
6.1	Optical simulations in ZEMAX . . . . .	63
6.2	Rotating diffuser in the 4-f imaging system . . . . .	63
6.3	Sinusoidal rotating grating . . . . .	65
<b>7</b>	<b>Conclusion and further work</b>	<b>67</b>
	<b>Bibliography</b>	<b>69</b>
	<b>Appendices</b>	
<b>A</b>	<b>Article</b>	<b>73</b>
<b>B</b>	<b>Poster</b>	<b>81</b>
<b>C</b>	<b>MATLAB code</b>	<b>83</b>
C.1	Load images . . . . .	83
C.2	Analyse images . . . . .	84
C.3	Create graphs . . . . .	85
<b>D</b>	<b>Datasheets</b>	<b>87</b>
D.1	Datasheet for the laser . . . . .	87
D.2	Datasheet for the polarizers . . . . .	90
D.3	Datasheet for the beamsplitter . . . . .	91
D.4	Datasheet for the photodetector . . . . .	92
D.5	Datasheet for the beam expander . . . . .	98
D.6	Datasheet for the diffusers . . . . .	101
D.7	Datasheet for the lenses . . . . .	103
D.8	Datasheet for the camera . . . . .	106

---

D.9 Datasheet for the camera lens . . . . .	110
D.10 Datasheet for the spatial light modulator . . . . .	113



# 1. Introduction

Most of the projectors on today's market employ incandescent lamps as light sources, but other sources, such as LEDs and lasers, are also available. The decisive benefits of lasers compared to conventional sources are improved color gamut, higher contrast, greater brightness and deeper focus [1]. In addition, lasers provide a longer lifetime. There are however some drawbacks, such as cost, availability of wavelengths, power consumption, cooling and laser safety [2]. Yet, the main issue is speckle.

Figure 1.1 demonstrates how a laser emits coherent light onto an optically rough screen. The light is scattered, and then detected by an intensity detector with a finite aperture, e.g. an observer's eye. This makes the scattered rays interfere either constructively, causing bright spots, or destructively, causing dark spots, and thus creating a varying intensity pattern known as speckle [3]. Practically all surfaces are known to be rough on the scale of optical wavelengths [4].

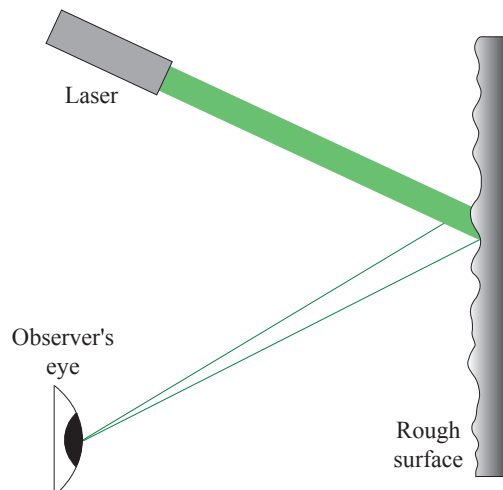


**Figure 1.1:** The origin of speckle.

Since speckle imposes a serious degradation of the image quality, developing methods to reduce the speckle contrast is the key to make the laser a favourable source. Some essential limitations to these methods are that they should not reduce the laser intensity too much, or cancel out its other advantages. Another condition they have to satisfy is that the speckle contrast should have a value below what is recognizable for the human eye, which is approximately 5% according to [5] and [6]. A common approach for reducing the speckle contrast is to degrade the spatial and/or temporal coherence of the laser beam. This could be performed by placing a modulator, such as a diffuse object [7] or a diffractive optical element [8], in the beam path between the source and the imaging system.

In this thesis the investigated speckle reduction methods are a rotating diffuser, and a sinusoidal rotating grating. A rotating diffuser is positioned in the Fourier plane of a 4-f imaging system and rotated discretely. The measurements are performed with a lens in the object plane, and also with an empty object plane. In order to inquire whether it is advantageous or not to perform the speckle reduction in the Fourier plane, other positions between the two lenses creating the 4-f imaging system are also investigated. Furthermore, a discretely rotated sinusoidal grating implemented on a transmissive spatial light modulator is examined. Measurement series for different grating periods are performed with the sinusoidal grating rotated both around its center and in a spiral.

The speckle patterns are stationary for all the measurements, and an image is captured for each rotation. Thus the modulator speckle contrast, that is the speckle contrast caused by the rotating object, and its deviation from the theoretical contrast can be calculated for each measurement series.

In addition, ZEMAX, which is an optical system design software, will be employed for speckle simulations. The intention is to be able to simulate different methods for speckle reduction, e.g. a varying aperture and a rotating diffuser. However, to simulate a speckle pattern is the first challenge.

## 2. Theory

### 2.1 Speckle statistics

First-order statistical properties of optical speckle will be presented in section 2.1. The statistics are from John W. Goodman's book *Speckle Phenomena in Optics: Theory and Applications* [1], and further details of the calculations can be found there.

The purpose is to find the probability density function of the intensity for the sum of several speckle patterns. This function contains information about how the speckle behaves, i.e. how the different intensities in the speckle pattern are distributed. Another goal is to find a function for the theoretical speckle contrast when several statistically independent speckle patterns are averaged. Before these functions can be derived the functions for a single pattern has to be found.

#### 2.1.1 Random phasor sum

A typical time-harmonic signal is expressed by

$$\mathbf{A}(x, y; t) = A(x, y; t)\cos[2\pi\nu_0 t - \theta(x, y; t)], \quad (2.1)$$

where  $A(x, y; t)$  denotes the amplitude or the envelope of the signal,  $\theta(x, y; t)$  denotes the phase and  $\nu_0$  gives the carrier frequency. In complex notation the sinusoidal signal can be represented by

$$\mathbf{A}(x, y; t) = A(x, y; t)e^{j\theta(x, y; t)}, \quad (2.2)$$

where  $A(x, y; t)$  and  $\theta(x, y; t)$  still represent the amplitude and the phase, respectively. When several of these signals are added together they constitute what is known as a random walk. This random phasor sum is given by

$$\mathbf{A} = Ae^{j\theta} = \frac{1}{\sqrt{N}} \sum_{n=1}^N \mathbf{a}_n = \frac{1}{\sqrt{N}} \sum_{n=1}^N a_n e^{j\phi_n}, \quad (2.3)$$

where  $\mathbf{A}$  is the resultant phasor,  $A$  is the length and  $\theta$  is the phase of the resultant phasor. Further,  $\mathbf{a}_n$  is the  $n$ th component phasor in the sum. The fraction  $\frac{1}{\sqrt{N}}$  is a scaling factor, where  $N$  is the number of phasor components. The scaling factor is introduced to keep finite second moments of the sum, even when  $\mathbf{a}_n$  approaches infinity. At last  $a_n$  represents the length and  $\phi_n$  represents the phase of  $\mathbf{a}_n$ . The resultant phasor  $\mathbf{A}$  can be either constructive or destructive depending on each component in the sum. This is shown in figure 2.1.

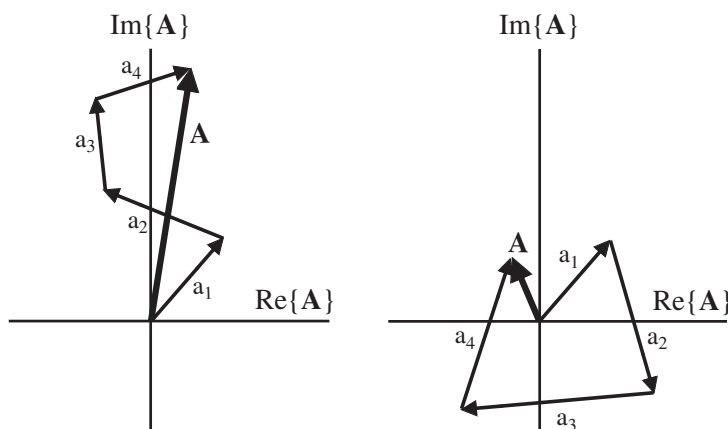


**Figure 2.1:** Constructive and destructive random phasor sums of the resultant phasor  $\mathbf{A}$ .

For the calculations, the random phasor sum in equation (2.3) is divided into its real and imaginary parts,

$$\begin{aligned} \mathcal{R} = Re\{\mathbf{A}\} &= \frac{1}{\sqrt{N}} \sum_{n=1}^N a_n \cos \phi_n \\ \mathcal{I} = Im\{\mathbf{A}\} &= \frac{1}{\sqrt{N}} \sum_{n=1}^N a_n \sin \phi_n. \end{aligned} \quad (2.4)$$



In order to find the probability density function of the intensity, the following assumptions are made:

1.  $a_n$  and  $\phi_n$  are statistically independent of  $a_m$  and  $\phi_m$  for  $n \neq m$ , which means that knowledge of one phasor's amplitude and/or phase does not imply knowledge of another phasor's amplitude and/or phase.
2.  $a_n$  and  $\phi_n$  are statistically independent, which means that knowledge of a phasor's amplitude does not imply knowledge of the same phasor's phase, and the other way around.
3. The phases  $\phi_n$  are uniformly distributed between  $-\pi$  and  $\pi$ , which means that all phase values are equally likely. Then the screen has to be rough on the order of visible wavelengths.

These assumptions are the basis for the following calculations.

### 2.1.2 Means, variances and correlation of the resultant phasor

The means of the real,  $\mathcal{R}$ , and imaginary,  $\mathcal{I}$ , parts of the resultant phasor are calculated to be

$$\begin{aligned} E[\mathcal{R}] &= 0 \\ E[\mathcal{I}] &= 0. \end{aligned} \tag{2.5}$$

The third assumption imposes the expectation values of  $\cos \phi_n$  and  $\sin \phi_n$  to be zero. The means of  $\mathcal{R}$  and  $\mathcal{I}$  are then equal to zero.

The variances of the real and imaginary parts of the resultant phasor are found to be

$$\begin{aligned} \sigma_{\mathcal{R}}^2 = E[\mathcal{R}^2] &= \frac{1}{N} \sum_{n=1}^N \frac{E[a_n^2]}{2} \\ \sigma_{\mathcal{I}}^2 = E[\mathcal{I}^2] &= \frac{1}{N} \sum_{n=1}^N \frac{E[a_n^2]}{2}. \end{aligned} \tag{2.6}$$

Thus it is seen that also the variances of the real and imaginary parts of the resultant phasor are identical,

$$\sigma_{\mathcal{R}}^2 = \sigma_{\mathcal{I}}^2. \quad (2.7)$$

Finally, the correlation between the real and imaginary parts is considered. The correlation coefficient,  $\rho$ , is proportional to the covariance,  $\Gamma$ , by the relation

$$\rho = \frac{\Gamma_{\mathcal{R},\mathcal{I}}}{\sigma_{\mathcal{R}}\sigma_{\mathcal{I}}}, \quad (2.8)$$

where  $\sigma_{\mathcal{R}}$  and  $\sigma_{\mathcal{I}}$  denotes the standard deviations of the real and imaginary parts [9]. Hence the correlation coefficient is seen to be

$$\rho \propto \Gamma_{\mathcal{R},\mathcal{I}} = E[\mathcal{R}\mathcal{I}] = 0. \quad (2.9)$$

This means that there is no correlation between the real and imaginary parts of the resultant phasor given that all three assumptions are fulfilled.

### 2.1.3 Statistics of the length $A$ and the phase $\theta$ of the resultant phasor

When assuming that the number of phasor components,  $N$ , is large the real and imaginary parts of the resultant phasor, given by (2.4), have a large number of independent random variables. The central limit theorem is then applicable [9]. It says that under certain general circumstances the statistics of the sum of  $N$  independent random variables are close to Gaussian when  $N \rightarrow \infty$ .

There is no correlation between the real and imaginary parts of the resultant phasor and the random variables are statistically independent because they have a Gaussian distribution [9]. The joint probability density function for the real and imaginary parts of the resultant phasor when considering the results for the means, variances and correlation, given by equations (2.5), (2.6) and (2.9), then becomes

$$p_{\mathcal{R},\mathcal{I}}(\mathcal{R},\mathcal{I}) = \frac{1}{2\pi\sigma^2} \exp\left(-\frac{\mathcal{R}^2 + \mathcal{I}^2}{2\sigma^2}\right), \quad (2.10)$$

where  $\sigma^2 = \sigma_{\mathcal{R}}^2 = \sigma_{\mathcal{I}}^2$ .

The joint probability density function of the length  $A$  and the phase  $\theta$  is then

$$p_{A,\theta}(A, \theta) = \frac{A}{2\pi\sigma^2} \exp\left(-\frac{A^2}{2\sigma^2}\right), \quad (2.11)$$

for  $A \geq 0$  and  $-\pi \leq \theta \leq \pi$ , otherwise it is zero.

The next step is to find the marginal statistics of the length  $A$  and phase  $\theta$  separately. The marginal statistics of the length  $A$  is

$$p_A(A) = \frac{A}{\sigma^2} \exp\left(-\frac{A^2}{2\sigma^2}\right), \quad (2.12)$$

for  $A \geq 0$ . This is known as the Rayleigh density function.

The marginal statistics of the phase  $\theta$  is found by integrating equation (2.11) with respect to the amplitude  $A$ , which gives

$$p_\theta(\theta) = \frac{1}{2\pi}, \quad (2.13)$$

for  $-\pi \leq \theta \leq \pi$ . Here it is used that the integral of the Rayleigh density function must be unity.

#### 2.1.4 Statistics of the intensity and the phase

The amplitude  $A$  is related to the intensity  $I$  by  $I = A^2$ .

When there is a large number of random phasors, i.e.  $N$  is large, it is possible to show that the amplitude  $A$  has a Rayleigh distribution. By using equation (2.12),  $I$  is seen to have a negative exponential distribution,

$$p_I(I) = \frac{1}{2\sigma^2} \exp\left(-\frac{I}{2\sigma^2}\right), \quad (2.14)$$

where  $I \geq 0$ . The expectation value of the intensity  $I$  is given by

$$E[I] = 2\sigma^2 \equiv \bar{I}. \quad (2.15)$$

Then the probability density function of the intensity  $I$  is found to be

$$p_I(I) = \frac{1}{\bar{I}} \exp\left(-\frac{I}{\bar{I}}\right). \quad (2.16)$$

This is known as *fully developed* speckle because the phases of the component phasors are uniformly distributed. This gives the greatest variation of intensity in the speckle pattern.

Figure 2.2 shows the distribution of the intensity. This means that there is a large amount of speckle grains with low intensity and a small amount of speckle grains with high intensity. This can be seen in the image in figure 2.3, which is showing bright speckle grains on a black background.

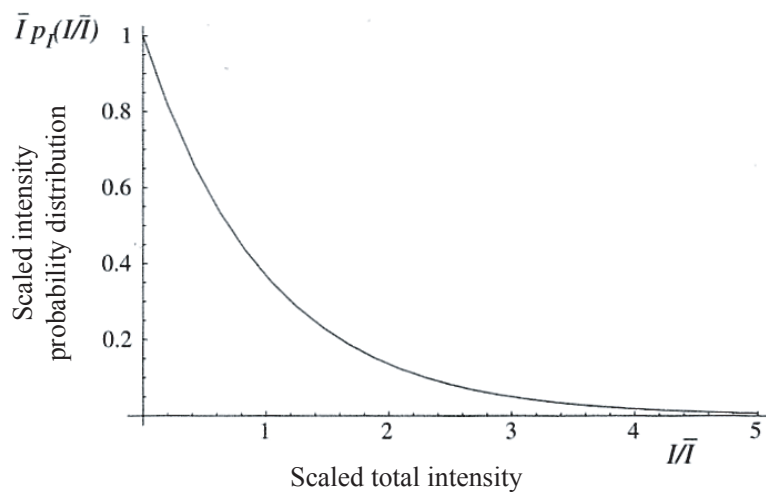


**Figure 2.2:** Negative exponential distribution of the intensity. The graph is from [1].

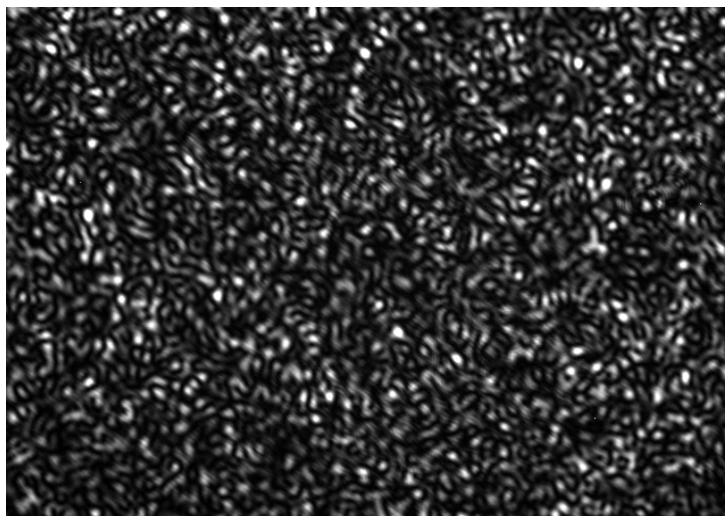


**Figure 2.3:** Image taken in the laboratory showing a speckle pattern.

For fully developed speckle the second moment, variance and standard deviation of the intensity are given by

$$\begin{aligned}\overline{I^2} &= 2\bar{I}^2 \\ \sigma_I^2 &= \bar{I}^2 \\ \sigma_I &= \bar{I}.\end{aligned}\tag{2.17}$$

The speckle contrast is a measure that shows how the fluctuations of intensity in the speckle pattern behave with respect to the average intensity. The contrast is defined by

$$C = \frac{\sigma_I}{\bar{I}}.\tag{2.18}$$

By using the standard deviation from equation (2.17) the contrast for fully developed speckle becomes

$$C = 1.\tag{2.19}$$

This means that the fluctuations of intensity are the same as the average intensity, which would cause serious image degradation. To overcome this the speckle contrast should be reduced. According to [5] and [6] a speckle contrast of approximately 5% is acceptable.

## 2.1.5 Sums of speckle patterns

### Two speckle patterns

The statistics of sums of fully developed speckle patterns on an intensity basis will be investigated. The total intensity of two independent speckle patterns is given by

$$I_s = I_1 + I_2. \quad (2.20)$$

From equation (2.16) it is seen that the probability density function of each pattern is given by

$$\begin{aligned} p_1(I_1) &= \frac{1}{\bar{I}_1} \exp\left(-\frac{I_1}{\bar{I}_1}\right) \\ p_2(I_2) &= \frac{1}{\bar{I}_2} \exp\left(-\frac{I_2}{\bar{I}_2}\right). \end{aligned} \quad (2.21)$$

The total probability density function is a convolution of the two probability density functions in equation (2.21). An easier way to find the total probability density function is by means of the characteristic functions. The characteristic function of the intensity fluctuations is a Fourier transformation of the probability density function,

$$\mathbf{M}_I(\omega) \equiv E[e^{j\omega I}] = \int_0^\infty e^{j\omega I} p_I(I) dI = \frac{1}{1 - j\omega \bar{I}}. \quad (2.22)$$

Then the characteristic function of the sum is found by multiplication of the characteristic functions of the two probability density functions,

$$\mathbf{M}_s(\omega) = \mathbf{M}_1(\omega) \mathbf{M}_2(\omega) = \frac{1}{1 - j\omega \bar{I}_1} \frac{1}{1 - j\omega \bar{I}_2}. \quad (2.23)$$

By performing an inverse Fourier transform the probability density functions of the total intensity become

$$\begin{aligned} p_s(I_s) &= \frac{1}{\bar{I}_1 - \bar{I}_2} \left[ \exp\left(-\frac{I_s}{\bar{I}_1}\right) - \exp\left(-\frac{I_s}{\bar{I}_2}\right) \right] && \text{when } \bar{I}_1 > \bar{I}_2 \\ p_s(I_s) &= \frac{I_s}{\bar{I}^2} \exp\left(-\frac{I_s}{\bar{I}}\right) && \text{when } \bar{I}_1 = \bar{I}_2 = \bar{I}. \end{aligned} \quad (2.24)$$

### Multiple speckle patterns

The calculations of the sum of  $N$  independent speckle patterns are similar to the case of two independent speckle patterns. An extension of equation (2.20) for  $N$  independent speckle patterns gives the total intensity,

$$I_s = \sum_{n=1}^N I_n. \quad (2.25)$$

Then the characteristic function for  $N$  speckle patterns becomes

$$\mathbf{M}_s(\omega) = \prod_{n=1}^N \mathbf{M}_n(\omega) = \prod_{n=1}^N \frac{1}{1 - j\omega \bar{I}_n}. \quad (2.26)$$

When assuming that all the average intensities are similar, i.e.  $\bar{I}_n = I_0$ , the probability density function of  $N$  speckle patterns is

$$p_s(I_s) = \frac{I_s^{N-1}}{\Gamma(N)I_0^N} \exp\left(-\frac{I_s}{I_0}\right) = \frac{N^N I_s^{N-1}}{\Gamma(N)\bar{I}^N} \exp\left(-N\frac{I_s}{\bar{I}}\right), \quad (2.27)$$

where  $\bar{I} = NI_0$  is the total mean intensity.

Figure 2.4 shows the intensity distribution of the probability density function of speckle patterns for different values of  $N$ . When  $N$  becomes large the probability density function approaches a Gaussian distribution. Hence the total speckle pattern will be smeared out and then less prominent compared to the speckle patterns for small  $N$ .

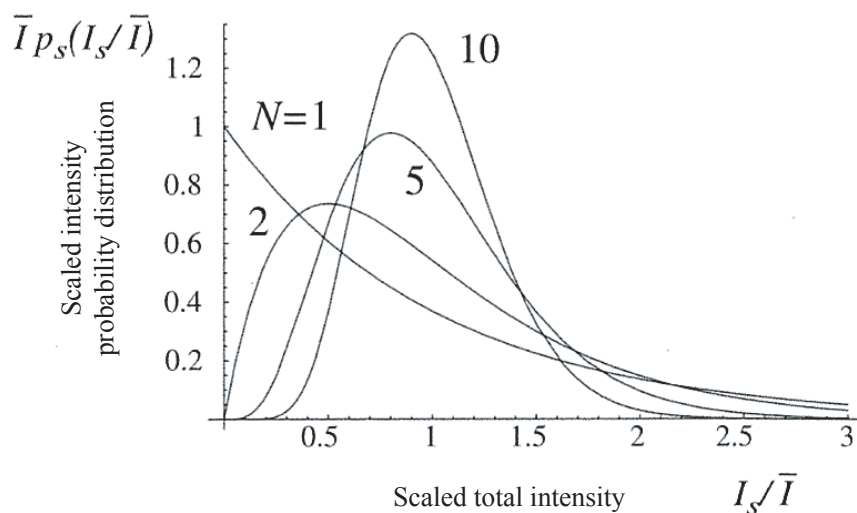


**Figure 2.4:** Probability density functions for different values of  $N$ . The graph is from [1].

The mean value of the total intensity is

$$\bar{I}_s = \sum_{n=1}^N \bar{I}_n, \quad (2.28)$$

and the second moment of the total intensity is given by

$$\bar{I}_s^2 = \sum_{n=1}^N \bar{I}_n^2 + \bar{I}_s^2. \quad (2.29)$$

The variance of the total intensity is then

$$\sigma_s^2 = \bar{I}_s^2 - \bar{I}_s^2 = \sum_{n=1}^N \bar{I}_n^2. \quad (2.30)$$

The speckle contrast is given by the standard deviation and the mean value of the total intensity,



$$C = \frac{\sigma_s}{\bar{I}_s} = \frac{\sqrt{\sum_{n=1}^N \bar{I}_n^2}}{\sum_{n=1}^N \bar{I}_n}. \quad (2.31)$$

This function reduces to

$$C = \frac{1}{\sqrt{N}}, \quad (2.32)$$

which is valid when all the  $N$  statistically independent speckle patterns have the same mean intensity, that is  $\bar{I}_n = I_0$ . This can be shown to be the maximum attainable reduction of speckle contrast for any values of the individual intensities  $I_n$ .

## 2.2 Fourier optics

The light intensity in a plane with coordinates  $x$  and  $y$ , perpendicular to the direction of incoming light, is going to be examined. Then the interesting quantities for Fourier theory are the positions  $(x, y)$  and the spatial frequencies  $(\nu_x, \nu_y)$ . The Fourier optics in sections 2.2 and 2.3 are from the book *Fundamentals of Photonics* written by B.E.A. Saleh and M.C. Teich [10].

### 2.2.1 Fourier transforms

Looking at one dimension reduces the position to one coordinate ( $x$ ) and one corresponding spatial frequency ( $\nu$ ).

The fundamental spatial harmonic function in Fourier calculations is  $F(\nu)e^{j2\pi\nu x}$ , where  $F(\nu)$  is the complex amplitude and  $\nu$  is the spatial frequency. When several of these functions, which have their own complex amplitude and frequency, are added together, they will form the function  $f(x)$ . Then the complex amplitude  $F(\nu)$  is known as the Fourier transform of the function  $f(x)$ . This can be written as

$$F(\nu) = \int_{-\infty}^{\infty} f(x)e^{-j2\pi\nu x} dx. \quad (2.33)$$

The inverse Fourier transform is then

$$f(x) = \int_{-\infty}^{\infty} F(\nu)e^{j2\pi\nu x} d\nu. \quad (2.34)$$

This can be used in the analysis of linear systems. A system is linear if the superposition principle is valid; that is when the response of the sum of two or more inputs is similar to each of the inputs' responses added together.

Similarly, the fundamental harmonic function for two variables can be written as  $F(\nu_x, \nu_y)e^{-j2\pi(\nu_x x + \nu_y y)}$ , where  $F(\nu_x, \nu_y)$  is the complex amplitude and  $\nu_x$  and  $\nu_y$  are the spatial frequencies in the  $x$  and  $y$  directions, respectively. When several of these functions are added together they will form the function  $f(x, y)$ . The two-dimensional Fourier transform can then be written as

$$F(\nu_x, \nu_y) = \int_{-\infty}^{\infty} \int_{-\infty}^{\infty} f(x, y)e^{j2\pi(\nu_x x + \nu_y y)} dx dy. \quad (2.35)$$

The inverse Fourier transform is then

$$f(x, y) = \int_{-\infty}^{\infty} \int_{-\infty}^{\infty} F(\nu_x, \nu_y)e^{-j2\pi(\nu_x x + \nu_y y)} d\nu_x d\nu_y. \quad (2.36)$$

## 2.2.2 Linear shift-invariant systems

A system is shift-invariant if the output is shifted in the same direction and by the same length as the input is shifted. Otherwise the output remains the same. The output signal  $f_2(x, y)$  of a linear system with the input signal  $f_1(x, y)$  is given by the integral

$$f_2(x, y) = \int_{-\infty}^{\infty} \int_{-\infty}^{\infty} h(x - x', y - y') f_1(x', y') dx' dy', \quad (2.37)$$

where  $h(x - x', y - y')$  is the impulse-response function. This function describes how the output of a system responds to an incoming impulse.

The transfer function  $H(\nu)$  is the Fourier transform of the impulse-response function, and is related to the Fourier transforms  $F_1(\nu)$  and  $F_2(\nu)$  by

$$F_2(\nu) = H(\nu)F_1(\nu). \quad (2.38)$$

A linear shift-invariant system can be described by either its impulse response function  $h(x, y)$  or by its transfer function  $H(\nu_x, \nu_y)$ .

### 2.2.3 Optical system

A plane wave can be seen as a spatial harmonic function

$$U(x, y, z) = Ae^{-j(k_x x + k_y y + k_z z)}, \quad (2.39)$$

where  $A$  is a complex constant and  $(k_x, k_y, k_z)$  are components of the wave vector  $\vec{k}$ . These components are related by  $k_x^2 + k_y^2 + k_z^2 = \frac{\omega^2}{c^2} = (\frac{2\pi}{\lambda})^2$ .

Since  $f(x, y)$  can be expressed as a superposition of harmonic functions the traveling wave  $U(x, y, z)$  can be seen as a superposition of plane waves.

When a plane wave is traveling through an optical system in the  $z$ -direction it is given by  $U(x, y, 0)$  at the input plane. This is equal to the harmonic function  $f(x, y) = Ae^{-j2\pi(\nu_x x + \nu_y y)}$ , where  $\nu_x = \frac{k_x}{2\pi}$  and  $\nu_y = \frac{k_y}{2\pi}$  are the spatial frequencies and  $k_x$  and  $k_y$  are the angular spatial frequencies. When this plane wave reaches the output plane it is given by  $U(x, y, d) = g(x, y)$ . This is shown in figure 2.5.

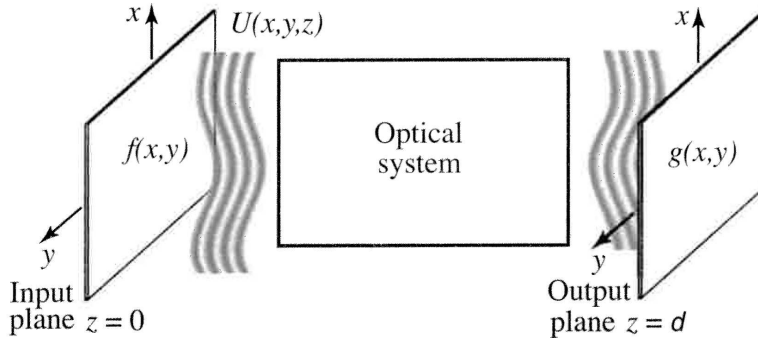


**Figure 2.5:** A plane wave traveling through an optical system. The illustration is from [10].

### 2.2.4 Optical Fourier transform

A wave is composed of several plane waves. The components of these waves can be separated by use of a lens, and focused into one common plane known

as the focal plane of the lens. The plane wave will arrive at the lens with small angles  $\theta_x$  and  $\theta_y$ . When the angles are small,  $\tan \theta_x \approx \theta_x$  and  $\tan \theta_y \approx \theta_y$ . Since  $f$  is the focal length, the point where the now paraboloidal wave is focused will be  $(x, y) = (\theta_x f, \theta_y f)$ . Hence, the lens will separate each of the plane waves' contributions.

A beam of light is a resultant wave that consists of several plane waves with a complex amplitude proportional to the Fourier transform  $F(\nu_x, \nu_y)$ , traveling with small angles  $\theta_x = \lambda \nu_x$  and  $\theta_y = \lambda \nu_y$ . Since the angles are small,  $\sin \theta_x \approx \theta_x$  and  $\sin \theta_y \approx \theta_y$ , the light will be focused by a lens into the focal point  $(x, y) = (\theta_x f, \theta_y f) = (\lambda f \nu_x, \lambda f \nu_y)$ . Evaluated at the spatial frequencies  $\nu_x = \frac{x}{\lambda f}$  and  $\nu_y = \frac{y}{\lambda f}$  the Fourier transform of the lens will be proportional to the distribution in the output plane,

$$F\left(\frac{x}{\lambda f}, \frac{y}{\lambda f}\right) \propto g(x, y). \quad (2.40)$$

This is known as a 2-f imaging system, shown in figure 2.6.

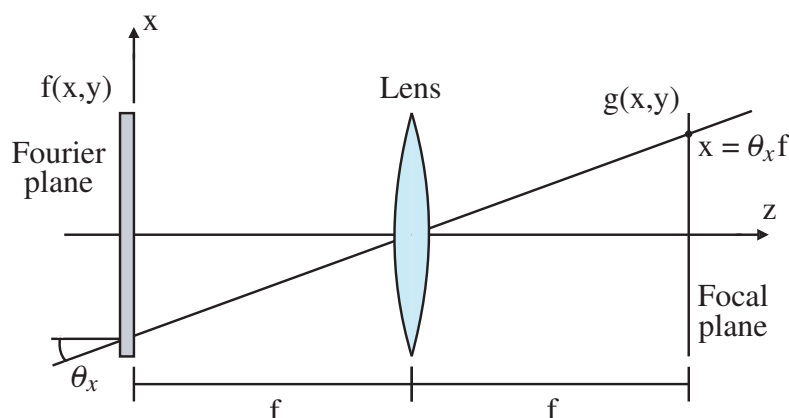


**Figure 2.6:** The 2-f imaging system.

## 2.3 4-f imaging system

The 4-f imaging system is described by figure 2.7. The system can be seen as two subsystems put together, the first between the object plane and the Fourier plane, and the second between the Fourier plane and the image plane. Each subsystem is a Fourier-transformator. The focal length of the two lenses are the same. The distances from each lens to the Fourier plane and from a

lens to its respective object or image plane are all equal to the focal length, hence the name 4-f.

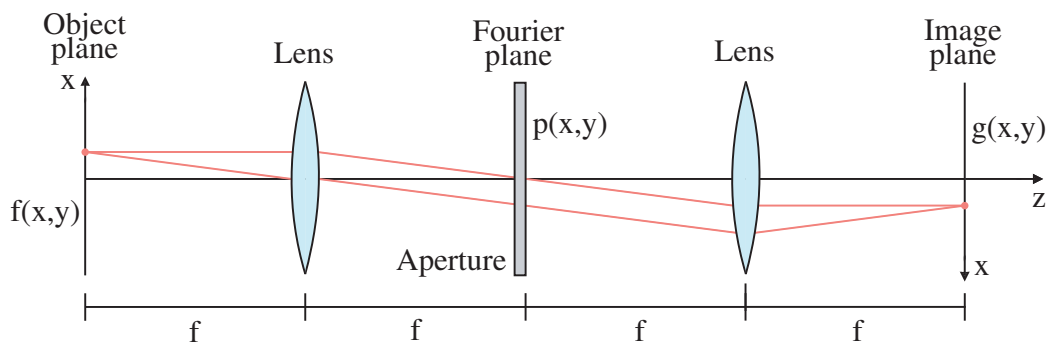


**Figure 2.7:** The 4-f imaging system.

After a beam of light enters through the object plane, it passes through the first lens and becomes Fourier transformed. In the Fourier plane all the spatial frequencies are separated in space, making it possible to filter individual frequencies. Then the light continues through the second lens, which inversely transforms the light distribution back to the spatial domain. When there is no mask blocking any of the spatial frequencies in the Fourier plane there will not be any magnification and the image has the same transverse light distribution as imposed by the object, but rotated  $180^\circ$ .

Imagine that a transparency, e.g. an image of a person, is placed in the object plane. The amplitude and phase distributions given by the transparency are described by the complex function  $f(x, y)$ . When the light passes the Fourier plane, the mask works as a filter that blocks some spatial frequencies and transmits others, and it is described in terms of phase and amplitude by the complex pupil function  $p(x, y)$ . In the frequency domain, this function is proportional to the transfer function  $H(\frac{x}{\lambda f}, \frac{y}{\lambda f})$ . Finally, the amplitude and phase of the light in the image plane is given by  $g(x, y)$ .

Right before the light passes the mask in the Fourier plane, the amplitude and phase distribution  $f(x, y)$  has been transformed into  $F(\nu_x, \nu_x)$ . Then the mask is applied and produces  $H(\nu_x, \nu_x)F(\nu_x, \nu_x)$  which is equal to the Fourier transform of  $G(\nu_x, \nu_x)$ . In the image plane,  $G(\nu_x, \nu_x)$  has been inverse transformed into  $g(x, y)$ .

## 2.4 Temporal and spatial coherence

A laser is a coherent light source, and speckle arises for such sources. Coherence can be divided into two types, which are temporal and spatial coherence.

Temporal coherence is the coherence measured when light waves generated at different times interfere. The coherence time is how long a source maintains its phase, and it is used to characterize the temporal coherence. A uniform phase in a plane that is perpendicular to the propagation direction is known as a perfect plane wave. This wave is said to be spatially coherent. All the points in such a wave will have fluctuations that are identical [11].

The temporal coherence function  $G(\tau)$  contains information about the intensity,  $I = G(0)$ , and also the degree of correlation, known as coherence, of stationary light. Equation (2.41) provides a measure of coherence which is not sensitive to the intensity. This equation is known as the complex degree of temporal coherence.

$$g(\tau) = \frac{G(\tau)}{G(0)} = \frac{\langle U^*(t)U(t + \tau) \rangle}{\langle U^*(t)U(t) \rangle}, \quad (2.41)$$

where its absolute value has to be less than unity and the different forms of  $U(t)$  are complex wave functions [10].

The mutual coherence function for temporal and spatial coherences is known as

$$G(\mathbf{r}_1, \mathbf{r}_2, \tau) = \langle U^*(\mathbf{r}_1, t)U(\mathbf{r}_2, t + \tau) \rangle, \quad (2.42)$$

where the different forms of  $U(\mathbf{r}, t)$  also are complex wave functions. In a normalized form this equation becomes

$$g(\mathbf{r}_1, \mathbf{r}_2, \tau) = \frac{G(\mathbf{r}_1, \mathbf{r}_2, \tau)}{\sqrt{I(\mathbf{r}_1)I(\mathbf{r}_2)}}, \quad (2.43)$$

where  $I(\mathbf{r})$  denotes the intensity. This function is known as the complex degree of coherence, and it is the cross-correlation coefficient of  $U^*(\mathbf{r}_1, t)$  and  $U(\mathbf{r}_2, t + \tau)$  which are random variables. Its absolute value also has to be less than unity [10].

In order to reduce the spatial coherence it is possible to place a moving diffuser in the beam path of the optical system, and hence produce independent speckle patterns. This is shown in figure 2.8.

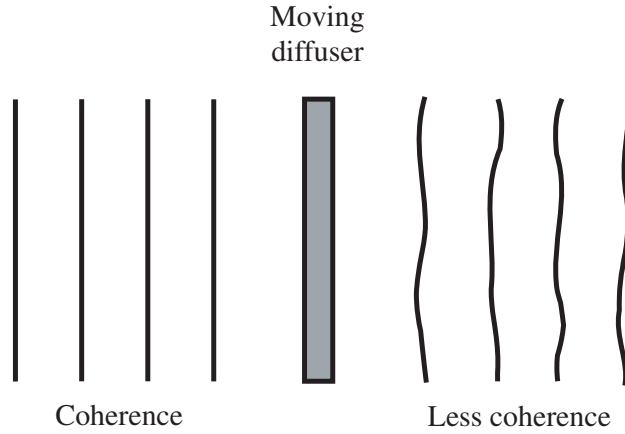


**Figure 2.8:** Moving diffuser reduces spatial coherence.

## 2.5 Speckle size

There are two types of observable speckle [12], objective speckle and subjective speckle. Objective speckle is when the pattern is reflected from a rough surface and on to a screen where it is observed, shown in figure 2.9. Subjective speckle is when the pattern is reflected from a rough surface and imaged on to a screen through a lens, displayed in figure 2.10. The last case is how the speckle will be observed in this thesis. It is possible to calculate the subjective speckle size,  $\sigma_s$ , which is different from the objective speckle size,  $\sigma_o$ .

$$\sigma_s = \frac{\lambda b}{D}, \quad (2.44)$$

where  $\lambda$  is the wavelength,  $b$  is the distance from the lens to the screen and  $D$  is the diameter of the lens. The aperture number is known to be

$$F = \frac{f}{D}, \quad (2.45)$$

where  $f$  is the focal length. Thus the subjective speckle size becomes

$$\sigma_s = (1 + m)\lambda F, \quad (2.46)$$

where  $m = \frac{(b-f)}{f}$  is known to be the magnification of the imaging system. From (2.46) it is seen that when the aperture is getting smaller, that is when the aperture number,  $F$ , increases, the speckle size will become larger. This can be applied in a speckle reduction system where the opening of an aperture is varied, and thus produces independent speckle patterns.

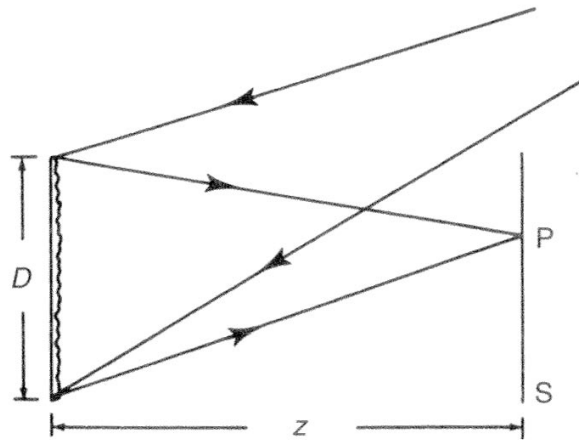


**Figure 2.9:** Objective speckle. The illustration is from [12].

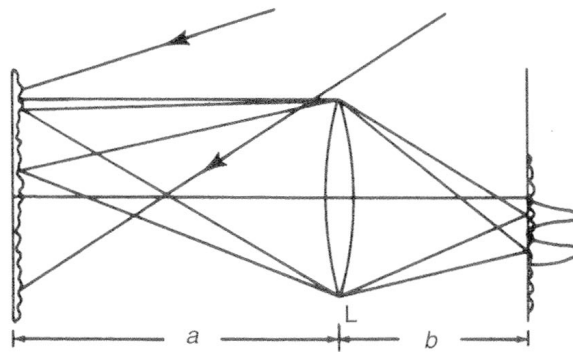


**Figure 2.10:** Subjective speckle. The illustration is from [12].



## 3. Optical simulations in ZEMAX

ZEMAX is an optical system design software. For a complete description of it see the *User's Manual* [13]. The software has several different areas of application, such as sequential lens design, analysis, optimization, tolerancing, physical optics, non-sequential optical system design, polarization, thin-film modeling and mechanical CAD Import/Export [14].

The intention of using the program is to simulate a 4-f imaging system for speckle reduction [15], and the first challenge is to simulate speckle. First the sequential mode of Zemax is explored. A beam expander is designed and two lenses are inserted from the lens catalog. Further, a diffuser is desired in the setup, but because of the scattering restrictions in the sequential mode the non-sequential mode has to be employed.

The specifications for the components used in the different designs can be found in the datasheets in appendices D.1 - D.10.

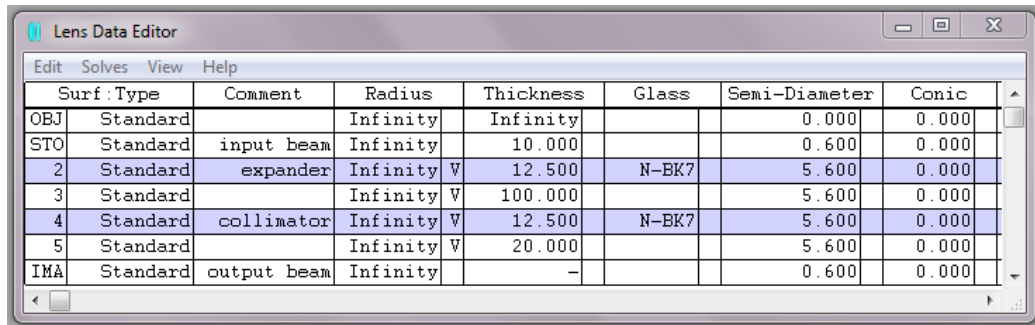
### 3.1 Sequential mode

In the sequential mode each surface of an object is described in the lens data editor. The parameters are surface type, radius, thickness, glass type, semi-diameter and conic. In addition it is possible to insert a comment.

#### Beam expander

In order to expand the laser beam a beam expander should be designed. The lens data editor in figure 3.1 is from the zip archive folder which is attached to the article *How to Design Afocal Systems* from [16]. The semi-diameter of the input beam has been changed to 0.6 mm, the thicknesses of the expander and the collimator have been increased to 12.5 mm, and the

distance between them has been set to 100 mm for them to correspond to the actual components used in the laboratory. The 2D layout of the setup before it has been optimized is shown in figure 3.2.



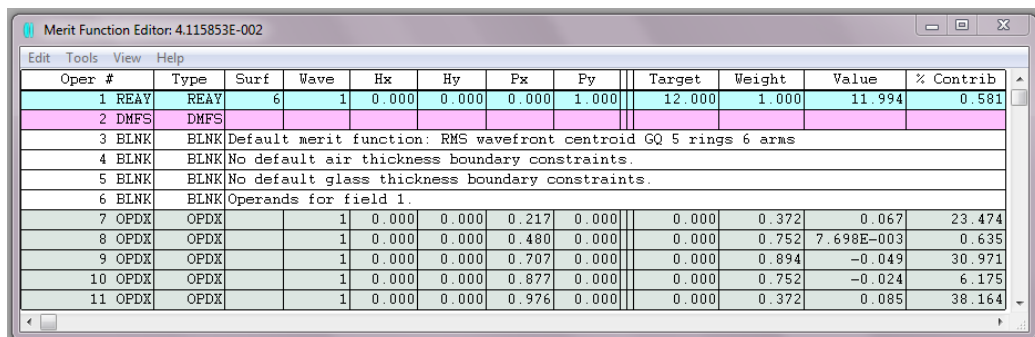
Surf	Type	Comment	Radius	Thickness	Glass	Semi-Diameter	Conic
OBJ	Standard		Infinity	Infinity		0.000	0.000
STO	Standard	input beam	Infinity	10.000		0.600	0.000
2	Standard	expander	Infinity	12.500	N-BK7	5.600	0.000
3	Standard		Infinity	100.000		5.600	0.000
4	Standard	collimator	Infinity	12.500	N-BK7	5.600	0.000
5	Standard		Infinity	20.000		5.600	0.000
IMA	Standard	output beam	Infinity	-		0.600	0.000

**Figure 3.1:** Lens data editor for the beam expander before the design has been optimized.



**Figure 3.2:** 2D layout of the beam expander before the design has been optimized.

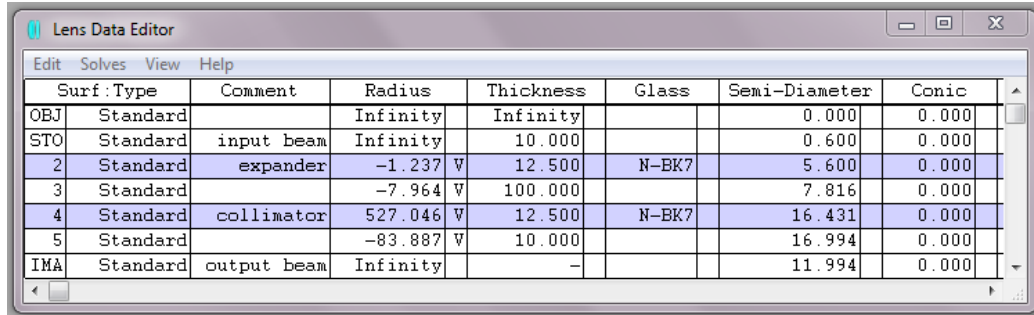
The input beam has a wavelength of 532 nm and a diameter of 1.2 mm. The beam expander has a 20 $\times$  magnification. The output beam should then have a diameter of 24 mm. The merit function editor is displayed in figure 3.3. The merit function is a numerical representation indicating how close the optical system is to the specified goals [13]. Here the target is 12.000 mm and the value is 11.994 mm for the first operand in the editor.



Oper #	Type	Surf	Wave	Hx	Hy	Px	Py	Target	Weight	Value	% Contrib	
1	REAY	REAY	6	1	0.000	0.000	0.000	12.000	1.000	11.994	0.581	
2	DMFS	DMFS										
3	BLNK	BLNK Default merit function: RMS wavefront centroid GQ 5 rings 6 arms										
4	BLNK	BLNK No default air thickness boundary constraints.										
5	BLNK	BLNK No default glass thickness boundary constraints.										
6	BLNK	BLNK Operands for field 1.										
7	OPDX	OPDX		1	0.000	0.000	0.217	0.000	0.000	0.372	0.067	23.474
8	OPDX	OPDX		1	0.000	0.000	0.480	0.000	0.000	0.752	7.698E-003	0.635
9	OPDX	OPDX		1	0.000	0.000	0.707	0.000	0.000	0.894	-0.049	30.971
10	OPDX	OPDX		1	0.000	0.000	0.877	0.000	0.000	0.752	-0.024	6.175
11	OPDX	OPDX		1	0.000	0.000	0.976	0.000	0.000	0.372	0.085	38.164

**Figure 3.3:** Merit function editor for optimization of the beam expander.

As a consequence of the optimization of the optical system the values in the lens data editor change, which means that the layout changes too. This is shown in figures 3.4 and 3.5.



Surf	Type	Comment	Radius	Thickness	Glass	Semi-Diameter	Conic
OBJ	Standard		Infinity	Infinity		0.000	0.000
STO	Standard	input beam	Infinity	10.000		0.600	0.000
2	Standard	expander	-1.237	12.500	N-BK7	5.600	0.000
3	Standard		-7.964	100.000		7.816	0.000
4	Standard	collimator	527.046	12.500	N-BK7	16.431	0.000
5	Standard		-83.887	10.000		16.994	0.000
IMA	Standard	output beam	Infinity	-		11.994	0.000

**Figure 3.4:** Lens data editor for the beam expander when the design has been optimized.

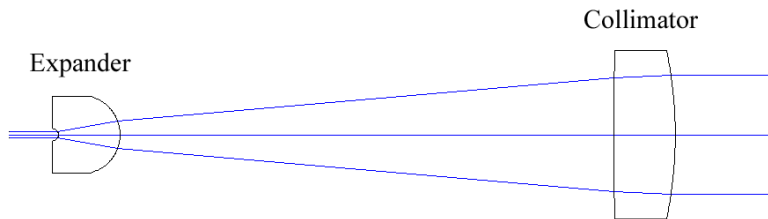


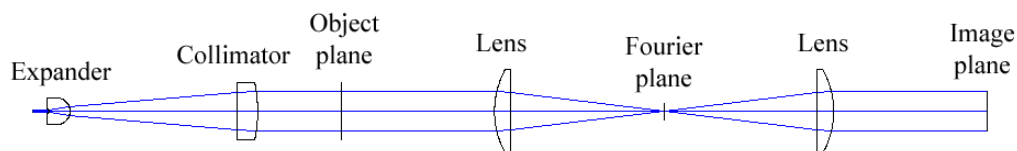
**Figure 3.5:** 2D layout of the beam expander when the design has been optimized.

## Lenses

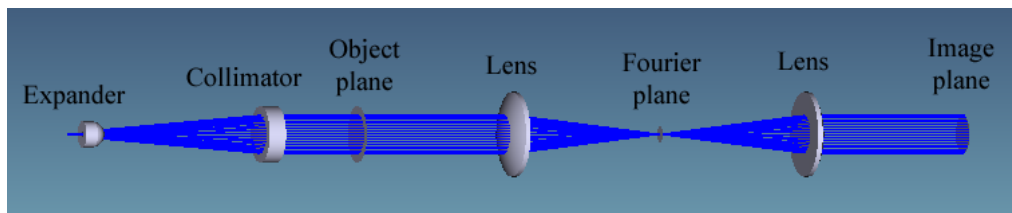
In order to create a 4-f imaging system two lenses have to be inserted from the lens catalog included in Zemax. They should be placed with the flat surfaces against each other in order to reduce the spherical aberrations, and hence the second lens has to be inverted. The surfaces of the second lens are then switched, and the radius of the curved surface is set to be negative. The lens data editor with the beam expander and the two lenses inserted is shown in figure 3.6. The layout of the 4-f imaging system is shown in 2D in figure 3.7(a) and as a shaded 3D model in figure 3.7(b). The surface in the middle of the two lenses indicates the Fourier plane.

Surf	Type	Comment	Radius	Thickness	Glass	Semi-Diameter	Conic
OBJ	Standard		Infinity	Infinity		0.000	0.000
STO	Standard	input beam	Infinity	10.000		0.600	0.000
2	Standard	expander	-1.237	12.500	N-BK7	5.600	0.000
3	Standard		-7.964	100.000		7.816	0.000
4	Standard	collimator	527.046	12.500	N-BK7	16.431	0.000
5	Standard		-83.887	50.000		16.994	0.000
6	Standard	object plane	Infinity	92.000		16.990	0.000
7*	Standard	LA1050	51.500	9.690	N-BK7	25.400	U
8*	Standard		Infinity	92.000		25.400	U
9	Standard	Fourier plane	Infinity	92.000		5.000	U
10*	Standard	LA1050	Infinity	9.690	N-BK7	25.400	U
11*	Standard		-51.500	92.000		25.400	U
IMA	Standard	output beam	Infinity	-		11.990	0.000

Figure 3.6: Lens data editor for the beam expander and the two lenses.



(a) 2D layout.



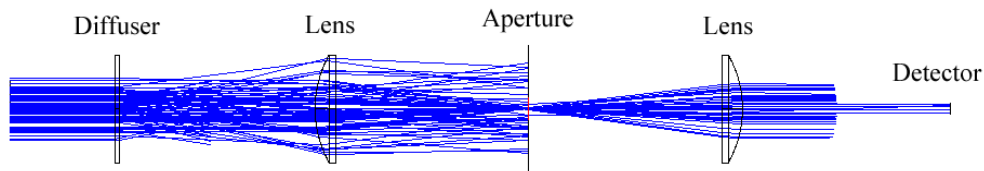
(b) Shaded 3D model.

Figure 3.7: 2D layout and shaded 3D model of the beam expander and the 4-f imaging system.

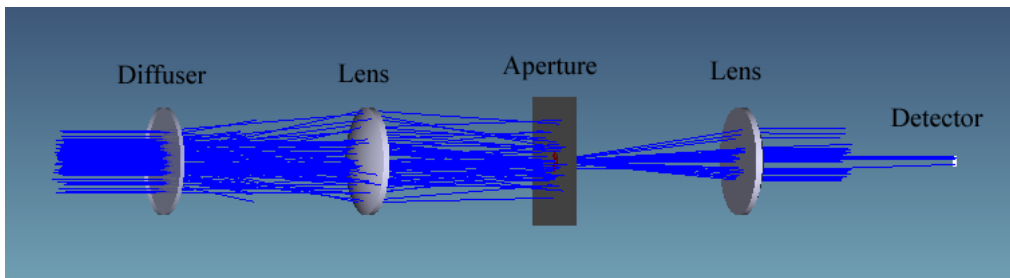
In order to simulate speckle an object that scatters light is needed. Because scattering is not possible in the sequential mode, the non-sequential mode has to be employed.

## 3.2 Non-sequential mode

In the non-sequential mode each object is described in the non-sequential component editor. The object types have some parameters in common, and other parameters are specific for a certain type. The setup for a 4-f imaging system, with a diffuser in the object plane and an aperture in the Fourier plane, is described in the non-sequential component editor in figure 3.9, and the components are described subsequently. A 2D layout of the setup is displayed in figure 3.8(a) and a shaded 3D model is shown in figure 3.8(b).



(a) 2D layout.



(b) Shaded 3D model

**Figure 3.8:** 2D layout and shaded 3D model of the 4-f imaging system, with a diffuser in the object plane and an aperture in the Fourier plane.

The screenshot shows the 'Non-Sequential Component Editor' window. The table below represents the data visible in the main window.

Object Type	Comment	Ref...	Z Position	Tilt About X	Material																
1 Source Gaussian		0	0.000	0.000	-	50000000	100	4.000	1	12.000											
2 Cylinder Volume	Diffuser	1	50.000	0.000	N-BK7	2.00	25.400	25.400													
3 Standard Lens	LA1050	2	94.770	0.000	N-BK7	0.00	51.500	25.400	25.400	0.000											
4 Rectangle	Aper. abs.	3	101.400	0.000	ABSORB	30.0	5.000														
5 Ellipse	Aper. open	4	0.000	0.000		5.00															
6 Standard Lens	LA1050	5	101.400	180.000	N-BK7	0.00	51.500	25.400	25.400	0.000											
7 Detector Rect		5	200.000	0.000	ABSORB	2.45	2.900	640	480	0											

**Figure 3.9:** Non-sequential component editor for the 4-f imaging system, with a diffuser in the object plane and an aperture in the Fourier plane.

## **Source**

A Gaussian source is placed in the non-sequential component editor. The source represents a HeNe laser with a wavelength of 532 nm and output power of 4 mW. The beam waist is set to have a radius of 12 mm, and consequently the beam expander is left out of the design. The number of layout rays shown in figures 3.8(a) - (b) is 100, and the number of analysis rays is 5 millions in order to achieve enough hits on the detector.

## **Diffuser**

A cylinder volume made of the material N-BK7 represents the diffuser. The object follows a Gaussian scattering at the front and the back face, and the angle scattering is set to  $10^\circ$ . The diameter of the diffuser is 50.8 mm and its thickness is 2 mm.

## **Lenses**

There are two lenses placed in the optical setup in order to form a 4-f imaging system. Their specifications are taken from the design in the sequential mode. The second lens is inverted by rotating it  $180^\circ$  about the x-axis. The first lens is placed a focal length from the diffuser, and the second lens is placed two focal lengths from the first lens.

## **Aperture**

An aperture is placed in the Fourier plane, which is in the middle of the two lenses. The aperture is made of an absorbtive rectangle with the size  $60\text{ mm} \times 60\text{ mm}$ . Then a circle with 5 mm radius made of air is placed at the same position as the rectangle. The circle of air surrounded by an absorbtive rectangle will thus let through parts of the laser beam and block the rest of it.

## **Detector**

At the end of the setup there is a coherent detector placed in the image plane of the 4-f imaging system. The size of the detector is  $5.8\text{ mm} \times 4.9\text{ mm}$  and

the number of pixels is  $640 \times 480$ . Hence the size of each pixel is  $9.06 \mu\text{m} \times 10.02 \mu\text{m}$ . This is the same specifications as the CCD sensor in the camera.

A ray trace has been performed and the detector viewer shows the simulated speckle pattern in figure 3.10.

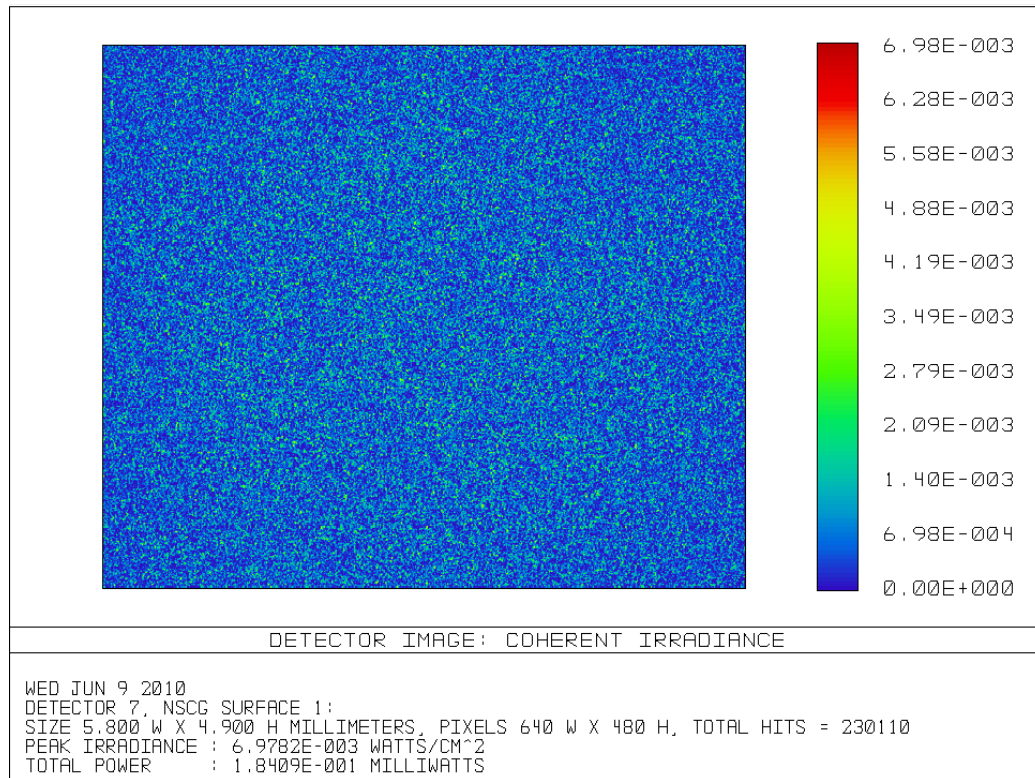


**Figure 3.10:** Simulated speckle pattern.



## 4. Instrumentation and methods

### 4.1 Components used in the laboratory setups

The components used in the subsequent speckle reduction methods are listed in table 4.1. Datasheets for most of them can be found in appendices D.1 - D.10.

<i>Component</i>	<i>Manufacturer</i>	<i>Model</i>
Laser	Photonic Products	300-0088-01
DC power supply	Mascot	719
Polarizers	Edmund Optics	NT52-557
Beamsplitter	Edmund Optics	NT49-004
Photodetector	Thorlabs	DET100A
Multimeter	Simpson	464
Beam expander	Edmund Optics	NT55-582
Diffusers	Thorlabs	DG20-(120,220,600,1500)
Lenses	Thorlabs	LA1050, LA1401
CCD camera	Lumenera	Lu070
Camera lens	VS Technology	L-VS-LD75
Spatial light modulator	Holoeye	LC 2002
Aperture and stop	-	-
Screen	Stewart Filmscreen	StudioTek 130 G3

**Table 4.1:** The components used in the laboratory setups.

### 4.2 Rotating diffuser in the 4-f imaging system

In order to reduce the speckle contrast an idea is to place a rotating diffuser in the Fourier plane of a 4-f imaging system, which is described in section 2.3.

The diffuser will reduce the coherence of the laser beam, and an interference pattern is created at the detector, as described in section 2.4. Ideally the rotation should be done continuously within the integration time of a human eye, which is 10 – 20 ms according to [17] and [18]. This corresponds to approximately one frame of the CCD camera. There is no equipment available at the laboratory to accomplish that, hence the diffuser is rotated by hand as a proof-of-concept. An image of the speckle pattern is captured for each  $10^\circ$  rotation of the diffuser from  $0^\circ$  to  $350^\circ$ . These images are averaged and the relative speckle contrast is found for each measurement series.

In order to compare the results of the measurement series in the Fourier plane it is necessary to conduct measurement series outside the Fourier plane, but between the two lenses. Most of the measurements have been performed at least two times in order to verify the results. The diffuser used in all the measurements have a grit size of 1500, because a shorter exposure time results in less scattering as explained in more detail in section 5.1.3.

### 4.2.1 The general setup

The general setup is shown in figure 4.1. A diode pumped solid state (DPSS) laser module is emitting light with a wavelength of 532 nm. The laser light is passed through two polarizers which control the intensity of the laser beam. The first polarizer has the position  $0^\circ$  and the second polarizer has the position  $50^\circ$  in all the measurements.

A beamsplitter is located after the polarizers. A part of the beam is passed on to the photodetector which is attached to a multimeter. The intensity of the laser beam is checked during the measurements in order to monitor the stability of the laser. The other part of the beam continues straight through the beamsplitter, and the beam is expanded  $20\times$  by the beam expander.

After the beam has been expanded it reaches the 4-f imaging system, which consists of an object plane, a lens, a Fourier plane, another lens and an image plane. The lenses (LA1050) are asymmetrical and they have a focal length of  $f = 100$  mm. Both are placed with the curved surface facing the collimated beam in order to minimize spherical aberrations. A diffuser, which is rotated discretely in the following measurements, is placed in the Fourier plane. The laser beam should not cover the center of the diffuser and is therefore passed through the upper part of it.

At the end of the setup there is a CCD camera which captures the speckle pattern and displays it on the computer by means of the program *LuCam*

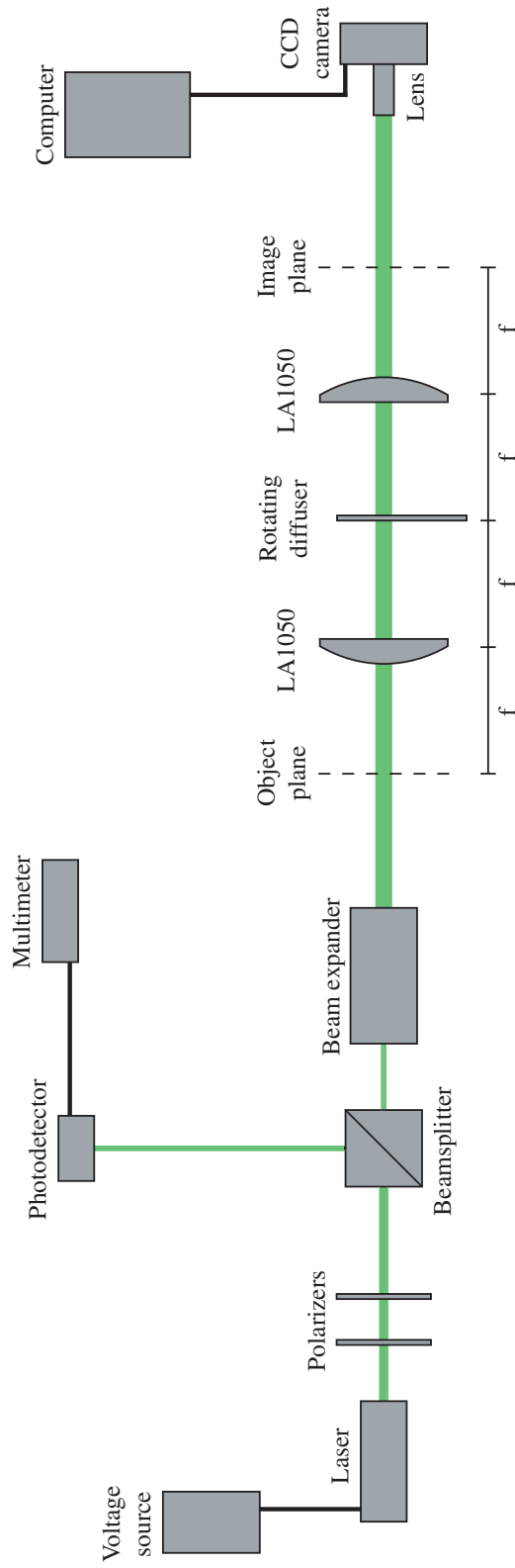


**Figure 4.1:** The general setup for speckle reduction using a rotating diffuser in the Fourier plane of the 4-f imaging system. The axis of rotation for the diffuser is not centered with the beam.

*Capture v4.5.0.* A lens with a focal length of  $f = 75$  mm is attached to the camera in order to focus the laser beam onto its CCD chip.

## 4.2.2 Speckle reduction methods

### Empty object plane

One method investigated in order to reduce the speckle contrast is shown in figure 4.1. The diffuser is rotated by hand and an image is captured for each  $10^\circ$  rotation, from  $0^\circ$  to  $350^\circ$ . In order to determine whether it is reasonable to do the speckle reduction in the Fourier plane several other positions between the two lenses should also be investigated. The ray propagation in the 4-f imaging system has been simulated with ZEMAX and is shown in figure 4.2. In the Fourier plane the laser beam is focused into a very small spot and hence the speckle grains created by the diffuser are very large compared to when the diffuser is placed elsewhere.

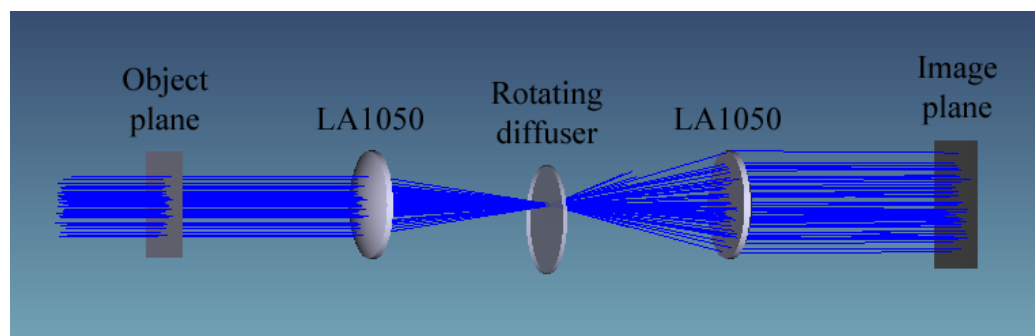


**Figure 4.2:** The ray propagation in the 4-f imaging system with an empty object plane.

### A lens in the object plane

In order to spread the light in the Fourier plane a third lens (LA1401) with a shorter focal length  $f = 60.0$  mm, is placed in the object plane of the 4-f imaging system. Otherwise the setup, shown in figure 4.3, is identical to the setup in figure 4.1. An image of the setup in the laboratory is shown in figure 4.4. The measurement series for this setup are also done with the diffuser at different positions between the two lenses in the 4-f imaging system. The ray propagation in the 4-f imaging system is displayed in figure 4.5.

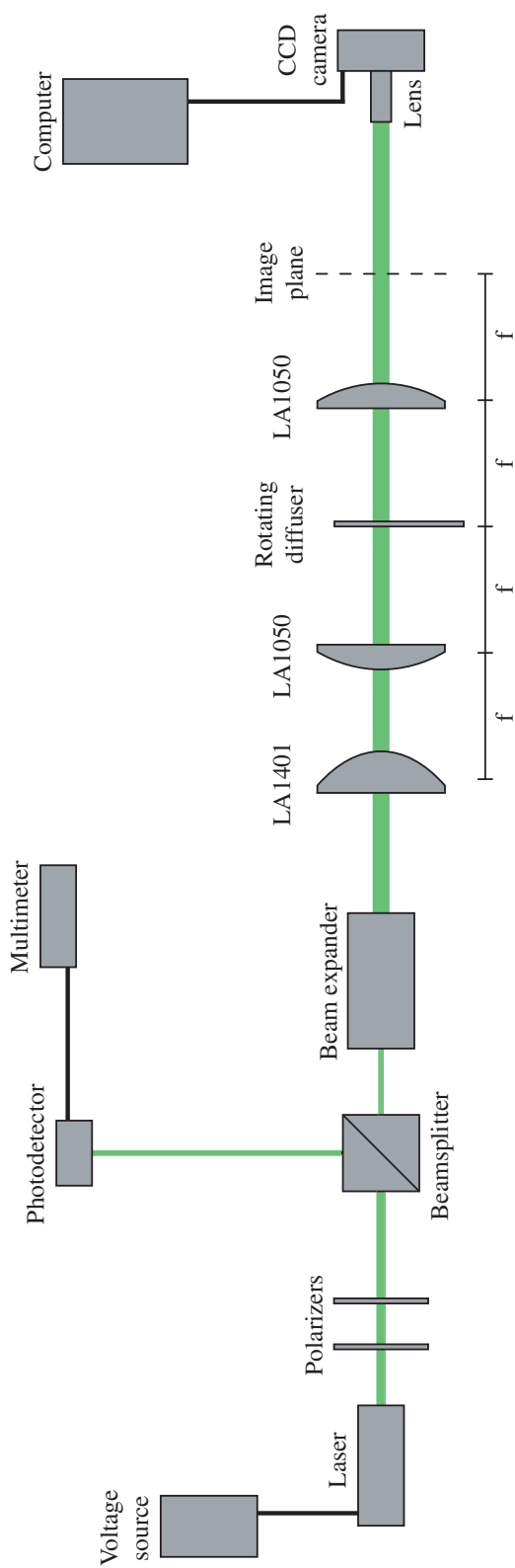


**Figure 4.3:** The setup for speckle reduction using a rotating diffuser in the Fourier plane of the 4-f imaging system with a lens in the object plane. The diffuser has an axis of rotation not centered with the beam.

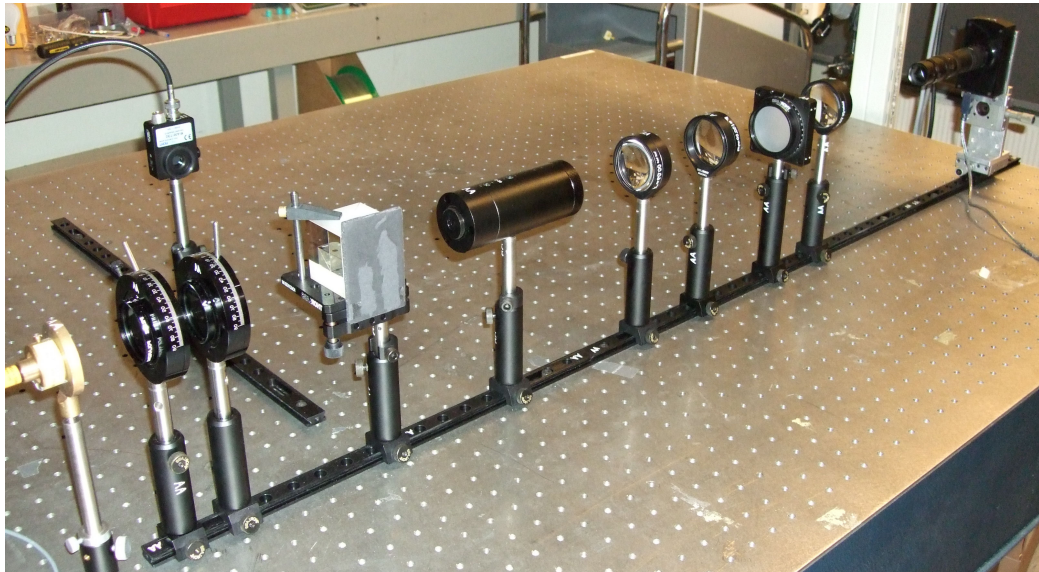


**Figure 4.4:** The laboratory setup corresponding to the schematics in figure 4.3.

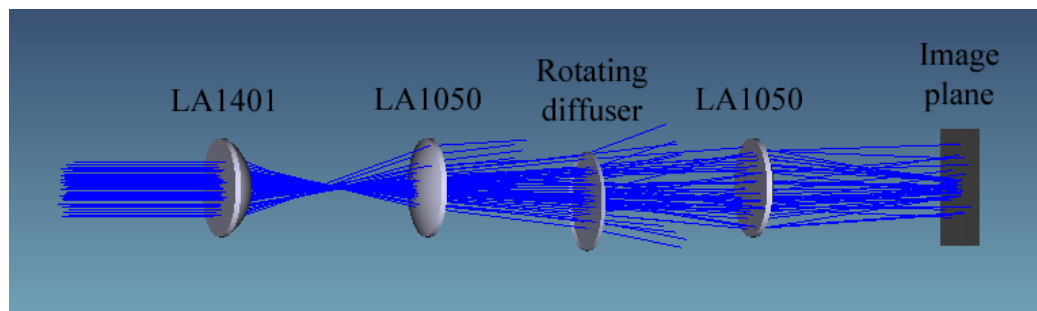


**Figure 4.5:** The ray propagation in the 4-f imaging system with a lens in the object plane.

Diffusers with different grit sizes, that is 120, 220, 600 and 1500, should also be investigated for the current setup. It is necessary to determine whether one of them is advantageous compared to the other ones. Measurement series should be done in the Fourier plane and outside the Fourier plane of the 4-f imaging system.

### 4.2.3 Calibration of the setup

The laser is connected to a voltage source which is set to 8 V, and it has a warm up time of about 30 minutes. The polarizers are set to  $0^\circ$  and  $50^\circ$ , respectively. It is important that the laser, the beamsplitter and the beam expander are aligned so that the beam passes straight through the latter.

Figure 4.6 show the properties of the lenses used in the measurements.  $D$  is the diameter of the lens,  $f$  is the focal length,  $R$  is the radius of curvature,  $t_c$  is the center thickness,  $n_l$  is the index of refraction,  $f_b$  is the length from the back plane of the lens to the right focal point and  $f_f$  is the length from the front plane of the lens to the left focal point plus the center thickness of the lens.  $H''$  is the distance from the focal plane to the back plane of the lens, and is given by equation

$$H'' = f - f_b = \frac{t_c}{n_l}. \quad (4.1)$$

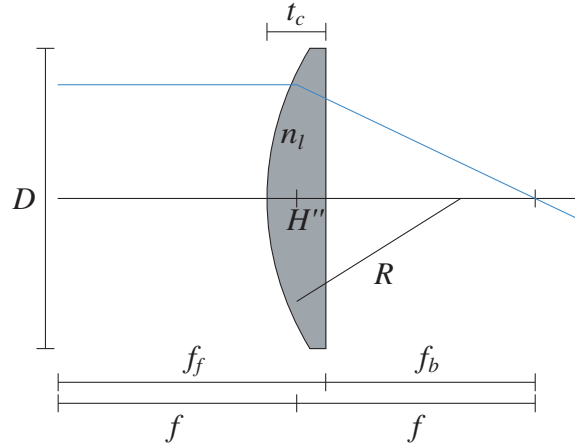


**Figure 4.6:** Properties of the lenses used in the measurements.

The specifications of the lenses are given for a wavelength of 633 nm in the datasheet, appendix D.7, and they are summarized in table 4.2. It is then necessary to do some calculations in order to get correct values for a wavelength of 532 nm. The simplified thick lens equation, from the datasheet, is given by equation (4.2), and it is used to find the new focal length. The new index of refraction is from the graph in the same datasheet.

$$\frac{1}{f} = (n_l - 1) \left[ \frac{1}{R} \right] \quad (4.2)$$

Equation (4.1) is used to find the new back focal length, and then the new front focal length is found by adding the thickness of the lens to the new back focal length. The specifications achieved for the lenses when the wavelength is 532 nm are shown in table 4.3. The diameter of the lens, the radius of curvature and the center thickness remain the same.

	$D$ [mm]	$f$ [mm]	$R$ [mm]	$t_c$ [mm]	$n_l$	$f_b$ [mm]	$f_f$ [mm]
LA1050	50.8	100.0	51.5	9.69	1.515	93.6	106.4
LA1401	50.8	60.0	30.9	16.29	1.515	49.2	70.8

**Table 4.2:** The specifications for the lenses when  $\lambda = 633$  nm.

	$D$ [mm]	$f$ [mm]	$R$ [mm]	$t_c$ [mm]	$n_l$	$f_b$ [mm]	$f_f$ [mm]
LA1050	50.8	99.1	51.5	9.69	1.519	92.8	105.5
LA1401	50.8	59.5	30.9	16.29	1.519	48.8	70.2

**Table 4.3:** The specifications for the lenses when  $\lambda = 532$  nm.

By using the values in table 4.3 the distances between the components in the 4-f imaging system can be found. A sketch with the distances applied is illustrated in figure 4.7. For the measurements without a lens in the object plane the distance from the object plane to the back plane of the first lens is 105.5 mm.

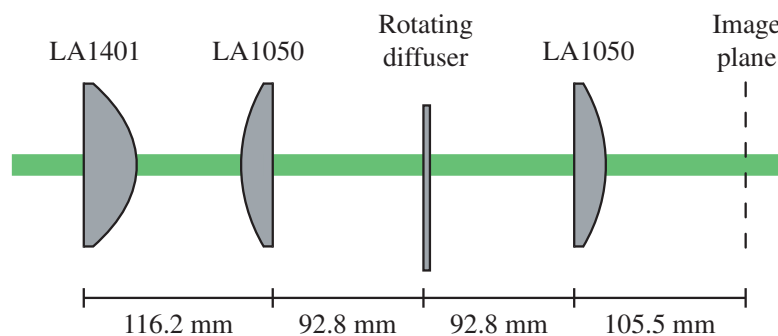


**Figure 4.7:** Distances between the components in the 4-f imaging system.

The proper distance from the image plane to the CCD camera with the lens attached has to be found. A screen was placed in the image plane and strongly illuminated with an incoherent light source. The camera was then adjusted so that the screen was in focus.



### 4.3 Sinusoidal rotating grating

Another method for reducing the speckle contrast is to place a sinusoidal rotating grating in the beam path of the laser. The sinusoidal grating will diffract the beam into a line of spots. When the grating is rotated the line of spots will also rotate, and thus cover different areas of the screen. Hence independent speckle patterns will be created. The zeroth order maxima will be stationary for all rotations, and therefore not contribute to changes in the speckle patterns. In order to remove it without losing power a phase delay of 4.8 radians will be employed [19]. The principle is shown in figure 4.8. A more thorough description of the method can be found in the article *Speckle reduction using a sinusoidal rotating grating* written by Sigbjørn Vindenes Egge in appendix A, where I have contributed with the measurements. A poster of the subject is found in appendix B.

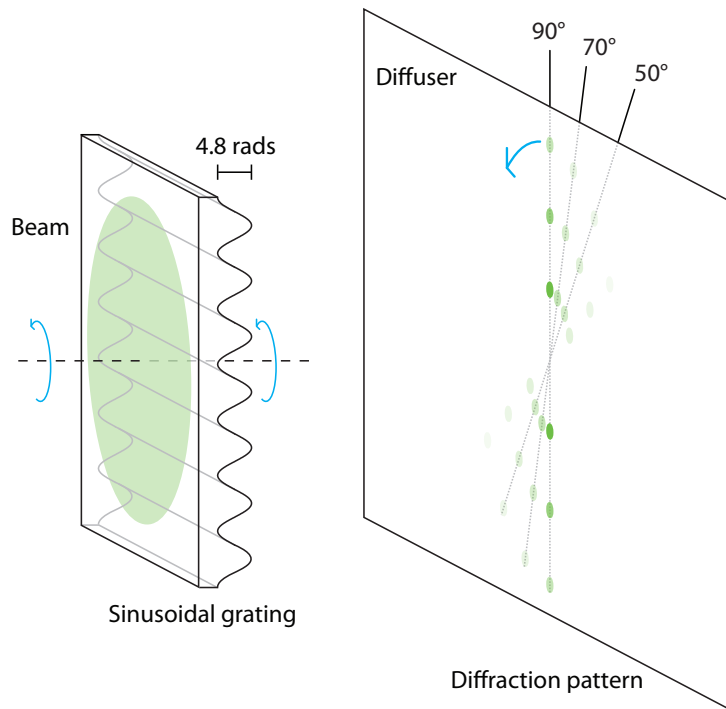


**Figure 4.8:** Principle of speckle reduction using a sinusoidal rotating grating. The illustration is from the article in appendix A.

The sinusoidal grating is introduced by poLight AS through the spatial light modulator with a deformable polymer layer (SLMDPL) [20]. The deformable layer can assume a sinusoidal shape that is controlled by a 1D array of electrodes. In order to rotate the sinusoidal grating poLight AS is working on

implementing a 2D array of electrodes.

Because a sinusoidal rotating grating is not available at the moment a transmissive spatial light modulator (SLM) will be employed as a proof-of-concept. The sinusoidal gratings are created by means of gray levels, and implemented on the SLM. It is not possible to achieve a continuous rotation of the sinusoidal gratings, because of the inherent pixelation of the SLM. Consequently the sinusoidal grating is rotated discretely from  $0^\circ$  to  $170^\circ$  with an angle increment of  $10^\circ$ , and an image is captured for each rotation. A rotation of  $180^\circ$  will give the same speckle pattern as when the grating is positioned at  $0^\circ$ . The sinusoidal grating is also rotated in a spiral in order to get different intensity distributions for rotations of  $0^\circ$  and  $180^\circ$ . Thus the grating is rotated from  $0^\circ$  to  $350^\circ$ , and an image is recorded for each  $10^\circ$  rotation.

Three measurement series will be performed for each method with different phase periods, that is 4, 8 and 12 pixels. As for the rotating diffuser in the 4-f imaging system the recorded speckle patterns are to be averaged and the modulator speckle contrast will be found for each measurement series.

### 4.3.1 The setup

The setup for speckle reduction using a sinusoidal rotating grating is shown in figure 4.9, and an image from the laboratory is displayed in figure 4.10. The DPSS laser module is emitting light with a wavelength of 532 nm and it has an applied voltage of 8 V. The spatial light modulator is sandwiched between a polarizer, positioned at  $330^\circ$ , and an analyser, positioned at  $0^\circ$ , in order to obtain the desired range of phase retardation. When the sinusoidal gratings are implemented into the SLM by means of the *LC2002 Control Program* a diffraction pattern is created.

A filter, which is used to remove undesirable diffraction maximas, followed by a stationary diffuser with a grit size of 1500 is placed a long distance from the SLM, that is 78 cm from the SLM to the diffuser. The 1500 grit is chosen because it scatters light less than the diffusers with lower grits, see section 5.1.3. The diffuser is used to decorrelate and homogenize the beam.

Further, the light is reflected onto the CCD camera by a screen, and the speckle patterns are captured by means of the software program *LuCam Capture v4.5.0*. The exposure time was 30 ms for all measurements, and no gain was applied. A lens with a focal length of  $f = 75$  mm is attached to the camera in order to focus the beam onto the CCD sensor. The angle

between the beam paths before and after hitting the screen is about  $22^\circ$ . Subsequently, the SLM and the filter are described more thoroughly.

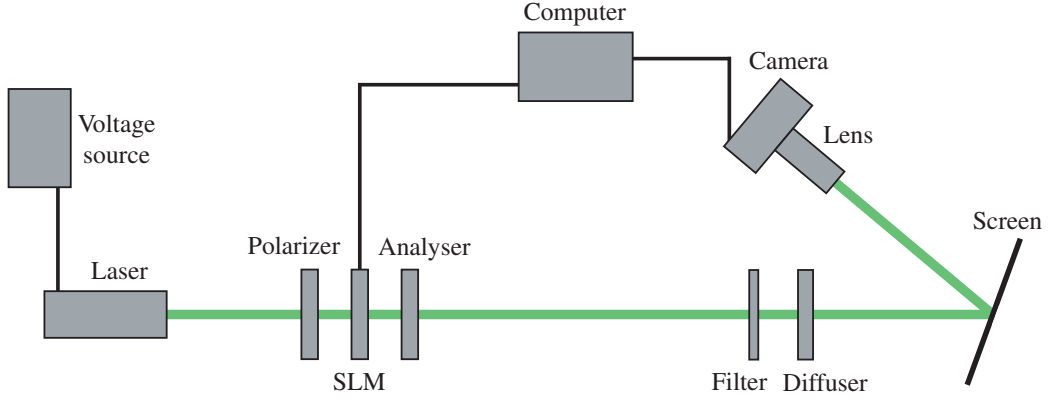


**Figure 4.9:** The setup for speckle reduction using a sinusoidal rotating grating.

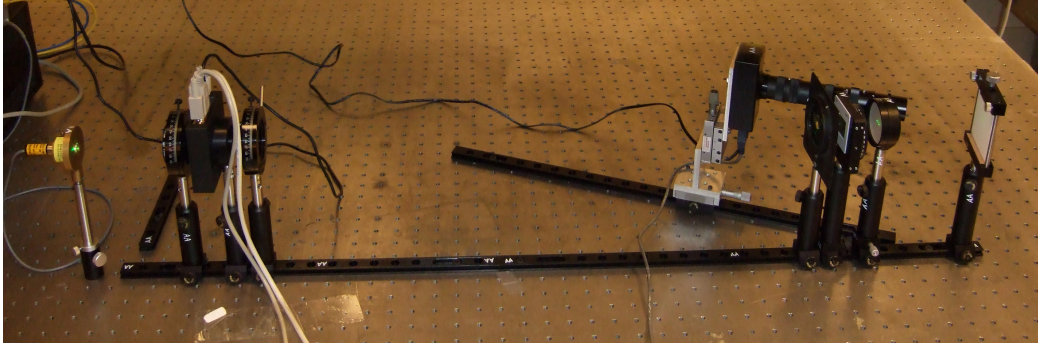


**Figure 4.10:** The laboratory setup corresponding to the schematics in figure 4.9.

### The spatial light modulator and the filter

The intensity distribution of the diffraction pattern with a peak-to-peak phase delay  $m$  results in the following equation [19],

$$I(x, y) \approx \left(\frac{A}{\lambda z}\right)^2 \sum_{q=-\infty}^{\infty} J_q^2\left(\frac{m}{2}\right) \text{sinc}^2\left(\frac{2wy}{\lambda z}\right) \times \text{sinc}^2\left[\frac{2w}{\lambda z}(x - qf_0\lambda z)\right]. \quad (4.3)$$

Here  $A$  is the area of the aperture,  $\lambda$  is the wavelength,  $z$  is the distance from the aperture to the observation plane,  $J_q$  is a Bessel function of first kind and order  $q$ ,  $w$  is the half-width of the aperture and  $f_0$  is the spatial frequency of the grating. The peak-to-peak phase delay is equal to 4.8 radians in order to cancel out the central diffraction maxima.

Every pixel in the matrix forming the SLM is individually alternating the phase of the laser beam, and can be considered as wave retarders [21]. A completely black pixel, with gray level 0, will cause no retardation, and a completely white pixel, with gray level 255, will cause a retardation of  $2\pi$  radians. The phase retardation as a function of gray level for the SLM, shown in figure 4.11, had to be measured because it was not linear. The function was used to make a lookup-table for correction of the sinusoidal gratings before they were implemented on the SLM. Such a correction is necessary for the sinusoidal gratings to actually give a sinusoidal phase retardation. A section of the matrix before and after the correction is shown in figures 4.12(a) - (b).

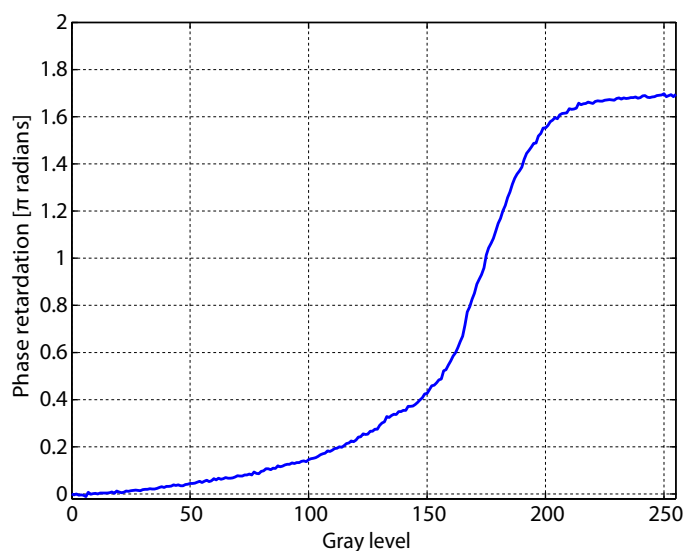


**Figure 4.11:** Phase retardation as a function of gray level for the SLM. The graph is from the article in appendix A.

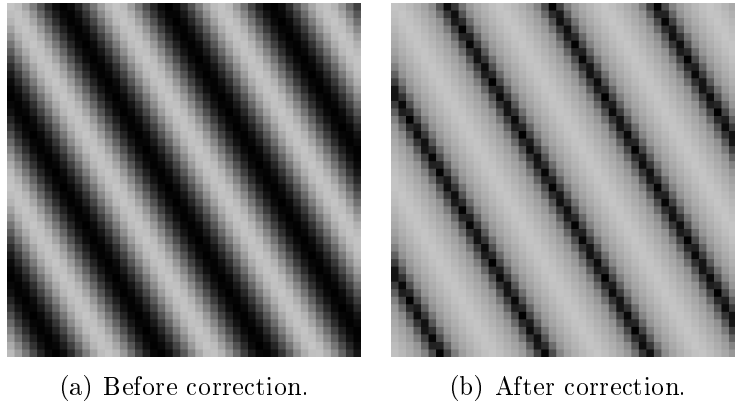


**Figure 4.12:** Correction of the sinusoidal grating. The images are from the article in appendix A.

When the SLM is turned off its pixels act as a grating because of the low fill factor of 55%. Thus a diffraction pattern, as illustrated in figure 4.13(a), is created. The distances between the spots at the filter were about 12 mm in both horizontal and vertical directions. The sinusoidal grating displayed on the SLM causes the laser beam to diffract each of these maximas, and they will be centers for a line of spots, as shown in figure 4.13(b). The spot sizes changes with respect to the grating periods, i.e. shorter periods lead to larger spots. The maximas created by the SLM are undesired, and hence a filter consisting of an aperture and a stop is employed. The aperture removes the higher order maximas and their corresponding lines of spots, while the stop blocks the zeroth order maxima. The filter utilised is shown in figure 4.13(c). The stop has to cover the zeroth diffraction order completely, and its size is therefore changed for the different grating periods. The size of the aperture opening is 9 mm for all the measurements, and the stop sizes are 3 mm, 2 mm and 1.5 mm for grating periods of 4, 8 and 12 pixels, respectively.

### 4.3.2 Speckle reduction methods

There are two similar speckle reduction methods investigated for this setup. In the first method the sinusoidal gratings are rotated around their centers, and an image is captured for each  $10^\circ$  rotation from  $0^\circ$  to  $170^\circ$ . The measurements are performed for grating periods of 4, 8 and 12 pixels.

In the second method the sinusoidal gratings are rotated in a spiral with their starting points in the center of the gratings. When the grating period is 4 pixels the grating is shifted one pixel for a rotation of  $10^\circ$ , two pixels for

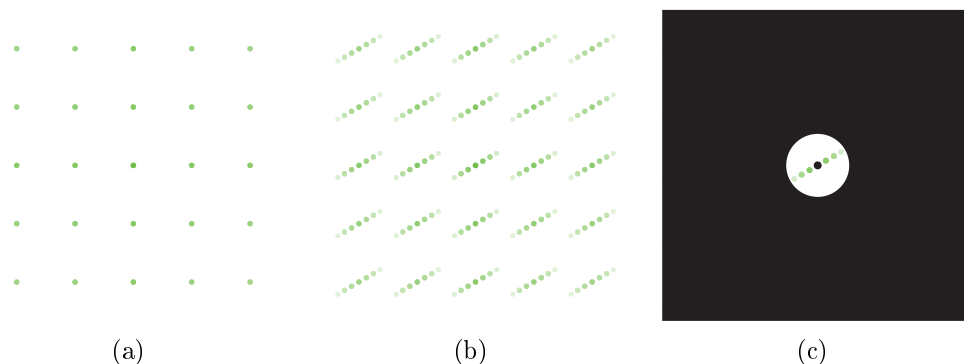


**Figure 4.13:** (a) The diffraction pattern caused by the pixels in the SLM. (b) Each maxima will be the source of a line of spots when a sinusoidal grating is displayed on the SLM. (c) The filter, consisting of an aperture and a stop, removing undesired elements. The illustrations are from the article in appendix A.

$20^\circ$ , three pixels for  $30^\circ$ , and then zero pixels for  $40^\circ$ , one pixel for  $50^\circ$ , and so forth. The same shifting method is applicable to the phase periods of 8 and 12 pixels, where the maximum shifts are 7 and 11 pixels, respectively.

The shift theorem stated below [19] proves that the diffraction patterns for the same grating periods in the two methods will not change when the gratings are shifted:

If

$$\mathcal{F}\{g(x, y)\} = G(f_x, f_y), \quad (4.4)$$

then

$$\mathcal{F}\{g(x - a, y - b)\} = G(f_x, f_y)\exp[-j2\pi(f_x a + f_y b)]; \quad (4.5)$$

that is, translation in the space domain introduces a linear phase shift in the frequency domain.

The idea is that the shifting of the rotating gratings in the second method will result in a change of the intensity distribution in the spots. Hence more independent speckle patterns will be obtained compared to the first method where there is no shifting. Because  $0^\circ$  and  $180^\circ$  rotations should result in different speckle patterns, an image is captured for each of the  $10^\circ$  angle increments from  $0^\circ$  to  $350^\circ$ . Thus a better speckle contrast reduction should be achieved.

## 4.4 Post-processing of the speckle patterns

Both the diffuser positioned in the 4-f imaging system and the sinusoidal grating implemented on the SLM are rotated discretely with an angle increment of  $10^\circ$ . An image is captured for each rotation, and saved in the folder corresponding to its measurement series.

When  $n$  independent elements contribute in the speckle reduction, the total speckle contrast is given by [1]

$$C = c_1 \cdot c_2 \cdots c_m \cdots c_n. \quad (4.6)$$

The contribution imposed by the rotating element is known as the modulator speckle contrast,  $c_m$ , while the rest of the contributions are caused by other elements in the setup. The speckle reduction achieved without the rotating element is known as the reference contrast, given by  $C_{\text{ref}} = c_1 \cdot c_2 \cdots c_{m-1} \cdot c_{m+1} \cdots c_n$ , which corresponds to

$$c_m = \frac{C}{C_{\text{ref}}}. \quad (4.7)$$

Hence the contrast reduction caused by the rotating element has been isolated. In this thesis,  $C$  is the contrast of the average speckle pattern, while  $C_{\text{ref}}$  is the average contrast of a set of speckle patterns.

The recorded images have to be averaged in order to calculate the modulator speckle contrast. For different numbers of averaged images,  $N$ , the speckle patterns are chosen with the same angle increment,  $\Delta\alpha$ , from one image to the next, given by

$$\Delta\alpha = \frac{360^\circ}{N}. \quad (4.8)$$

Thus, a larger amount of averaged images requires a smaller angle increment. For the measurement series with the sinusoidal grating rotated around its center,  $360^\circ$  changes to  $180^\circ$  in equation (4.8).

The MATLAB code used to create the graphs that display the modulator speckle contrasts for  $N$  averaged images and their deviations from the theoretical contrast is found in appendix C, and described subsequently.

An image of the background light is captured for each measurement series, and subtracted from the speckle patterns. To avoid negative matrix elements, negative values are treated as errors and set to zero. The outer edges of the images are removed to avoid potential edge effects caused by the CCD sensor. The intensities of the speckle patterns within one measurement series are scaled in order to achieve equal mean intensities for all images. At last, the modulator speckle contrasts are found for different numbers of averaged speckle patterns for the measurement series, as well as the deviations from the theoretical contrast.



## 5. Results

The brightness for all the speckle patterns displayed throughout section 5 has been increased in order to show the variations of the intensities better.

### 5.1 Rotating diffuser in the 4-f imaging system

#### 5.1.1 Empty object plane

The images in figures 5.1(a) - (f) show the speckle patterns at  $0^\circ$  for each of the measurements. The measurement series are performed between the two lenses in the 4-f imaging system shown in figure 4.1, and the distances given beneath each image are measured from the back plane of the first lens to the front plane of the diffuser. The Fourier plane is located where the speckle grains are largest, that is at 9.4 cm from the back plane of the first lens.

In order to reduce the speckle contrast images recorded for each rotation of  $10^\circ$ , from  $0^\circ$  to  $350^\circ$ , have to be averaged. This results in the images shown in figures 5.2(a) - (f), which represents the average speckle patterns when 36 images are averaged for each measurement series.

The graph in figure 5.3 displays the modulator speckle contrast, which is described in the theory, when  $N = 2, 3, 4, 6, 9, 12, 18, 36$  images are averaged for all series of measurements. The modulator speckle contrast is compared to the theoretical contrast of  $N$  independent images, which is given by  $C = \frac{1}{\sqrt{N}}$  in section 2.1, and the deviation in percent is showed by the graphs in figures 5.4(a) - (b).

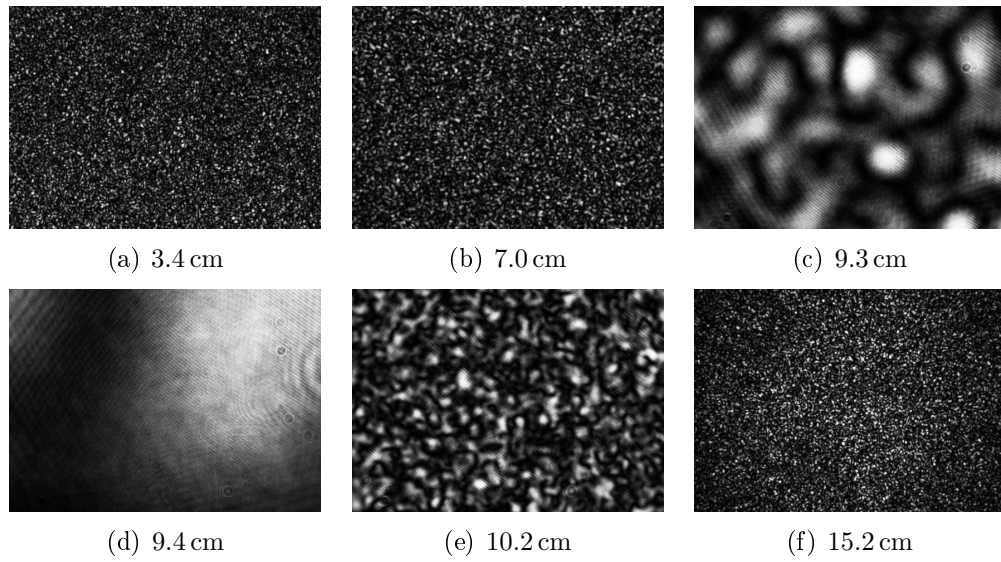


**Figure 5.1:** Speckle patterns at  $0^\circ$  for each measurement series at different positions in the 4-f imaging system.

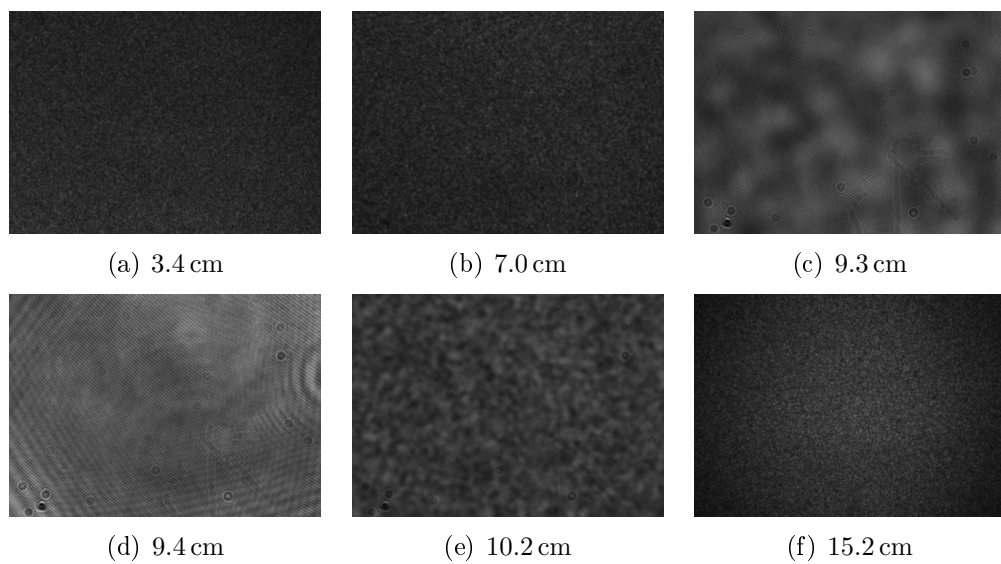


**Figure 5.2:** Average of 36 speckle patterns for each measurement series at different positions in the 4-f imaging system.

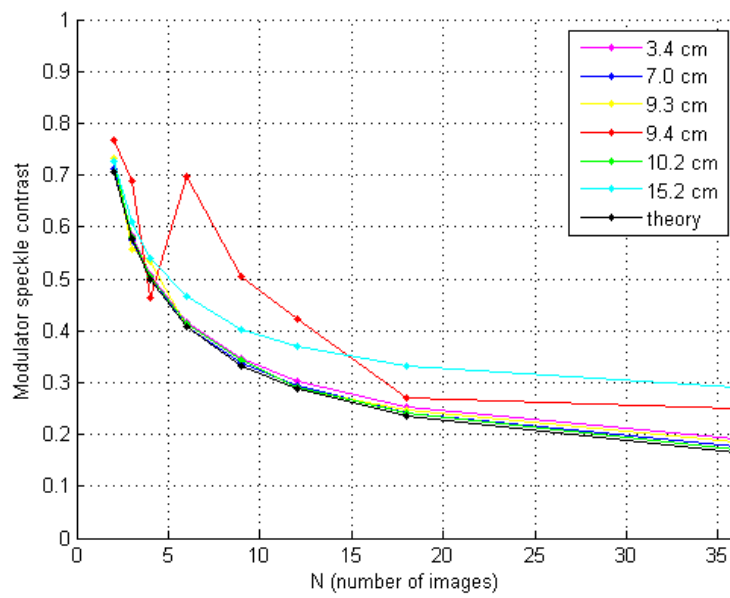
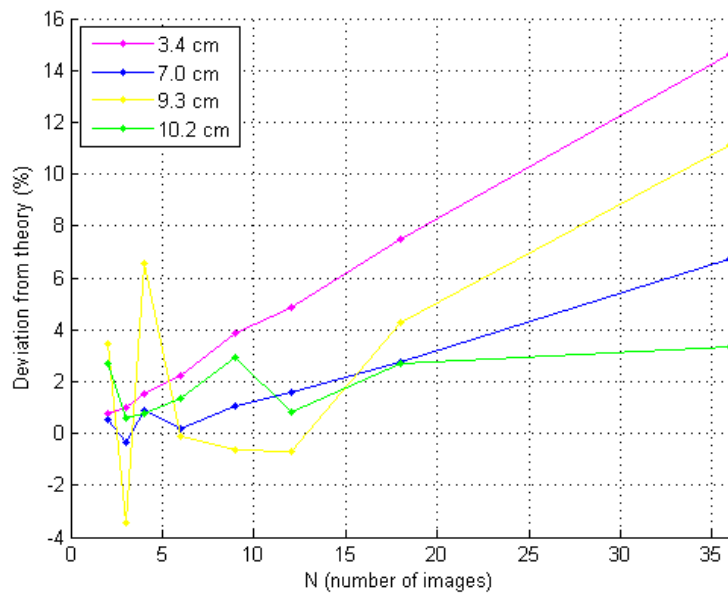
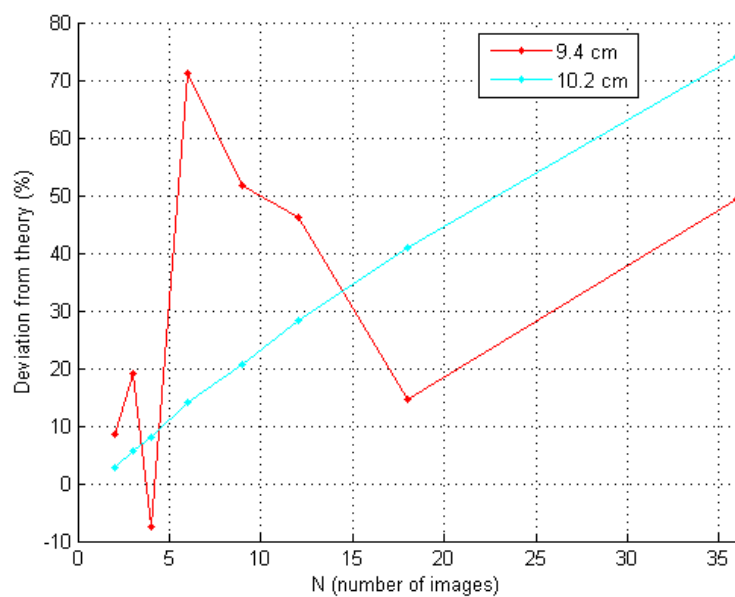


**Figure 5.3:** Modulator speckle contrast for  $N$  averaged images for the measurement series at different positions in the 4-f imaging system.



(a) Measurements close to theory.



(b) Measurements far from theory.

**Figure 5.4:** Deviation of modulator speckle contrast from theory for  $N$  averaged images for the measurement series at different positions in the 4-f imaging system.

### 5.1.2 A lens in the object plane

A lens is placed in the object plane of the 4-f imaging system, as shown in figure 4.3, in order to spread the light in the Fourier plane, and then avoid that just a small spot is illuminated. The images in figures 5.5(a) - (e) show the speckle patterns at  $0^\circ$  for each series of measurements. The measurement series are performed at different positions between the two similar lenses in the 4-f imaging system. The distances beneath the images in the figures are from the back focal plane of the first lens to the front plane of the diffuser. Calculations, displayed in figure 4.7, show that the Fourier plane is close to 9.3 cm from the back plane of the first lens. As opposed to the measurement series with an empty object plane the speckle grains are about the same size.

In order to achieve speckle reduction the images captured for each rotation of  $10^\circ$ , from  $0^\circ$  to  $350^\circ$ , have to be averaged. This leads to the images shown in figures 5.6(a) - (e) which display averaged speckle patterns for 36 different images for each measurement series.

The graphs in figures 5.7(a) and 5.7(b) display the modulator speckle contrast and its deviation from theory in percent for  $N = 2, 3, 4, 6, 9, 12, 18, 36$  different speckle patterns for each measurement series.

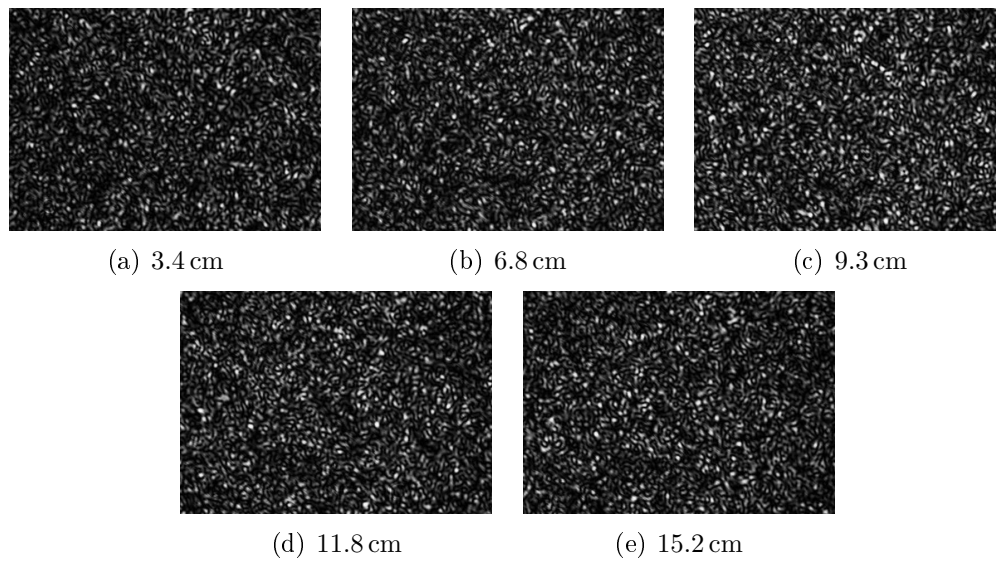


**Figure 5.5:** Speckle patterns at  $0^\circ$  for each measurement series at different positions in the 4-f imaging system.

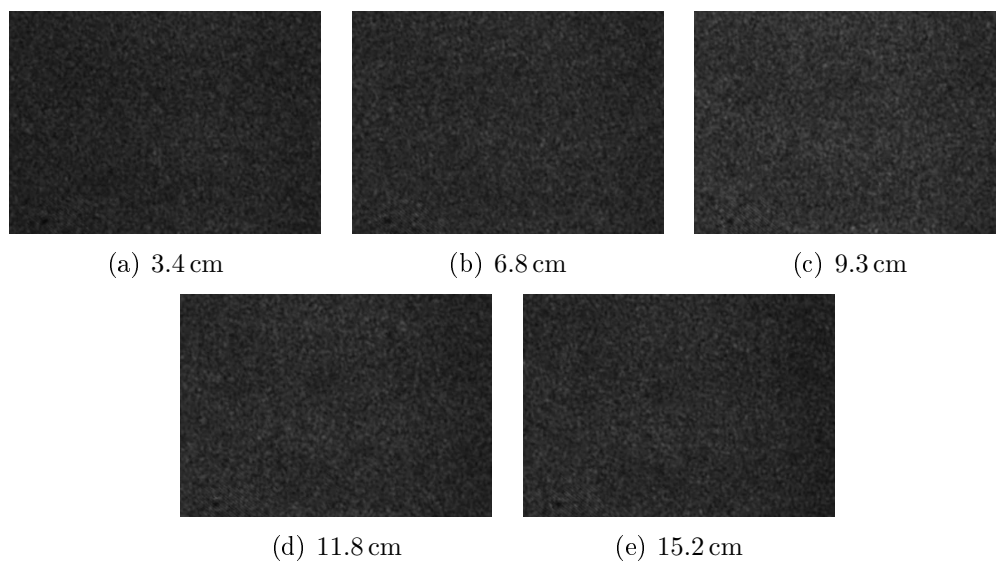
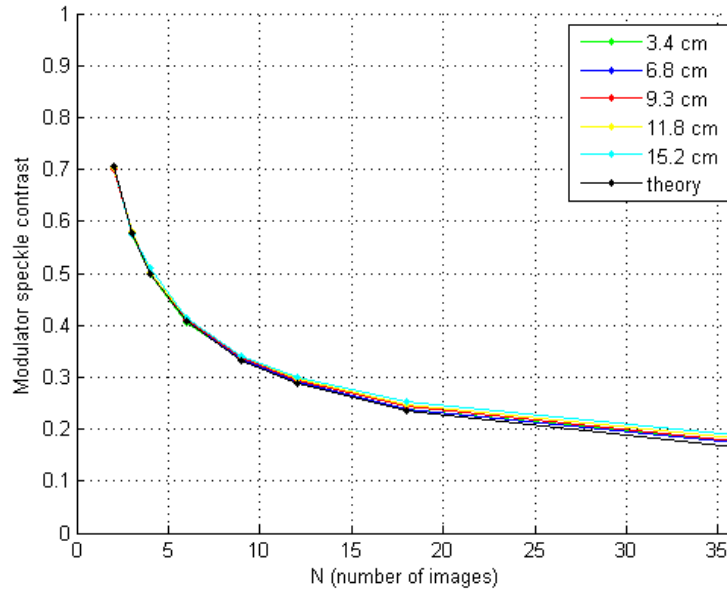
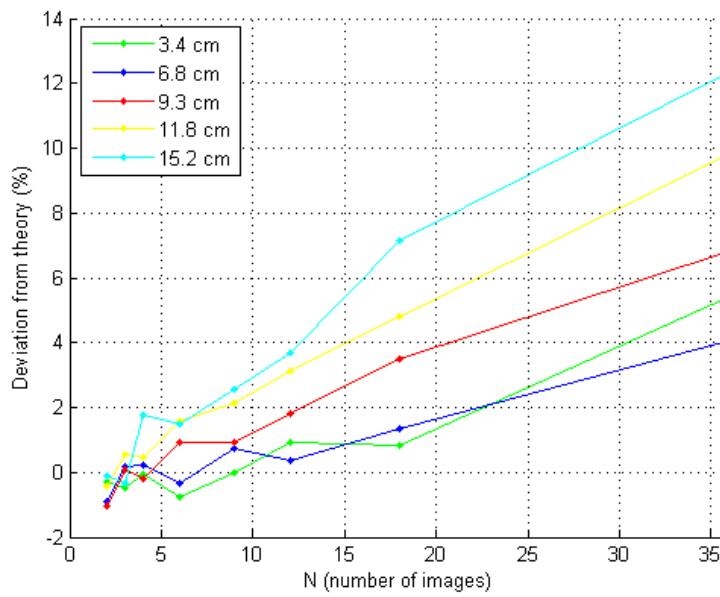


**Figure 5.6:** Average of 36 speckle patterns for each measurement series at different positions in the 4-f imaging system.



(a) Modulator speckle contrast for  $N$  averaged images.



(b) Deviation of modulator speckle contrast from theory for  $N$  averaged images.

**Figure 5.7:** Modulator speckle contrast and its deviation from theory for  $N$  averaged images for the measurement series at different positions in the 4-f imaging system.

### 5.1.3 Diffusers with different grit sizes

In order to find out whether the speckle reduction was dependent on the diffusers or not, different grit sizes were investigated. The images in figures 5.8(a) - (d) show the speckle patterns at  $0^\circ$  when the different diffusers are placed in the Fourier plane. The images in figures 5.9(a) - (d) display the average of the 36 different speckle patterns when rotating the diffuser with a  $10^\circ$  angle increment from  $0^\circ$  to  $350^\circ$ .

The graphs in figures 5.10(a) and 5.10(b) show the modulator speckle contrast and its deviation from the theoretical contrast when the diffusers are placed in the Fourier plane of the 4-f imaging system. It is seen that the diffuser with 600 grit has a larger deviation from theory than the other diffusers, and that is the reason why it is left out in the subsequent measurements. Table 5.1 show the exposure times for the different diffusers.

Diffuser	120 grit	220 grit	600 grit	1500 grit
Exposure time	12.0 ms	13.0 ms	6.0 ms	8.0 ms

**Table 5.1:** The exposure time for diffusers with different grit sizes positioned in the Fourier plane of the 4-f imaging system.

In order to determine the exposure times for the different diffusers some test images were captured. It is important that the maximum intensity of the images do not exceed 255, because then the images are saturated. Nevertheless, it is preferable that the images have a maximum intensity close to 255 for them to be as bright as possible.

Further, the same measurements were performed outside the Fourier plane, at the position 11.8 cm from the back plane of the first lens. Hence the speckle patterns for  $0^\circ$  are shown in figures 5.11(a) - (c), and the average of the 36 different speckle patterns can be seen in figures 5.12(a) - (c). Here the diffuser with a grit size of 600 was left out.

The graphs in figures 5.13(a) and 5.13(b) present the modulator speckle contrast and its deviation from the theoretical contrast when the diffusers are located 11.8 cm from the back plane of the first lens. The exposure times for the different diffusers are shown in table 5.2.



Diffuser	120 grit	220 grit	1500 grit
Exposure time	15.0 ms	15.0 ms	8.0 ms

**Table 5.2:** The exposure time for diffusers with different grit sizes positioned 11.8 cm from the back plane of the first lens in the 4-f imaging system.

Since the modulator speckle contrast for the different diffusers are similar the one with the shortest exposure time is preferable. That is because a shorter exposure time results in less scattering. The diffuser with a grit size of 1500 has thus been used in all the measurement series.

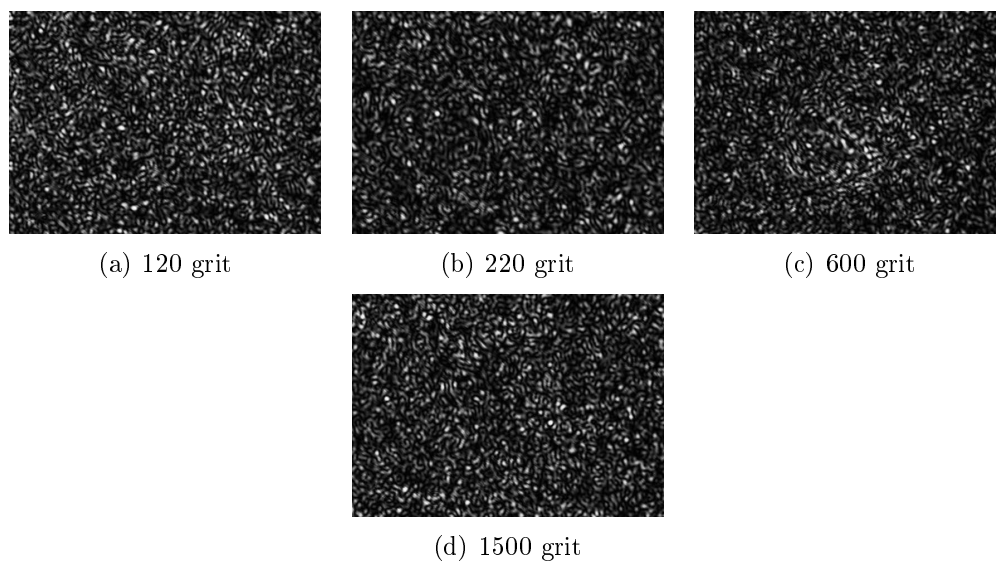


**Figure 5.8:** Speckle patterns at  $0^\circ$  for diffusers with different grit sizes positioned in the Fourier plane of the 4-f imaging system.

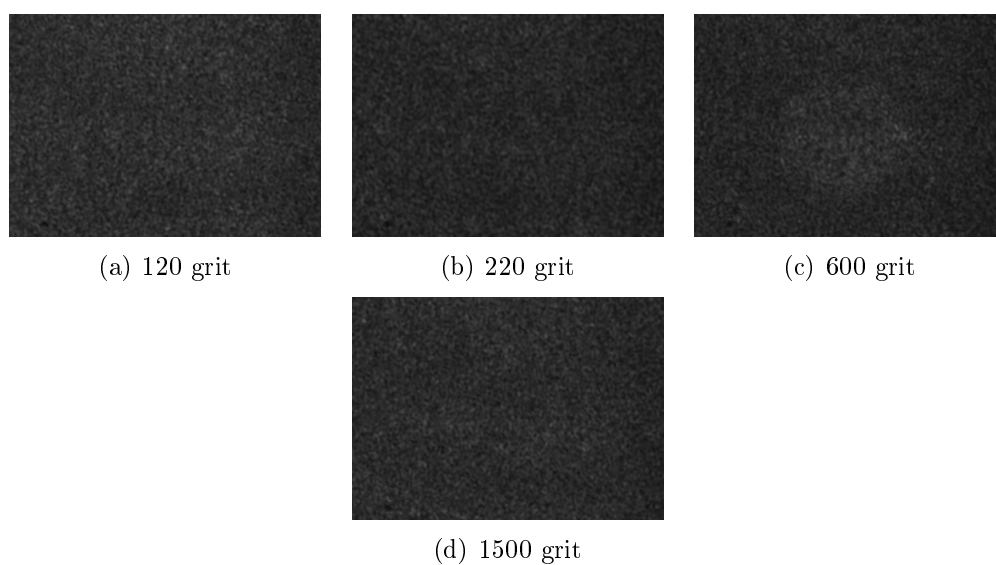
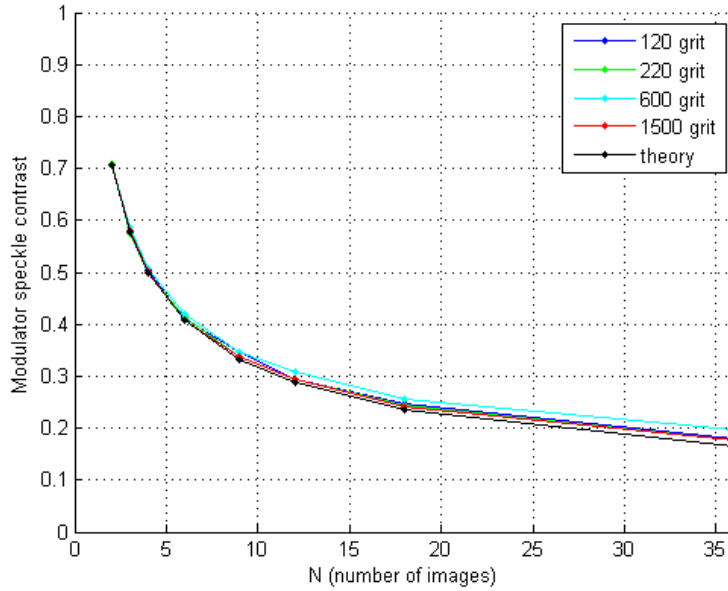
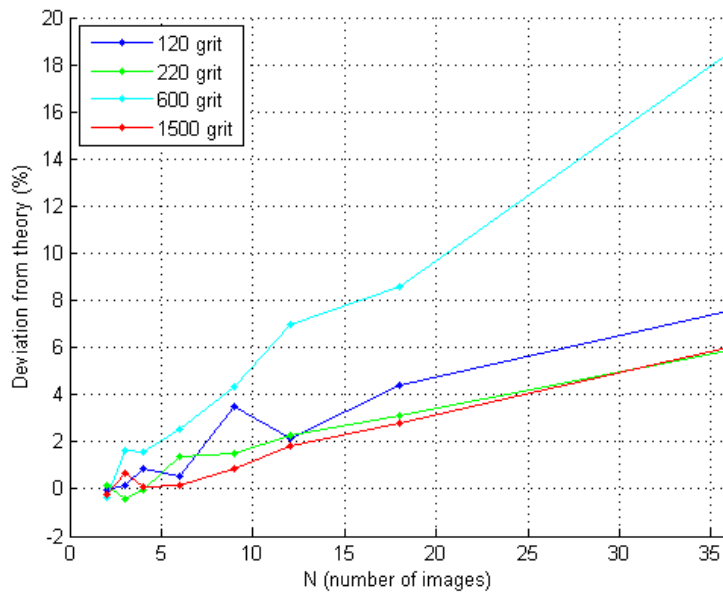


**Figure 5.9:** Average speckle patterns of 36 different images for diffusers with different grit sizes in the Fourier plane of the 4-f imaging system.



(a) Modulator speckle contrast for  $N$  averaged images.



(b) Deviation from theoretical contrast for  $N$  averaged images.

**Figure 5.10:** Modulator speckle contrast and its deviation from theoretical contrast for  $N$  averaged images when a rotating diffuser with different grit sizes positioned in the Fourier plane of the 4-f imaging system.

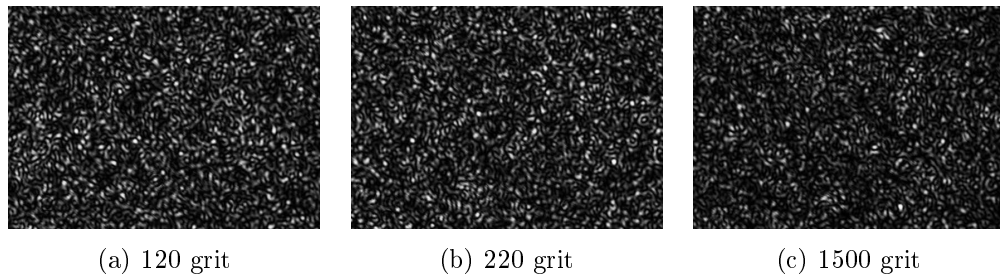


**Figure 5.11:** Speckle patterns at  $0^\circ$  for diffusers with different grit sizes positioned 11.8 cm from the back plane of the first lens in the 4-f imaging system.

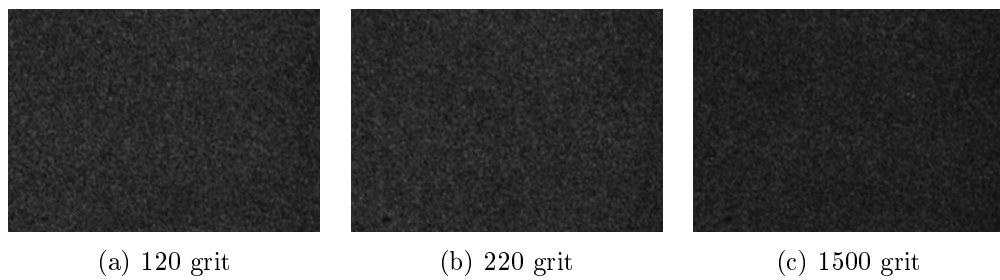
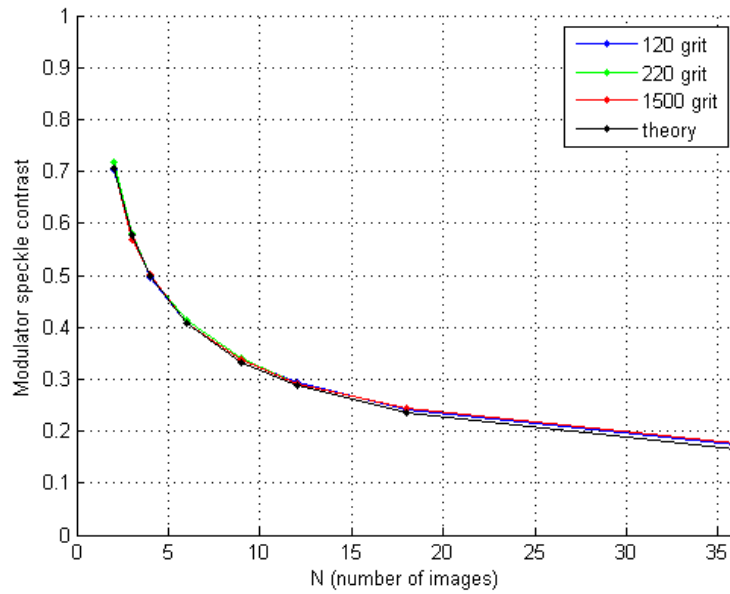
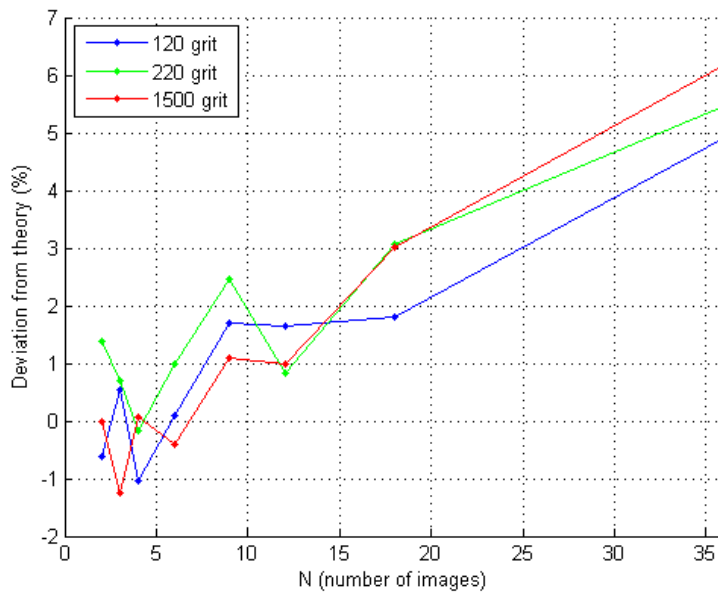


**Figure 5.12:** Average speckle patterns of 36 different images for diffusers with different grit sizes positioned 11.8 cm from the back plane of the first lens in the 4-f imaging system.



(a) Modulator speckle contrast for  $N$  averaged images.



(b) Deviation from theoretical contrast for  $N$  averaged images.

**Figure 5.13:** Modulator speckle contrast and its deviation from theoretical contrast for  $N$  averaged images when a rotating diffuser with different grit sizes is positioned 11.8 cm from the back plane of the first lens in the 4-f imaging system.

## 5.2 Sinusoidal rotating grating

### 5.2.1 Rotation around the center

In this method the sinusoidal gratings were rotated around their centers for each of the measurement series, that is for grating periods of 4, 8 and 12 pixels, and an image was captured for each rotation. A speckle pattern for a rotation of  $30^\circ$  and a grating period of 12 pixels is shown in figure 5.14(a). In order to reduce the speckle contrast the images captured for each  $10^\circ$  rotation from  $0^\circ$  to  $170^\circ$  had to be averaged. The average speckle pattern for  $N = 18$  different images is shown in figure 5.14(b). Similar images can be obtained for 4 and 8 pixels grating periods.

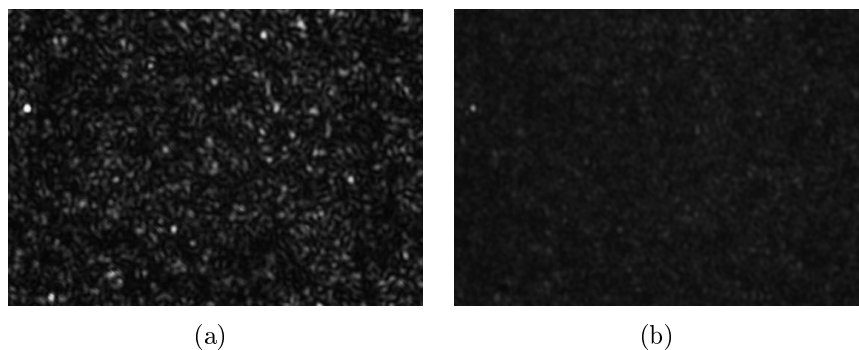
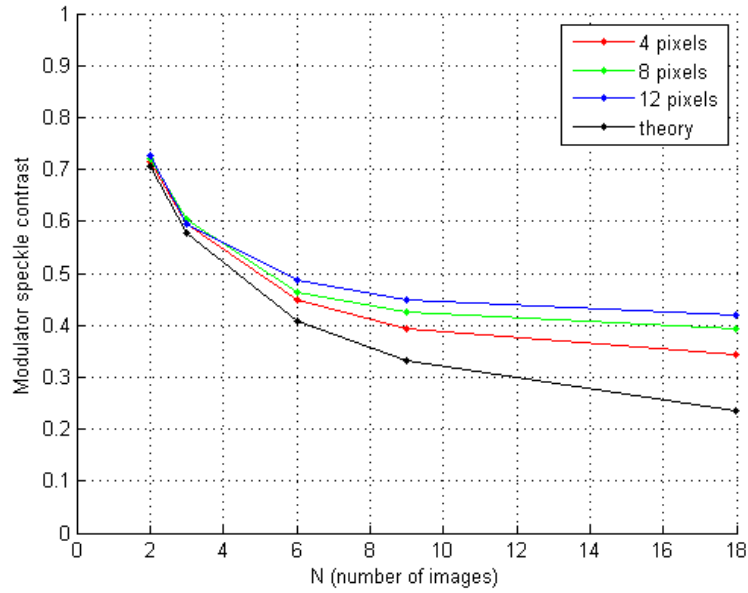


**Figure 5.14:** (a) Speckle pattern at  $30^\circ$  for a grating period of 12 pixels. (b) Average speckle pattern for  $N = 18$  with 12 pixels grating period.

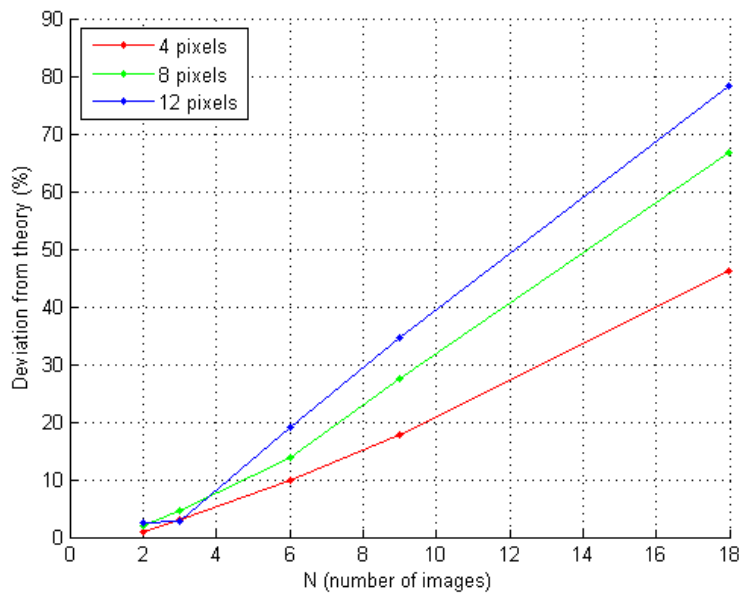
The modulator speckle contrasts for the different periods of the sinusoidal gratings for  $N = 2, 3, 6, 9, 18$  different speckle patterns are displayed in figure 5.15(a). Their deviations from the theoretical contrast,  $C = \frac{1}{\sqrt{N}}$ , are shown in figure 5.15(b). Table 5.3 gives the values of the modulator speckle contrasts for all  $N$ .

Period [px]	4	8	12
$c_m(N = 2)$	0.71	0.72	0.73
$c_m(N = 3)$	0.60	0.60	0.59
$c_m(N = 6)$	0.45	0.46	0.49
$c_m(N = 9)$	0.39	0.43	0.45
$c_m(N = 18)$	0.34	0.39	0.42

**Table 5.3:** Summary of the modulator speckle contrasts for all measurements.



(a) Modulator speckle contrasts for  $N$  averaged images.



(b) Deviations of modulator speckle contrasts from theoretical contrast for  $N$  averaged images.

**Figure 5.15:** Modulator speckle contrasts and their deviations from theory for  $N$  averaged images for the measurement series with a sinusoidal grating rotated around the center of the grating.

## 5.2.2 Rotation in a spiral

In this method the sinusoidal gratings were rotated in a spiral with their starting points in the center of the gratings, and an image was captured for each rotation. A speckle pattern recorded for 12 pixels grating period at  $30^\circ$  is displayed in figure 5.16(a). For these measurement series an image is captured at each  $10^\circ$  angle increment from  $0^\circ$  to  $350^\circ$ , and they had to be averaged in order to reduce the speckle contrast. Figure 5.16(b) shows the average speckle pattern for  $N = 36$  different images when the grating period is 12 pixels. The grating periods of 4 and 8 pixels will result in similar images.

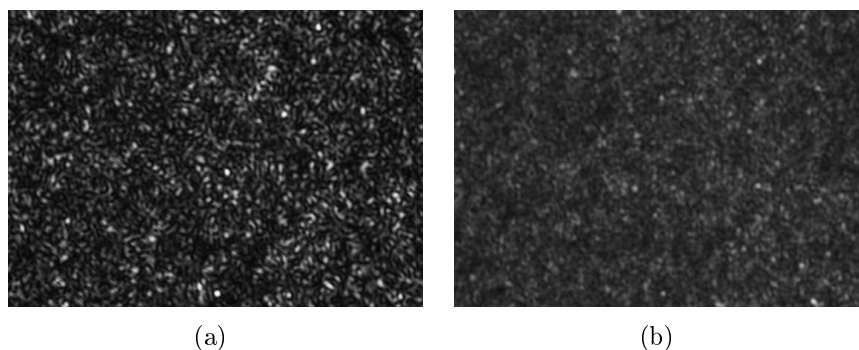


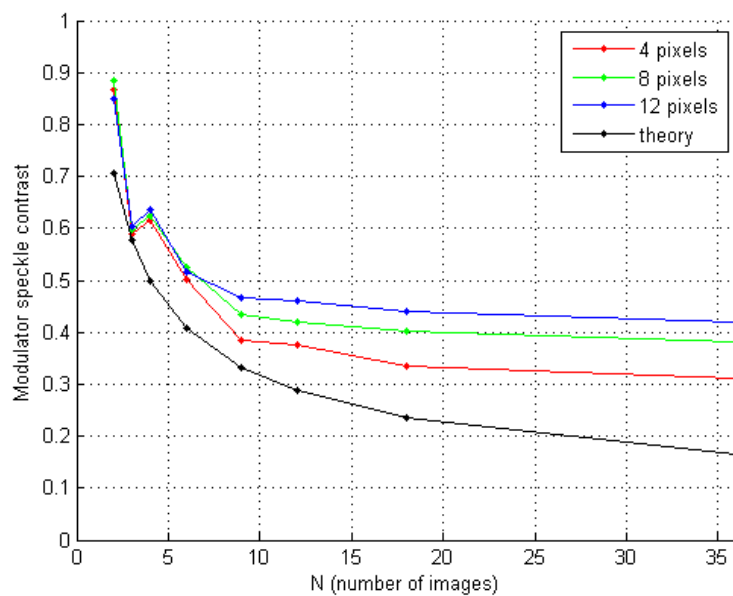
**Figure 5.16:** Speckle patterns at  $30^\circ$  for each measurement serie for different grating periods.

The graph in figure 5.17(a) shows the modulator speckle contrasts for  $N = 2, 3, 4, 6, 9, 12, 18, 36$  different images for all three grating periods. The graph in figure 5.17(b) displays their deviations from the theoretical contrast. The values for the modulator speckle contrasts for all  $N$  are given in table 5.4.

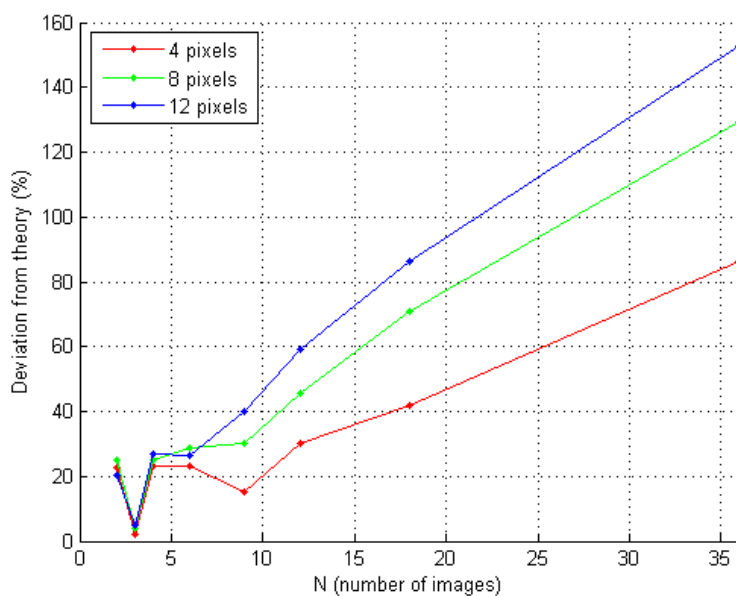
Period [px]	4	8	12
$c_m(N = 2)$	0.87	0.88	0.85
$c_m(N = 3)$	0.59	0.60	0.60
$c_m(N = 4)$	0.62	0.63	0.64
$c_m(N = 6)$	0.50	0.52	0.52
$c_m(N = 9)$	0.38	0.43	0.47
$c_m(N = 12)$	0.38	0.42	0.46
$c_m(N = 18)$	0.33	0.40	0.44
$c_m(N = 36)$	0.31	0.38	0.42

**Table 5.4:** Summary of the modulator speckle contrasts for all measurements.





(a) Modulator speckle contrasts for  $N$  averaged images.



(b) Deviations of modulator speckle contrasts from theoretical contrast for  $N$  averaged images.

**Figure 5.17:** Modulator speckle contrasts and their deviations from theory for  $N$  averaged images for the measurement series with a sinusoidal grating rotated in a spiral.



## 6. Discussion

### 6.1 Optical simulations in ZEMAX

According to the theory in section 2.5 the speckle size should become larger with a smaller aperture opening. Simulations with several aperture openings have been tested in ZEMAX, but all of them result in the same speckle size, which is shown in figure 3.10. It is very difficult to simulate the scattering properties of a diffuser, and it is reasonable to believe that the diffuser simulated in this setup does not qualify as a true diffuser. Therefore it is not certain that the pattern displayed in figure 3.10 represents speckle grains. Hence, simulating speckle turned out to be harder than expected, and due to the time limit for this thesis further experiments were not attempted.

### 6.2 Rotating diffuser in the 4-f imaging system

For the case with an empty object plane in the 4-f imaging system the images, when the diffuser is positioned at  $0^\circ$ , are displayed in figure 5.1. They show that the speckle grains have very different sizes when the diffuser is located at different positions between the two lenses. The speckle grains are largest when the diffuser is located in the Fourier plane, that is 9.4 cm from the back plane of the first lens, and they become smaller the closer the diffuser is positioned towards one of the lenses in the 4-f imaging system. When the diffuser is close to the second lens, that is 15.2 cm from the back plane of the first lens, more light is scattered and less light is incident on the CCD sensor. Consequently the images have dark outer edges.

The graphs in figures 5.3 and 5.4(b) show that the modulator speckle contrast in the Fourier plane fluctuates, and it is far from the theoretical contrast for almost all  $N$ . A reason may be the large sizes of the speckle grains

in the Fourier plane, seen in figure 5.1(d), causing them to overlap more frequently. As a consequence the speckle patterns will not be statistically independent. In addition, it is important to position the diffuser exactly in the Fourier plane, but the short Rayleigh range [10] makes this difficult. Thus, even a slight misalignment of the diffuser can cause incorrect results. The same graphs also show that when the diffuser is close to the second lens, the modulator speckle contrast has a large deviation from the theoretical contrast, i.e. 74% deviation for 36 averaged images. This is due to the nonuniform intensity distribution on the CCD sensor and the dark outer edges of the images.

The modulator speckle contrasts, shown by the graphs in figures 5.3 and 5.4(a), for the rest of the measurement series are fairly similar, and the deviation from theory ranges from about 4 – 15% for 36 averaged images. Hence it will not be advantageous to place the diffuser in the Fourier plane of the 4-f imaging system, nor close to the second lens, compared to elsewhere between the two lenses in the 4-f imaging system.

In order to spread the light in the Fourier plane a third lens with a shorter focal length was placed in the object plane of the 4-f imaging system. The speckle patterns, when the diffuser is positioned at  $0^\circ$  for different locations between the two lenses, are shown in figure 5.5, and it is seen that they have about the same grain size.

Further, the graphs in figure 5.7 show that the modulator speckle contrasts for  $N$  averaged images are fairly similar. The deviations from the theoretical contrast ranges from about 4 – 12% for 36 averaged speckle patterns, and the closer the diffuser is located towards the first lens of the 4-f imaging system the closer is the modulator speckle contrast to the theoretical contrast. As a result the Fourier plane does not seem to be advantageous for this case either.

Diffusers with different grit sizes were also investigated, both in the Fourier plane and outside of it. Figure 5.8 shows the speckle patterns when the diffusers are positioned at  $0^\circ$  and located in the Fourier plane. The speckle patterns for the diffusers with grit sizes of 120, 220 and 1500 are similar, but the speckle pattern for the diffuser with 600 grit is different. Instead of uniformly distributed speckle grains it is seen that there are more bright speckle grains towards the center of the CCD sensor. The same is seen in figure 5.9(c) when 36 speckle patterns are averaged. The graph in figure 5.10(b) shows that the 600 grit diffuser has a larger deviation from the theoretical contrast compared to the other diffusers, and hence it is left out for the measurement series performed outside the Fourier plane.

Figures 5.10 and 5.13 show that for the other measurement series the modulator speckle contrasts are close to the theoretical contrast, and also fairly similar. A short exposure time is desirable because it results in less scattering. Tables 5.1 and 5.2 show that the diffuser with 1500 grit requires the shortest exposure time, and hence it has been chosen for the measurement series.

Literature, such as [22], [23], [24] and [25] indicate that the Fourier plane of a 4-f imaging system could be advantageous for performing speckle reduction. Indeed none of them propose to place a diffuser in the Fourier plane, but, as can be seen in [26], [27] and [28], rotating or moving a diffuser is an effective method for speckle reduction. Therefore it was reasonable to believe that the speckle reduction measurements performed in the Fourier plane could prove to be superior compared to other measurement series. However, when considering the results achieved for a rotating diffuser located in the Fourier plane compared to a rotating diffuser positioned elsewhere the method does not appear to be advantageous.

### 6.3 Sinusoidal rotating grating

When the gratings are rotated around their centers, their deviations for the modulator speckle contrasts compared to the theoretical contrast are shown in figure 5.15(b). It is seen that the deviations increase when the number of averaged speckle patterns  $N$  increases. Because a smaller angle increment will cause the diffraction patterns to overlap more, this is as expected. Further, it is seen that the deviations are closer to theory when the grating periods are shorter. This is also as expected, because the 4 pixels grating period will create spots that are larger and more separated than the spots for the grating periods of 8 and 12 pixels. Thus the diffraction patterns for the 4 pixels grating period will overlap the least, and the diffraction patterns for the 12 pixels grating period will overlap the most.

The deviations for the modulator speckle contrasts compared to the theory when the gratings are rotated in a spiral show similar behaviour, and are displayed in figure 5.17(b). When  $N = 2$  the angle increment is given by  $\Delta\alpha = \frac{360^\circ}{2} = 180^\circ$ , see section 4.4, and consequently the images for  $0^\circ$  and  $180^\circ$  rotations are averaged for each of the grating periods. The averaged images have deviations from theory between 20 and 25 %, and as a result they have a large dependence. According to the shift theorem, see section 4.3.2, the diffraction spots for  $0^\circ$  and  $180^\circ$  rotations are perfectly overlapping.

However, if the two images had been alike the modulator speckle contrast would have been 1, but because it is not this indicates that the images have slightly different intensity distributions.

When  $N = 3$  and  $N = 9$ , tables 5.3 and 5.4 show that the modulator speckle contrasts are similar for the two methods. For the second method the angle increments are given by  $\Delta\alpha = \frac{360^\circ}{3} = 120^\circ$  and  $\Delta\alpha = \frac{360^\circ}{9} = 40^\circ$ , respectively. Hence none of the images have a rotation difference of  $180^\circ$  and a larger independence is achieved, as can be seen in figure 5.17(a). For  $N = 36$  a modulator speckle contrast of 0.31 is achieved for a grating period of 4 pixels. In comparison, a contrast of 0.34 is obtained for  $N = 18$  when the grating is rotated around its center. Consequently rotation in a spiral is promising and should be investigated further.

There are some drawbacks when it comes to the SLM used in the measurements. The steps of the sinusoidal gratings made of gray levels are more discretized for smaller grating periods. Furthermore, the gray levels ranged from 0 – 198 for the corrected sinusoidal gratings, thereby not using the maximum dynamic range of the SLM, which is 0 – 255. Moreover, because of the multiple maximas created by the SLM and their diffraction patterns shown in figure 4.13(b), spots from undesired maximas would pass through the aperture and mix with the desired spots. A larger grating period causes less mixing because the diffraction spots are closer to their respective zeroth order maximas. In addition, fewer grating periods are covered by the laser beam when the grating periods are larger, and thus equation (4.3) becomes less valid. Hence it could be fortunate to repeat the measurements with a beam expander positioned in front of the SLM.

## 7. Conclusion and further work

The intention with ZEMAX was to simulate a 4-f imaging system for speckle reduction, and the first challenge was to simulate speckle. It turned out to be a very challenging task, and as a consequence it was decided to end the simulations because of the time frame of this thesis. However, the work should be continued in a doctorate study. Other optical design and simulation software may be more suited to model speckle.

Further, a diffuser was rotated discretely with an angle increment of  $10^\circ$  from  $0^\circ$  to  $350^\circ$  in the Fourier plane of a 4-f imaging system. The diffuser was also placed at other positions between the two lenses forming the imaging system for comparison. Measurement series were performed both with an empty object plane and with a lens in the object plane in order to spread the light at the Fourier plane. When the object plane was empty the modulator speckle contrast was fluctuating compared to the theoretical contrast for the measurement series performed in the Fourier plane. Other positions resulted in a modulator speckle contrast much closer to the theoretical contrast. When the lens was placed in the object plane the modulator speckle contrasts were fairly similar and close to the theoretical contrast. Hence, the results impose that the Fourier plane of a 4-f imaging system is not an advantageous position for performing speckle contrast reduction with a rotating diffuser.

Lastly, sinusoidal rotating gratings made of gray levels were implemented on a transmissive spatial light modulator. Measurement series were performed with the sinusoidal gratings rotated discretely around their centers from  $0^\circ$  to  $170^\circ$  and in a spiral from  $0^\circ$  to  $350^\circ$ , both with an angle increment of  $10^\circ$ . The last method implied that the shifting of the sinusoidal gratings was not ideal to attain independent speckle patterns for rotations of  $0^\circ$  and  $180^\circ$ , but the rotation from  $180^\circ$  to  $350^\circ$  contributed to some additional speckle reduction. The modulator speckle contrasts for 4 pixels grating periods was 0.31 for  $N = 36$  averaged images when the SLM was rotated in a spiral, and 0.34 for  $N = 18$  averaged images when the SLM was rotated around its

center. The results from both methods indicate that rotation of sinusoidal gratings are promising for speckle contrast reduction, but because of the drawbacks of the SLM it is difficult to achieve good results. As a consequence, an SLM with a better fill factor and less discretization should be investigated. Moreover, a beam expander should be inserted in front of the SLM for the beam to cover even more grating periods. In addition, further measurements should be done with an improved method for rotating the sinusoidal gratings in a spiral, i.e. a method that results in independent speckle patterns for rotations of  $0^\circ$  and  $180^\circ$ .

By combining several reduction methods it is possible to achieve a better reduction of the speckle contrast, e.g. [26] and [29] suggest to employ several diffusers. It has also been proposed to use multiple light sources [30]. Hence, it could be interesting to place more than one SLM in the beam path in order to reduce the speckle contrast even further, and achieve the targeted 5% speckle contrast.



# Bibliography

- [1] J. W. Goodman, *Speckle Phenomena in Optics: Theory and Applications*. Ben Roberts & Company, 2007.
- [2] P. Janssens and K. Malfait, “Future prospects of high-end laser projectors,” *Proc. of SPIE*, vol. 7232, 2009.
- [3] J. I. Trisnadi, “Speckle contrast reduction in laser projection displays,” *Proc. of SPIE*, vol. 4657, 2002.
- [4] Z. Liao, T. Xing, G. Cheng, and W. Lin, “Speckle reduction in laser projection display by modulating illumination light,” *Proc. of SPIE*, vol. 6622, 2008.
- [5] L. Wang, T. Tschudi, M. Boeddinghaus, A. Elbert, T. Halldórsson, and P. R. Pétursson, “Speckle reduction in laser projections with ultrasonic waves,” *Society of Photo-Optical Instrumentation Engineers*, vol. 39, June 2000.
- [6] A. Furukawa, N. Ohse, Y. Sato, D. Imanishi, K. Wakabayashi, S. Ito, K. Tamamura, and S. Hirata, “Effective speckle reduction in laser projection displays,” *Proc. of SPIE*, vol. 6911, 2008.
- [7] T. Iwai and T. Asakura, “Speckle reduction in coherent information processing,” *IEEE*, vol. 84, May 1996.
- [8] L. Wang, T. Tschudi, T. Halldórsson, and P. R. Pétursson, “Speckle reduction in laser projection systems by diffractive optical elements,” *Applied Optics*, vol. 37, April 1998.
- [9] J. W. Goodman, *Statistical Optics*. John Wiley & Sons, 1985.
- [10] B.E.A.Saleh and M.C.Teich, *Fundamentals of Photonics*. John Wiley & Sons, Inc., second ed., 2007.
- [11] R. Guenther, *Modern Optics*. John Wiley & Sons, Inc., 1990.

- [12] K. J. Gåsvik, *Optical Metrology*. John Wiley & Sons, Ltd, third ed., 2002.
- [13] ZEMAX, *User's Manual*. April 14, 2010.
- [14] ZEMAX, "Getting Started Using ZEMAX, version 1.1.4." Website. <http://zemax.com/UserFiles/File/Getting%20Started%20With%20ZEMAX.pdf>.
- [15] G. April and H. Arsenault, "Nonstationary image-plane speckle statistics," *Optical Society of America*, vol. 1, July 1984.
- [16] ZEMAX, "ZEMAX User's Knowledge Base." Website. <http://www.zemax.com/kb/>.
- [17] A. Valberg, *Lys Syn Farge*. Tapir forlag, 1998.
- [18] B. B. Lee, J. Pokorny, V. C. Smith, P. R. Martin, and A. Valberg, "Luminance and chromatic modulation sensitivity of macaque ganglion cells and human observers," *Optical Society of America*, vol. 7, December 1990.
- [19] J. W. Goodman, *Introduction to Fourier Optics*. McGraw-Hill, 1996.
- [20] V. Kartashov, L. Henriksen, J. H. Ulvensøen, B. Svardal, T. Svortdal, R. Berglind, and G. Hedin, "Image improvement in a laser projection display with a spatial light modulator with a deformable polymer," *Journal of the Society for Information Display*, vol. 17, no. 7, 2009.
- [21] E. Hecht, *Optics*. Addison Wesley, fourth ed., 2002.
- [22] J. Maycock, B. M. Hennelly, J. B. McDonald, Y. Frauel, A. Castro, B. Javidi, and T. J. Naughton, "Reduction of speckle in digital holography by discrete Fourier filtering," *Optical Society of America*, vol. 24, June 2007.
- [23] N.-A. Chang and N. George, "Speckle in the 4F optical system," *Optical Society of America*, vol. 47, February 2008.
- [24] Y. Kawagoe, N. Takai, and T. Asakura, "Speckle reduction by a rotating aperture at the Fourier transform plane," *Optics and Lasers in Engineering*, vol. 3, 1982.
- [25] K. Jeong, L. Peng, D. D. Nolte, and M. R. Melloch, "Fourier-domain holography in photorefractive quantum-well films," *Applied Optics*, vol. 43, July 2004.

## BIBLIOGRAPHY

---

- [26] S. Lowenthal and D. Joyeux, "Speckle removal by a slowly moving diffuser associated with a motionless diffuser," *Optical Society of America*, vol. 61, July 1971.
- [27] M. A. A. Neil, F. Massoumian, R. Juškaitis, and T. Wilson, "Method for the generation of arbitrary complex vector wave fronts," *Optical Society of America*, vol. 27, November 2002.
- [28] S. C. Shin, S. S. Yoo, S. Y. Lee, C.-Y. Park, S.-Y. Park, J. W. Kwon, and S.-G. Lee, "Removal of hot spot speckle on laser projection screen using both the running screen and the rotating diffuser," *Elsevier B. V.*, 2006.
- [29] E. Schröder, "Elimination of granulation in laser beam projections by means of moving diffusers," March 1971.
- [30] S. An, A. Lapchuk, V. Yurlov, J. Song, H. W. Park, J. Jang, W. Shin, S. Kargapoltsev, and S. K. Yun, "Speckle suppression in laser display using several partially coherent beams," *Optics Express*, vol. 17, January 2008.



## A. Article

# Speckle reduction using a sinusoidal rotating grating

Sigbjørn Vindenes Egge,<sup>1</sup> Nadeem Akram,<sup>2</sup> Vladimir Khartashov,<sup>3</sup>  
Kristine Welde,<sup>1</sup> Zhaomin Tong,<sup>2</sup> Ulf Österberg,<sup>1</sup> and Astrid Aksnes<sup>1</sup>

<sup>1</sup>*Department of Electronics and Telecommunications,*

*Norwegian University of Science and Technology, 7491 Trondheim, Norway\**

<sup>2</sup>*Institute of Microsystems Technology, Vestfold University College, 3103 Tønsberg, Norway*

<sup>3</sup>*poLight AS, P.O. Box 163, 3192 Horten, Norway*

This paper describes a novel idea for reduction of speckle contrast in laser display projectors using the rotation of a diffraction pattern and a variable grating period. The feasibility of the proposed method was investigated by illuminating gratings with a sinusoidal phase on a transmissive spatial light modulator (SLM), where each phase grating pattern was rotated with respect to the previous one. Several series of measurements were done with different periods of the sinusoidal grating. For each series, an image of the speckle pattern was recorded at each rotation angle of the phase grating, and then an average image was calculated. Several series were also averaged together. Experimental results were compared with the theoretical speckle contrast of the sum of  $N$  independent speckle patterns. The experimental measurement results compare well to the theoretical predictions resulting in a minimum speckle contrast of 0.18, with further reduction possible.

PACS numbers: 000.0000, 999.9999.

## I. INTRODUCTION

Compared to ordinary display projectors based on incandescent lamps there are several advantages of using laser light, like improved color gamut, higher contrast, deeper focus, and higher brightness [1]. However, laser light, being highly coherent, causes interference at the detector (e.g. the observer's eye) when reflected off a rough screen and creates a random pattern of varying intensity over the image [2]. This noise pattern is called *speckle*. The decisive challenge with laser projectors is to reduce the speckle noise to an acceptable level without impairing the benefits of a laser light source or its power too much, or significantly degrading the image.

Techniques for reducing speckle noise are based on reducing the (spatial or temporal) coherence of the light before it arrives at the detector. A *partially* coherent beam will produce a time-varying interference pattern on the viewer's retina. These fluctuations will to a certain degree, depending on the correlation between speckle patterns at different instances, average out during the integration time of the eye. An overview of some speckle reduction techniques for laser projector displays can be found in Goodman's book [1].

A common approach to speckle reduction is to place a modulator in the path of light, between the light source and the imaging system, that reduces the coherence of the beam. Such a modulator can be based on the principle of diffraction. Wang *et al.* [3, 4] use a simple setup where the beam of a point-scanning projector is expanded and passed through a rotating diffractive optical element (DOE). The DOE transforms the beam into beamlets which cover different areas of a pixel. Rotation of the

DOE causes rotation of the beamlets and generates different speckle patterns. This is similar to [5] where the beam is sent through a rotating phase plate. Kamm *et al.* [6] apply a spatial light modulator (SLM) to modulate the phase across an expanded beam and divide it into sub-beams. The sub-beams are separated by a certain angle so they will produce uncorrelated speckle patterns, and then the phase differences between the beams are varied in order to produce a changing speckle pattern. In [7] the speckle noise is reduced by passing the light through a vibrating phase grating.

This paper presents a novel idea for a speckle reduction modulator based on diffraction and rotation. A beam of coherent light is passed through a sinusoidal phase grating which diffracts the light into a line of spots on the screen. When rotated, these spots will cover different areas of the screen and thus produce independent speckle patterns. However, the zeroth order maxima will be stationary when the diffraction pattern is rotated. That is why a *phase* grating is used, because a proper peak-to-peak phase delay of 4.8 radians will cancel the zeroth order without losing power [8]. In this laboratory experiment, the feasibility of the proposed speckle reduction method was investigated using an SLM. Other uses of SLMs include adaptive optics, optical communications, and image formation in display systems [9].

A modulator that can be used to implement the suggested method in a real projector is based on the spatial light modulator with a deformable polymer layer (SLMDPL) by poLight AS [10]. The deformable polymer layer is controlled by a 1D array of electrodes which can be used to give the polymer a sinusoidal shape that diffracts the incoming light. To incorporate *rotation* of the diffraction pattern poLight AS is working on an SLMDPL that is controlled by a 2D electrode array. However, the focus of this paper is on the proof-of-concept and not on any particular implementation.

---

\* sve@iet.ntnu.no

## II. SINUSOIDAL ROTATING GRATING MODULATOR

The proposed method for speckle reduction is to diffract an incoming beam of laser light into a line of spots on a diffuse surface and at the same time rotate the diffraction pattern, see Figure 1. The grating's axis of rotation is perpendicular to the surface of the diffuser such that the sinusoidal grating is always parallel with the diffuser. In a laser projector the diffuser would be followed by a light homogenizer with an image SLM at the end. When the sinusoidal grating is rotated, the diffraction orders will cover new areas of the diffuser and thus create different speckle patterns—except the zeroth order which will remain stationary. This order will not contribute to different speckle patterns and should thus be removed. One possibility is to block it, but that will cause an undesirable loss of power. Instead, the zeroth order can be eliminated without any loss of power by making the peak-to-peak phase delay in the sinusoidal grating equal to 4.8 radians, as shown in Figure 1. This can be derived using the expression for the intensity distribution of the diffraction pattern. For further reduction of speckle contrast the period of the sinusoidal grating can be varied. Then the period is changed for each 180° rotation of the grating such that the diffraction spots hit other parts of the diffuser. Of course, for a variable grating period to give any reduction of speckle contrast the different periods will have to be applied during the integration time of the eye.

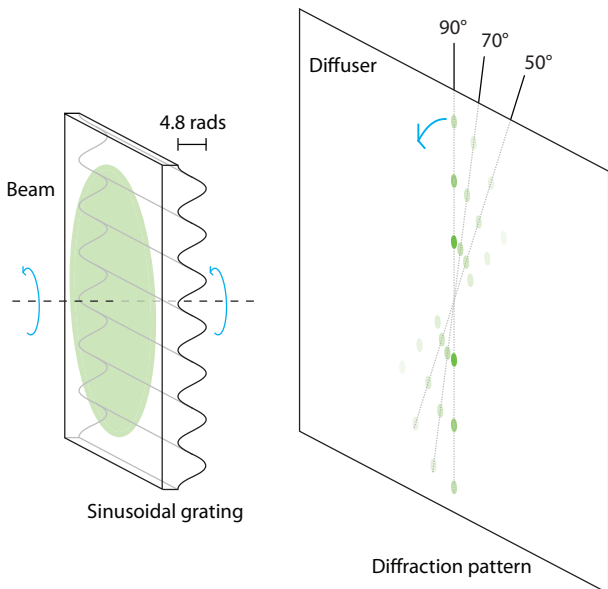


FIG. 1. Diffraction from a sinusoidal phase grating with a peak-to-peak phase delay of 4.8 radians produces a pattern with a vanishing zeroth order. Rotation of the diffraction pattern creates independent speckle patterns.

A sinusoidal phase grating oriented in the  $x$ -direction with a peak-to-peak phase delay  $m$  gives rise to a diffrac-

tion pattern with the following distribution [8],

$$I(x, y) \approx \left(\frac{A}{\lambda z}\right)^2 \sum_{q=-\infty}^{\infty} J_q^2\left(\frac{m}{2}\right) \text{sinc}^2\left(\frac{2wy}{\lambda z}\right) \times \text{sinc}^2\left[\frac{2w}{\lambda z}(x - qf_0\lambda z)\right]. \quad (1)$$

Here  $A$  is the area of the aperture,  $\lambda$  the wavelength,  $z$  the distance from the aperture to the observation plane,  $J_q$  a Bessel function of the first kind and order  $q$ ,  $w$  the half-width of the aperture, and  $f_0$  the spatial frequency of the grating. For a given  $y$ , the intensity distribution is a weighted sum of squared sinc-functions that each has a strong maximum for  $x = qf_0\lambda z$  and rapidly decays outside. Each sinc-function gives rise to one spot in the diffraction pattern. The zeroth order in the diffraction pattern is created by the sinc-function with a maximum at  $x = 0$ , when  $q = 0$ . In order to make the zeroth order of the diffraction pattern vanish,  $m$  has to be chosen such that  $m/2$  is a root of  $J_0$ . The first root is located at  $m/2 = 2.4$ , which gives a peak-to-peak phase delay of 4.8 radians.

When the phase grating is rotated there are two factors which contribute to a varying speckle pattern; the changing angle of the light rays incident on the diffuse surface and the relative displacement between this surface and the light spots. Independent speckle patterns are obtained by rotating the diffraction pattern an angle that makes the first order maxima non-overlapping before and after rotation. The more the maxima overlap, the less independent the speckle patterns become and the less speckle reduction is obtained. This is because the rotated diffraction pattern does not cover a completely different area on the diffuse surface with respect to the previous diffraction pattern, which is a criteria for independency.

The proposed modulator is intended to be implemented by a 2D SLM with a deformable polymer layer (SLMDPL) [10]. For proof-of-concept the sinusoidal phase grating was implemented in discretized steps on the transparent Holoeye LC 2002 SLM (800 × 600 pixels) in phase mode [11]. The SLM consists of a matrix of pixels which is used to alter the phase across a beam of light. Each pixel is individually modulating the phase of the incoming light such that every pixel is a wave retarder [12].

The SLM's phase retardation, as a function of gray scale, was not linear and had to be measured. The measured phase retardation is shown in Figure 2(a), and this was used to make a lookup-table to create gratings with a sinusoidal phase distribution when displayed on the SLM. The corresponding intensity modulation is shown in Figure 2(b). Since the SLM is slow at updating, with an image frame rate of maximum 60 Hz, speckle reduction measurements with the SLM were *not* performed in real time. The speckle patterns produced by the SLM were recorded separately at each rotation angle and then averaged.

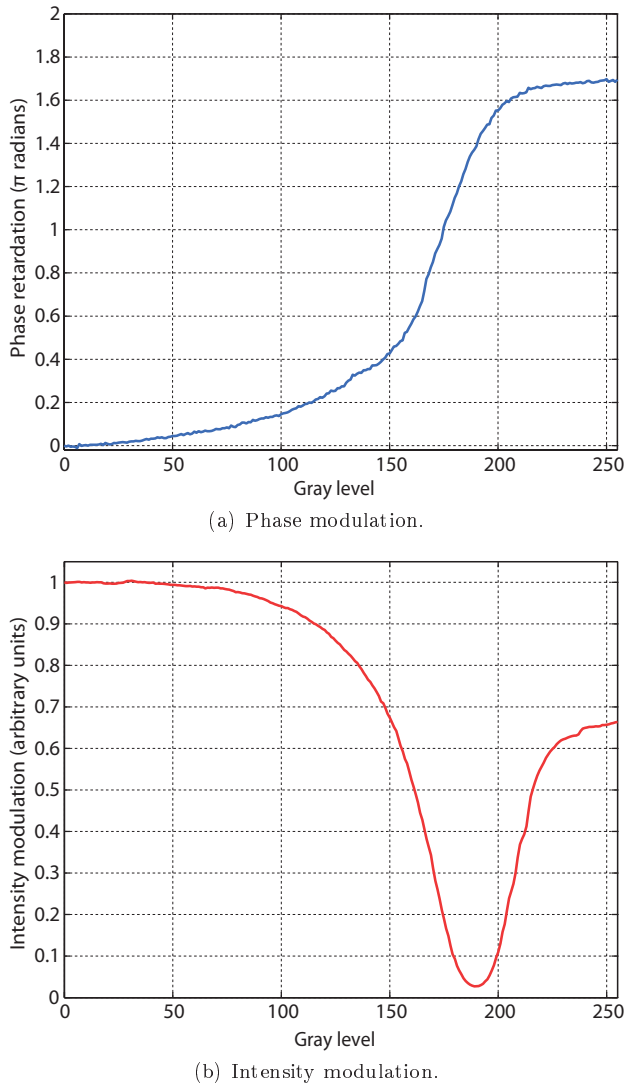


FIG. 2. (a) Phase retardation imposed by the SLM as a function of gray level, for the wavelength 532 nm. (b) The intensity also gets modulated when the SLM is used for phase modulation.

### III. SETUP AND METHOD

A schematic of the setup is shown in Figure 3. The laser emitted a beam with wavelength of 532 nm and  $1/e^2$ -diameter of 1.2 mm that was incident on the SLM with a pixel pitch of  $32 \mu\text{m}$ . To obtain the desired range of phase modulation the SLM was sandwiched between two polarizers. The polarizer and analyzer had axes of polarization oriented at respectively  $330^\circ$  and  $0^\circ$  relative to the vertical axis, measured counterclockwise while looking in the direction of the beam. The angles were chosen to get a large enough phase retardation. Passing through the SLM the light was diffracted, and the diffraction pattern was filtered to block unwanted maxima (the design of the filter will be explained below) before it passed

through a stationary diffuser in order to decorrelate and homogenize the beam. The distance between the SLM and the diffuser was 78 cm. The light was reflected off a sheet of the industry reference screen StudioTek 130 G3 from Stewart Filmscreen and imaged onto the CCD of the Lumenera Lu070 camera. The linearity of the CCD had been verified. The angle between the beam paths before and after hitting the screen is exaggerated in the figure; in reality the angle was about  $22^\circ$ .

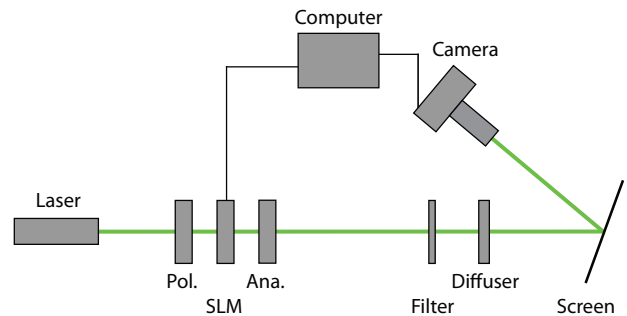


FIG. 3. A sketch of the measurement setup.

In order to use an SLM as a *phase* modulator, gray scale images of sinusoidal patterns were displayed on the SLM. This was done by connecting the SLM to a VGA port on a PC and then displaying the desired image. The retardation introduced by each pixel on an incoming light beam was determined by the value of the pixel's gray level. Black and white have the gray levels 0 and 255, respectively. A pixel in the gray scale image which is completely black caused no retardation, while a pixel that is completely white caused a retardation of approximately  $1.7\pi$  radians, as shown in Figure 2(a). The retardation depends both on the wavelength of the light and on the angle of the polarizers. Since the retardation was not a linear function of gray level the retardation-curve in Figure 2(a) had to be used to correct the sinusoidal gratings such that they actually gave a *sinusoidal* phase retardation. A section of a sinusoidal matrix before and after correction is shown in Figure 4.

The fill factor of the SLM is 55%. A major challenge using an SLM for speckle reduction is that the pixels act as a grating causing strong diffraction, as shown in Figure 5(a). The horizontal and vertical distances between the spots at the filter were about 12 mm. With a sinusoidal grating displayed on the SLM, each of these maxima would be the center of a line of diffraction spots, as shown in Figure 5(b). As mentioned earlier, the zeroth order maximum in the diffraction pattern from the sinusoidal grating should be cancelled out for a maximum phase retardation difference of 4.8 radians. Although the correct maximum phase retardation was implemented on the SLM, the reduction in the zeroth order was only relatively small since the zeroth order diffraction maximum from the SLM itself was overlapping. In order to avoid the maxima created by the SLM acting as a grating, light was passed through a filter after the SLM that con-



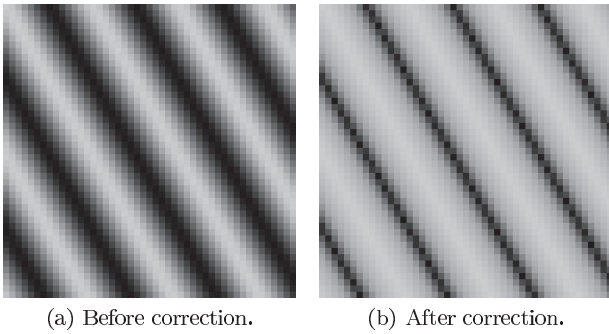


FIG. 4. Section of a sinusoidal matrix, before and after correcting for the non-linear behavior of the SLM. The matrix is rotated  $30^\circ$  and is from the set of matrices with a sinusoidal period of 12 pixels. One pixel in the images corresponds to one pixel on the SLM.

sisted of a circular aperture and an aperture stop. The circular aperture stopped light from all maxima except the zeroth, while the aperture stop removed the zeroth maximum, see Figure 5(c). The diameter of the aperture was 9 mm while the size of the aperture stop had to be chosen such that it completely blocked the zeroth diffraction order. The size of the diffraction orders depended on the period of the grating. For 4, 8, and 12 pixels period the diameter of the stop was 3 mm, 2 mm, and 1.5 mm, respectively. Measurements were performed with a DET100A photo detector from ThorLabs to verify that the power in the zeroth order was negligible.

Three series of measurements were performed that differed in the period of the sinusoidal gratings. The periods were 4, 8, and 12 pixels, which from (1) gives spot separations of respectively 3.0, 1.5, and 1.0 mm, and diffraction angles of  $0.24^\circ$ ,  $0.12^\circ$ , and  $0.078^\circ$ . All measurements were done by recording images of stationary speckle patterns. The exposure time was 30 seconds and no gain was used in the camera. Two factors accounted for the long exposure time; the filtering which took away most of the power and the camera's small aperture which was used to achieve large enough speckle grains. To avoid background light during measurements lights were turned off and the setup was covered with opaque material. For each measurement series, an image of the background light was taken and subtracted from the speckle patterns during post-processing. This subtraction yielded some negative intensity values due to discretization in the CCD, noise in the measurement system, and environmental disturbances. These negative intensity values were treated as errors and set to zero. In order to avoid any edge effects the speckle patterns were cropped. The intensity of each speckle pattern within a measurement series and between series was scaled such that all the patterns had the same mean intensity. Subsequently the speckle patterns were averaged.

When measuring the contrast of a fully developed speckle pattern it is often less than 1 because of dif-

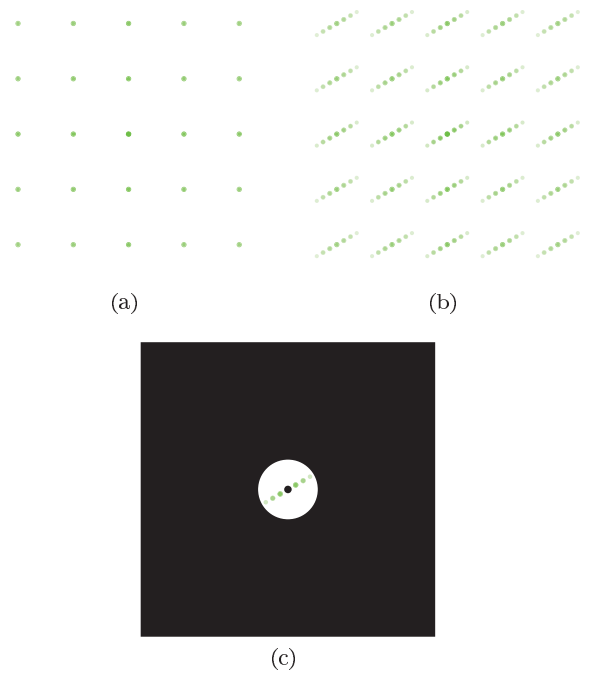


FIG. 5. (a) The pixel structure of the SLM acts as a grating and creates a diffraction pattern when the SLM is turned off. (b) When a sinusoidal grating is displayed on the SLM, each of the diffraction maxima from the pixel structure will have their own associated diffraction orders. (c) The filtered diffraction pattern. Because a smaller grating period gives a larger separation of diffraction spots, the number of spots passing through the filter depended on the grating period.

ferent factors that contribute to reducing the contrast. This means that it is the reduction of contrast imposed by the speckle reduction component under investigation that has to be the important parameter for judging any method's success in reducing the impact of speckle on an image.

The speckle contrast is calculated using the definition  $C = \frac{\sigma_I}{\langle I \rangle}$ , where  $\sigma_I$  is the standard deviation of the speckle pattern and  $\langle I \rangle$  its mean intensity. When  $n$  independent elements contribute to reducing the speckle contrast it is the product of the individual contributions [1],

$$C = c_1 \cdot c_2 \cdots c_m \cdots c_n. \quad (2)$$

Let  $c_m$  be the contribution from the element that implements the speckle reduction method under investigation. The other  $c_i$  are the contributions from other elements in the measuring system.

Define the reference contrast  $C_{\text{ref}}$  as the speckle contrast of the system *without* this speckle reduction element. Then  $C_{\text{ref}} = c_1 \cdot c_2 \cdots c_{m-1} \cdot c_{m+1} \cdots c_n$ , or

$$c_m = \frac{C}{C_{\text{ref}}}, \quad (3)$$

and the reduction of speckle contrast caused by the

method under investigation has been isolated. We will refer to  $c_m$  as the *modulator* speckle contrast. In our experiment, the speckle reduction method under investigation is based on averaging different speckle patterns. Then  $c_m$  is the contribution from this averaging to the total speckle contrast  $C$ .

#### IV. RESULTS AND DISCUSSION

Results from the measurement series are summarized in Table I. For each series, the angular position of the sinusoidal grating was varied between the measurements. When the speckle contrast was found for the average of different numbers of images  $N$ , the images were chosen with the same angle increment from one image to the next. A bigger  $N$  results in a smaller angle increment. The number  $N$  of averaged images and angle increment  $\Delta\alpha$  between diffraction patterns are related through  $N \cdot \Delta\alpha = 180^\circ$ . For instance, for  $N = 3$  the images correspond to gratings at positions  $0^\circ$ ,  $60^\circ$  and  $120^\circ$ . The period of the sinusoidal grating was constant within each series, and was equal to 4, 8, and 12 pixels, respectively. The angle increment used for the measurements were  $10^\circ$  and hence the maximum number  $N_{\max}$  of speckle patterns to average is 18.

TABLE I. Summary of measurement results. Speckle contrast is calculated for the periods 4, 8, and 12 pixels, for averages of 2, 3, 6, 9, and 18 images.  $P$  is the period of the sinusoidal grating, measured in pixels on the SLM. The number in parenthesis after  $c_m$  denotes the number of averaged speckle patterns.

$P$ [px]	4	8	12
$c_m(N = 2)$	0.71	0.72	0.73
$c_m(N = 3)$	0.60	0.60	0.59
$c_m(N = 6)$	0.45	0.46	0.49
$c_m(N = 9)$	0.39	0.43	0.45
$c_m(N = 18)$	0.34	0.39	0.42

In each measurement series an image was recorded for each rotation of the grating. An image of a speckle pattern is shown in Figure 6(a), created by a grating rotated  $30^\circ$  with a sinusoidal period of 12 pixels. The average image of all 18 speckle patterns in this measurement series is shown in Figure 6(b).

The contrasts obtained for the three measurement series are shown in Figure 7. The theoretical contrast  $C = \frac{1}{\sqrt{N}}$  obtained by summing independent speckle patterns is represented by a clean line while the measured data have lines labelled by geometrical objects. Triangle, square, and circle corresponds to periods of 4, 8, and 12 pixels, respectively. As can be seen from the figure the measured contrast's deviation from the theoretical contrast grows with the number of averaged patterns. This is as expected since a smaller angle increment will cause more overlapping of the diffraction patterns.

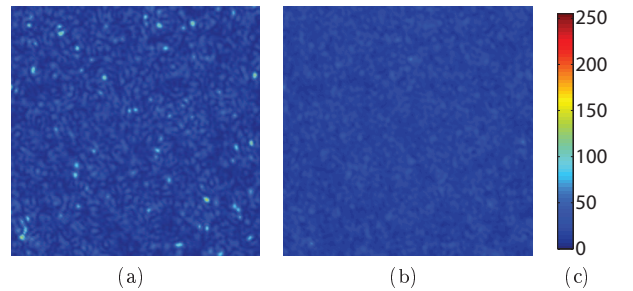


FIG. 6. Speckle patterns produced by sinusoidal gratings on the SLM with a period of 12 pixels. The intensities of the original gray scale images are represented by colors in order to show the relative intensities clearer. (a) Example of a speckle pattern, when the sinusoidal grating is rotated  $30^\circ$ . (b) The speckle pattern that is the average of 18 images. (c) The colorbar showing the mapping from gray value to color.

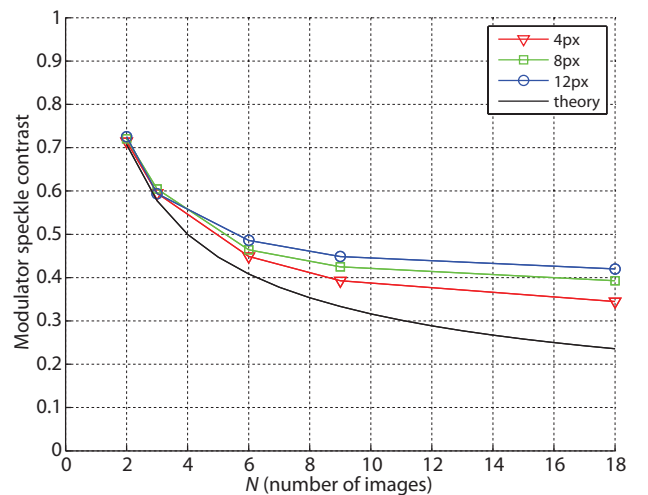


FIG. 7. Speckle contrast as a function of the number of images averaged together. The clean line shows the contrast of the sum of  $N$  independent speckle patterns, while the lines with triangles, squares, and circles are the experimental contrasts for 4, 8, and 12 pixels grating periods, respectively.

It is observed that the deviation becomes smaller with decreasing period of the sinusoidal grating. This is also expected since a smaller grating period will create maxima with greater separation that overlap less when rotated. For the series of measurements with a sinusoidal period of 4 pixels the deviation for  $N = 9$  is about the same as the deviation for  $N = 6$  for the series with 12 pixels period.

The speckle contrast for the average of several measurement series is calculated in Table II. The deviation from averaging *independent* speckle patterns is smallest when averaging together the 4 and 8 pixels periods and is then 14%. The deviation when averaging two measurement series is smaller than the deviation when averaging the 18 speckle patterns in *one* series. This could be

because the summation of two series creates a more uniform intensity distribution without too much overlapping of spots on the diffuser. When averaging all three series together the deviation rises because the chosen grating periods created more overlapping diffraction spots, but the deviation is still smaller than the deviation when averaging only one series.

TABLE II. Averaging of several series of measurements with differing periods, with 18 speckle patterns in each series. The row  $P$  shows the periods of the series which are averaged together.

$P$ [px]	4, 8	4, 12	8, 12	4, 8, 12
$N$	36	36	36	54
$c_m$	0.19	0.20	0.22	0.18

Some drawbacks are related to the SLM utilised for the proof-of-concept. The smaller the period of the grating, the more discretized steps its sinusoidal shape will have. Moreover, when the corrected sinusoidal matrices were displayed on the SLM, the range of gray values used were 0–198. An unfortunate property of the particular SLM is that when used in *phase* mode, the amplitude will be modulated as well, as shown in Figure 2(b). For the range of gray values employed the transmission decreased by an order of magnitude when the gray value went from 0 to 198, with the greatest decrease at large gray values. Equation (1) assumes an intensity that is independent of the imposed phase retardation.

Since the three grating periods yielded different separations between the spots, the number of spots which passed through the filter in Figure 5(c) varied with the grating period. Additionally, because the SLM produced a multitude of dotted diffraction lines, as shown in Figure 5(b), parts of the dotted lines closest to the aperture in Figure 5(c) would pass through the aperture and mix

with the one diffraction pattern that we wanted to observe. The smaller period used on the sinusoidal grating the more mixing. Diffraction spots from different grating angles could then be overlapped on the diffuser and produce correlated patterns. However, the overlapping spots were incident from different angles which should reduce the correlation. Also, the larger the period of the sinusoidal grating, the fewer of these periods are covered by the incoming laser spot on the SLM, and the less valid equation (1) becomes.

## V. CONCLUSION

The proposed speckle reduction method uses a sinusoidal rotating phase grating to create a rotating diffraction pattern with a zeroth order that is cancelled out due to destructive interference and optionally a *variable* grating period for further reduction of speckle contrast.

A setup was built for proof-of-concept and the measurements demonstrate the potential for using the principle of a sinusoidal rotating grating for reducing speckle contrast. It was found that averaging several measurement series with different grating periods gave a smaller deviation from theory than the average of only one measurement series.

Important next steps are to use SLMs with less discretization and a larger fill factor, that are able to produce sinusoidal gratings with optimized varying periodicities.

## VI. ACKNOWLEDGEMENTS

This work is part of a project funded by the Research Council of Norway (grant no. 182667/I40) and poLight AS.

- 
- [1] J. W. Goodman, *Speckle Phenomena in Optics: Theory and Applications* (Roberts and Company Publishers, 2006).
  - [2] J. W. Goodman, *Journal of the Optical Society of America*, **66**, 1145 (1976).
  - [3] L. Wang, T. Tschudi, T. Halldórsson, and P. R. Pétursson, *Applied Optics*, **37**, 1770 (1998).
  - [4] L. Wang *et al.*, *Method and device for eliminating image speckles in scanning laser image projection*, United States Patent (2002).
  - [5] M. Lai and M. J. Yuan, *Speckle free laser probe beam*, United States Patent (2005).
  - [6] M. Kamm and O. Ripoll, *Image generation unit and method to use an image generation unit*, United States Patent (2008).
  - [7] H. Lin, *Speckle mechanism in holographic optical coherence imaging* (2009).
  - [8] J. W. Goodman, *Introduction to Fourier Optics* (McGraw-Hill, 1996).
  - [9] U. Efron, *Spatial Light Modulator Technology: Materials, Devices, and Applications* (Marcel Dekker, 1995).
  - [10] V. Kartashov, L. Henriksen, J. H. Ulvensøen, B. Svardal, T. Svortdal, R. Berglind, and G. Hedin, *Journal of the SID*, **17**, 581 (2009).
  - [11] Holoeye, “Data sheet for LC 2002 SLM,” (2010), [www.holoeye.com/spatial\\_light\\_modulator\\_lc\\_2002.html](http://www.holoeye.com/spatial_light_modulator_lc_2002.html).
  - [12] E. Hecht, *Optics* (Addison Wesley, 2002).



## B. Poster

# Speckle Reduction Using a Sinusoidal Rotating Grating

Sigbjørn Vindenes Egge<sup>1</sup>, Muhammed Nadeem Akram<sup>2</sup>, Vladimir Kartashov<sup>3</sup>,  
Kristine Welde<sup>1</sup>, Zhaomin Tong<sup>2</sup>, Ulf Österberg<sup>1</sup>, Astrid Aksnes<sup>1</sup>

<sup>1</sup> Norwegian University of Science and Technology (NTNU), Department of Electronics and Telecommunications  
<sup>2</sup> Vestfold University College (HIVE), Institute of Microsystems Technology  
<sup>3</sup> poLight AS, Postboks 163, 3192 Horten

## Introduction

The coherent nature of laser light introduces the problem of *speckle* in laser display projectors. Speckle are random spatial intensity fluctuations which arise when coherent light is reflected off a rough surface. A novel idea for speckle reduction in laser display projectors uses the rotation of a diffraction pattern. To test the principle a test configuration was implemented. The setup consisted of sinusoidal phase gratings patterned on a transmissive spatial light modulator (SLM), with each phase grating rotated with respect to the previous one.

## Laser speckle

Improved color gamut, higher contrast, deeper focus, and higher brightness are some of the advantages of using laser light contra incandescent lamps in display projectors [1]. However, coherent light causes interference when reflected off a rough screen and creates a random pattern of varying intensity over the image. This noise pattern is called *speckle* and has to be reduced to an acceptable level without impairing the benefits of a laser light source or its power too much.

Speckle reduction methods are based on reducing the coherence of light. A *partially* coherent beam produces a time-varying interference pattern that is averaged during the integration time of the eye. The speckle contrast is defined as  $C = 1/\sqrt{N}$  for the sum of  $N$  independent speckle patterns. To get a good viewing experience  $C < 0.1$ .

## Sinusoidal rotating grating

A novel idea for a speckle reduction modulator is based on diffraction and rotation. A beam of coherent light is passed through a sinusoidal phase grating which diffracts the light into a line of spots on a diffuser. When rotated, these spots will cover different areas of the diffuser and produce independent speckle patterns if the zeroth order is removed. A phase grating with a retardation difference of 4.8 radians will extinct the zeroth order without losing power [2]. In a laser projector the diffuser would be followed by a light homogenizer with an image SLM at the end.

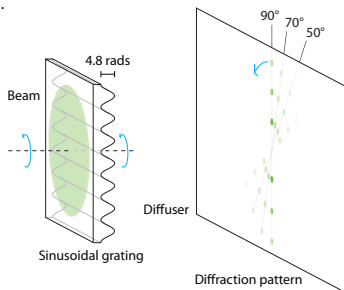


Figure 1: Diffraction on a sinusoidal phase grating with a peak-to-peak phase difference of 4.8 radians produces a pattern with a vanishing zeroth order. Rotation of the diffraction pattern creates independent speckle patterns.

The proposed modulator is intended to be implemented by a 2D SLM with a deformable polymer layer (SLMDPL) [3]. For proof-of-concept the sinusoidal phase grating was implemented in discretized steps on a Holoeye LC 2002 SLM (800x600 px). Its phase retardation as a function of gray scale was linearized by a lookup-table.

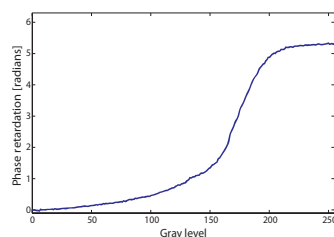


Figure 2: Phase retardation imposed by the SLM as a function of gray level, for the wavelength 532 nm.

## Laboratory setup

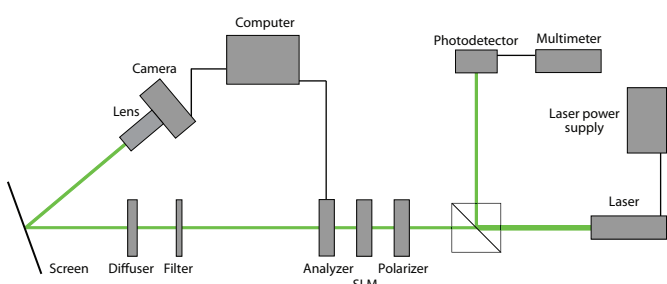


Figure 3: A sketch of the laboratory setup.

## Laboratory setup continued

To obtain the desired range of phase modulation the SLM was sandwiched between two polarizers. In order to decorrelate and homogenize the beam it was passed through a diffuser. The light was reflected off a Stewart Filmscreen and imaged onto a CCD. The laser power was continuously monitored by a photodetector.

## Results

The sinusoidal grating period was varied to characterize speckle contrast as a function of period. In each measurement series an image of the speckle pattern was recorded for each rotation, and average images were calculated for various angle increments.

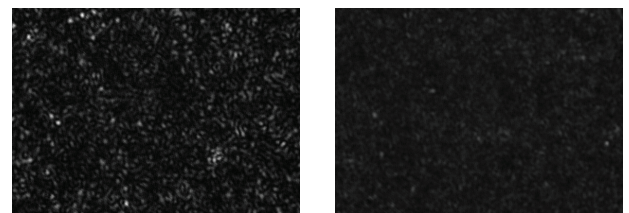


Figure 4: Speckle patterns produced by a sinusoidal grating with a period of 4 pixels. Left: Example of an individual speckle pattern, rotated 30 degrees. Right: The speckle contrast is reduced by averaging 18 individual patterns.

The grating period ranged from 4 to 8 pixels. Results were compared with the speckle contrast of the sum of  $N$  independent speckle patterns. The results are promising with deviation from minimum speckle contrast of 16 % when averaging 6 patterns with period of 4 pixels.

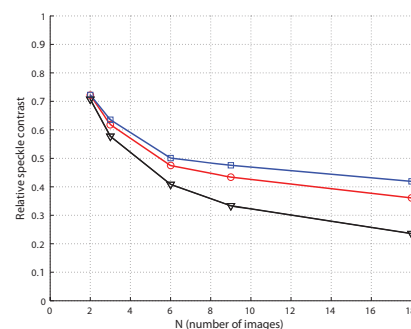


Figure 5: Speckle contrast as a function of the number of images averaged together. The black line shows the contrast of the sum of  $N$  independent speckle patterns, while the red and blue lines are the experimental contrasts for 4 and 8 pixels grating periods, respectively.

## Conclusion

The measurements indicate that the sinusoidal rotating grating principle for speckle contrast reduction is promising. Better results are expected when a true sinusoidal grating is implemented.

## References

1. J. W. Goodman. *Speckle Phenomena in Optics: Theory and Applications*. Roberts and Company Publishers, 2006.
2. J. W. Goodman. *Introduction to Fourier Optics*. McGraw-Hill, 1996.
3. V. Kartashov *et al.* Image improvement in a laser projection display with a SLM with a deformable polymer. *Journal of the SID* 17(7):581-587, 2009.

## Acknowledgements

This project was funded by the Research Council of Norway and poLight AS (project number 182667/I40).

## C. MATLAB code

### C.1 Load images

```
Ibg=imread('bg.bmp');
    %Load the background image

N=0;
M=36;

for N = (1:M)
    num = (N-1)*10;
    st = int2str(num);
    str = strcat(st, '.bmp');
    I(N).Ia = imread(str);
        %Load the speckle patterns
    Isub(N).Ia = I(N).Ia-Ibg;
        %Subtract the background image
    Icrop(N).Ia = Isub(N).Ia(41:440,41:600);
        %Remove the edges
    Iscale(N).Ia = (double(Icrop(N).Ia)/mean2(double(Icrop(N).Ia)))
        *mean2(double(Icrop(1).Ia));
        %Scale the images

    max(max(Icrop(N).Ia))
        %Maximum intensities
    min(min(Icrop(N).Ia))
        %Minimum intensities
    mean2(Iscale(N).Ia)
        %Mean intensities
end
```

## C.2 Analyse images

```

K=0;
for K = (1:36)
    Ci(K).std = std2(Icrop(K).Ia)/mean2(Icrop(K).Ia);
    %Speckle contrast of individual speckle patterns
end

L = [36 18 12 9 6 4 3 2];
a = [0 0 0 0 0 0 0 0];

N=0;
M=0;
for N = (1:8)
    Imean = zeros(400,560);

    for M = (1:(L(1)/L(N)):L(1))
        Imean = Imean+Iscale(M).Ia;
        %Sum of L speckle patterns
        a(N)=a(N)+Ci(M).std;
        %Sum of speckle contrasts of individual speckle
        patterns
    end

    mean(N).Im = Imean/(L(N));
    %Mean intensity of L speckle patterns

    Cref(N)=a(N)/L(N);
    %Average contrast of individual speckle patterns
    Cave(N)=std2(mean(N).Im)/mean2(mean(N).Im);
    %Contrast of averaged speckle pattern
    Cm(N)=Cave(N)/Cref(N);
    %Modulator speckle contrast
    Ctheory(N)=1/((L(N))^(0.5));
    %Theoretical contrast
    D(N)=100*(((Cm(N))-(Ctheory(N)))/(Ctheory(N)));
    %Deviation from theoretical contrast
end

```



### C.3 Create graphs

```
figure(1)
grid on
hold on
plot(L,Cm,'r.-')
plot(L,Ctheory,'k.-')
xlabel('N (number of images)')
ylabel('Modulator speckle contrast')
axis([0 36 0 1])

figure(2)
grid on
hold on
plot(L,D,'r.-')
xlabel('N (number of images)')
ylabel('Deviation from theory (%)')
axis([0 36 -2 16])
```

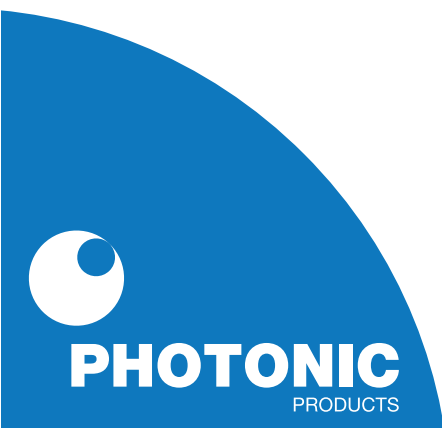


## D. Datasheets

### D.1 Datasheet for the laser

# sheet

# data



## DPSS green laser diode module 532nm

### Key features

- Visible light  $\lambda = 532\text{nm}$
- Output power 0.9mW and 4mW
- Circular beam 1.2mm typ.
- Adjustable lens
- Modulation 0-1kHz
- Compact and self-contained
- High reliability

### Applications

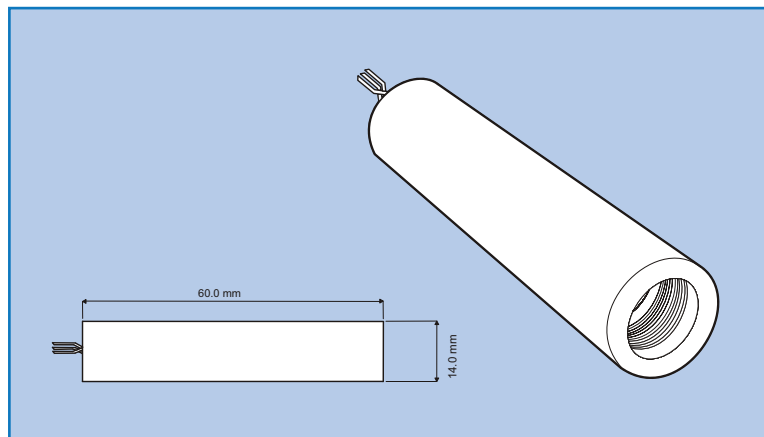
- Industrial alignment
- Medical alignment
- Scientific equipment

### 532nm DPSS Green Laser Diode Module

The 300-0088 series DPSS green laser diode module offers a circular output beam of 1.2mm diameter with beam divergence of  $<2.0\text{mrad}$ , output power of 0.9mW or 4mW, an operating voltage of 4-6V at an operating current of 350mA maximum, and operating temperature from  $+10^{\circ}\text{C}$  to  $+30^{\circ}\text{C}$ . Power stability is better than 5% over 7 hours.

The DPSS (Diode Pumped Solid State) laser diode module has been designed as a complete laser diode solution for OEM use.

It consists of an anodised aluminium housing, laser diode, drive circuit and user-adjustable collimating lens. Electrical connections are made via external flying leads.



## laser diode solutions

## DPSS green laser diode module 532nm

### Specifications (Tc=25°C)

ITEM / PART no.	300-0088-00	300-0088-01
Wavelength	532nm	532nm
Output Power (±10%)	0.9mW	4.0mW
Beam Size (typ 1/e <sup>2</sup> )	1.2 mm	1.2 mm
Beam Circularity	≤ 1.3:1	≤ 1.3:1
Beam Divergence	≤ 2.0 mrad	≤ 2.0 mrad
Warm up Time	4-5 minutes	4-5 minutes
Power Stability (over 7 hours after warm up at constant temperature)	< 5%	< 5%
Power Stability (over operating temperature range)	≤ 20%	≤ 20%
Mode	TEM <sub>00</sub>	TEM <sub>00</sub>
Operating Voltage	4-6V DC	4-6V DC
Operating Current (25°C)	< 300mA	< 350mA
Operating Temperature (ambient)	+10°C to +30°C	+10°C to +30°C
Storage Temperature	-40°C to +60°C	-40°C to +60°C
Housing Material	Anodised Aluminium	Anodised Aluminium
Weight	40g	40g
Lifetime MTTF (typ)	5000 hours	5000 hours
Modulation	0 to 1kHz, 5V=ON, 0V=OFF 0 to 1kHz, 5V=ON, 0V=OFF	
Mechanical	14mm ± 0.1mm diameter, 60mm length (66mm including rear cable strain relief)	

#### Heat Sinking

If the case temperature of the laser diode exceeds its maximum specification, premature or catastrophic failure may occur. To ensure the maximum life of the laser diode, it is recommended that an additional electrically insulated heatsink of at least 50 sq cm be used. Thermal transfer cream can be used to improve contact and heat dissipation. Do not restrict air circulation around the device.

#### Power Connections

These DPSS laser diode modules require a regulated input voltage of 4-6V. Connections are made via the 3 pre-tinned external flying leads, (red is positive, black is negative, yellow is modulation).

**WARNING:** The housing is internally connected to the positive supply rail. Damage to the external anodised surfaces will result in the housing being at positive potential.

Specifications subject to change without notice. E&OE

### Laser Safety

The light emitted from these devices has been set in accordance with IEC60825. However, staring into the beam, whether directly or indirectly, must be avoided. IEC60825 classifies laser products into three different categories depending on light emitted, wavelength and eye safety.

#### CLASS II

"Caution", visible laser light less than 1.0mW. Considered eye safe, normal exposure to this type of beam will not cause permanent damage to the retina.

#### CLASS III R

"Danger", visible laser light between 1.0mW and 5.0mW. Considered eye safe with caution. Focusing of this light into the eye could cause some damage.

#### CLASS III B

"Danger", infrared (IR), and high power visible lasers considered dangerous to the retina if exposed.

NB: It is important to note that while complying with the above classifications, unless otherwise stated, our laser diode products are not certified and are designed solely for use in OEM products. The way in which the device is used in the final product may alter its original design classification, and it is the responsibility of the OEM to ensure compliance with the relevant standards.



#### PHOTONIC PRODUCTS UK LIMITED

Pierce Williams, Sparrow Lane  
 Hatfield Broad Oak, Hertfordshire CM22 7BA, UK  
 Telephone: +44 (0) 1279 717170  
 Facsimile: +44 (0) 1279 717171  
 E-mail: [sales@photonic-products.com](mailto:sales@photonic-products.com)  
[www.photonic-products.com](http://www.photonic-products.com)

#### PHOTONIC PRODUCTS USA

Telephone: +1 714-841-1960  
 E-mail: [salesusa@photonic-products.com](mailto:salesusa@photonic-products.com)

#### PHOTONIC PRODUCTS GERMANY

Telefon: +49 (0) 8142 / 669 8364  
 E-mail: [salesgermany@photonic-products.com](mailto:salesgermany@photonic-products.com)  
[www.photonic-products.com](http://www.photonic-products.com)



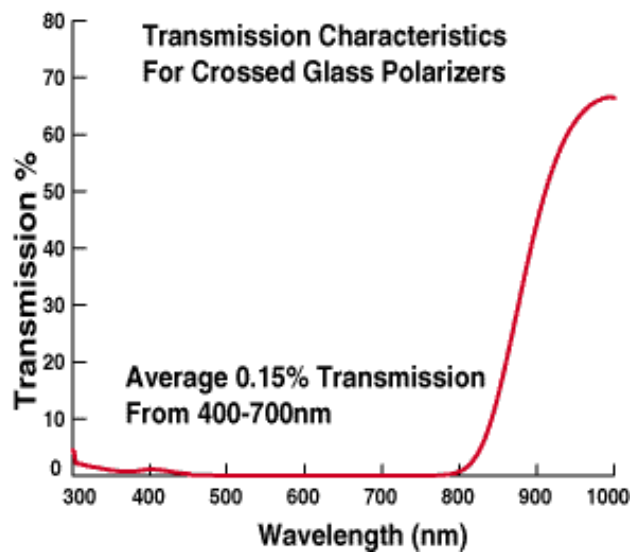
**PHOTONIC**  
 PRODUCTS

## D.2 Datasheet for the polarizers

### Specifications

Diameter Tolerance	Threaded diameter $\pm 0.1\text{mm}$
Clear Aperture	Outer Dia - 5mm (typical)
Operating Temperature	$-15^{\circ}\text{C}$ to $70^{\circ}\text{C}$ ( $5^{\circ}\text{F}$ to $158^{\circ}\text{F}$ )
Polarization Efficiency	95%
Transmission, single	30% typical over 400-700nm
Transmission, crossed	0.15% average over 400-700nm

### Technical Image



## D.3 Datasheet for the beamsplitter

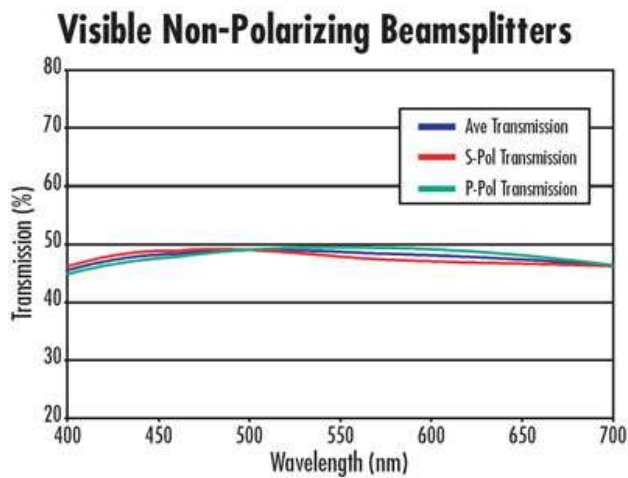
### Overall Specifications

Substrate	N-BK7
Dimensional Tolerance	$\pm 0.1\text{mm}$
Beam Deviation	$\pm 2$ arcmin
Surface Accuracy	$1/8 \lambda$
Surface Quality	40-20
Clear Aperture	$> 90\%$
Bevel	$0.3\text{mm} \times 45^\circ$

### Beamsplitter Coating Specifications

Design Wavelength	430-670nm VIS
Coating Type	Hybrid
AR Coating	$< 0.5\%$ 430-670nm
Transmittance	$45\% \pm 5\%$
Absorption	$< 10\%$
Polarization	$< 6\%$

### Technical Image



## **D.4 Datasheet for the photodetector**



## DET100A Operating Manual – Large Area Silicon Detector

### Description:

The Thorlabs DET100A is a ready-to-use large area photo detector. The unit comes complete with a photodiode and internal 12V bias battery enclosed in a rugged aluminum housing. The DET100A includes a removable 1" optical coupler (SM1T1), providing easy mounting of ND filters, spectral filters, fiber adapters (SMA, FC and ST style), and other Thorlabs 1" stackable lens mount accessories.

The DET100A includes two #8-32 tapped mounting holes with a 0.25" mounting depth, while the DET100A/M has two M4 tapped mounting holes. A 12V A23 battery is included.

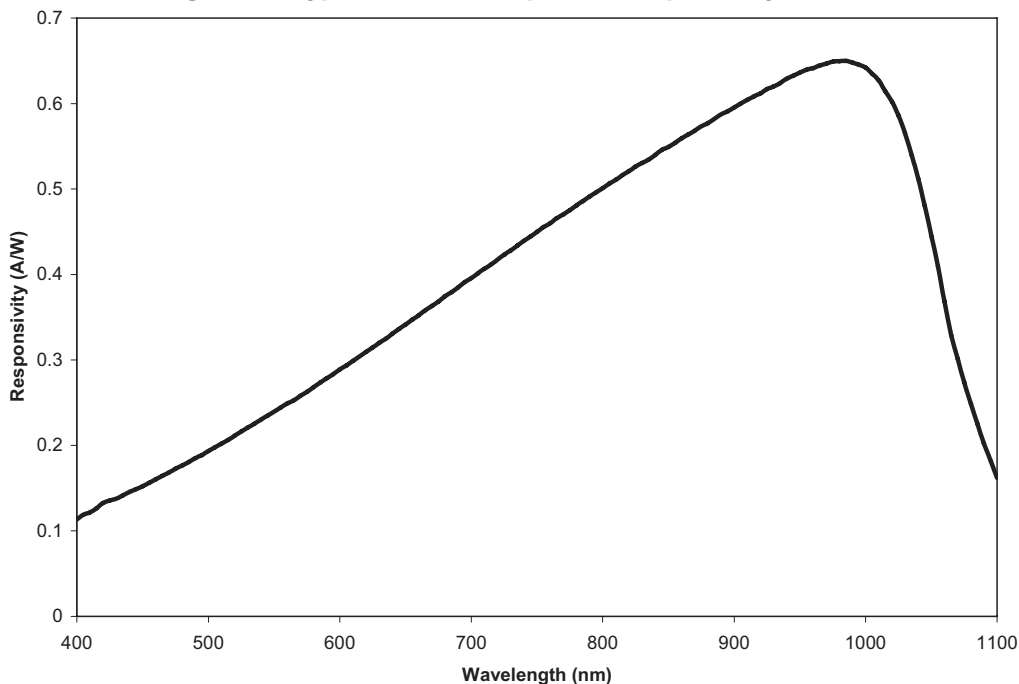
### Specifications:

Electrical		
Detector:		Silicon PIN
Active Area <sup>4</sup> :		75.4mm <sup>2</sup> (Ø9.8mm)
Wavelength Range:	$\lambda$	400 to 1100 nm
Peak Wavelength:	$\lambda_p$	970 nm (typ)
Peak Response (typ):	$\mathcal{R}(\lambda_p)$	0.65 A/W (typ)
Shunt Resistance:	$R_{sh}$	>10M $\Omega$
Diode Capacitance:	$C_J$	300pF
Rise/Fall Time:	$t_r$	43ns (max.)
Linearity Limit (Current):		1mA
(Power):		1.5mW (min @ $\lambda_p$ )
NEP (750nm):		$3.9 \times 10^{-14}$ W/ $\sqrt{\text{Hz}}$ (max.)
Bias Voltage:	$V_R$	10 V (9V min)
Dark Current <sup>2</sup> :	$I_D$	100nA (600nA max.)
Output Voltage:	$V_{OUT}$	0 to 10V
Damage Threshold:		100mW/cm <sup>2</sup>

General	
On / Off Switch:	Slide
Battery Check Switch:	Momentary Pushbutton
Output:	BNC (DC Coupled)
Package Size:	2.8"x1.9" x 0.83" 70mm x 48mm x 21mm
PD Surface Depth:	0.20" (5.1mm)
Weight:	0.2 lbs
Accessories:	SM1T1 Coupler SM1RR Retainer Ring
Storage Temp:	-20 to 70°C
Operating Temp:	10 to 50°C
Battery:	A23, 12V <sub>DC</sub> , 40mAh
Low Battery Voltage <sup>3</sup>	(See 'Battery Check')
$V_{OUT}$ (Hi-Z):	~9V
$V_{OUT}$ (50 $\Omega$ ):	~400mV

1. All measurements performed with a 50 $\Omega$  load unless stated otherwise.
2. Measured with specified Bias Voltage.
3. Assumes the battery voltage drops below 9.6V. The reverse protection diode generates a 0.6V drop.
4. Specified to Aperture size; detector size is 10 x 10mm square.

Figure 1 – Typical DET100A Spectral Responsivity Curve



## Operation

Thorlabs DET series are ideal for measuring both pulsed and CW light sources. The DET100A includes a reversed-biased PIN photo diode, bias battery, and ON/OFF switch packaged in a rugged housing. The BNC output signal is the direct photocurrent out of the photo diode anode and is a function of the incident light power ( $P$ ) and wavelength ( $\lambda$ ). The Spectral Responsivity,  $\mathfrak{R}(\lambda)$ , can be obtained from Figure 1 to estimate the amount of photocurrent to expect. Most users will wish to convert this photocurrent to a voltage ( $V_{OUT}$ ) for viewing on an oscilloscope or DVM. This is accomplished by adding an external load resistance,  $R_{LOAD}$ . The output voltage is derived as:

$$V_{OUT} = P * \mathfrak{R}(\lambda) * R_{LOAD}$$

It should be noted that the load resistor will react with the photodetector junction capacitance ( $C_J$ ) to limit the bandwidth. For best frequency response, a  $50\Omega$  terminator should be used. The bandwidth ( $f_{BW}$ ) and the rise-time response ( $t_R$ ) can be approximated using the diode capacitance ( $C_J$ ) and the load resistance ( $R_{LOAD}$ ) as shown below:

$$f_{BW} = 1 / (2 * \pi * R_{LOAD} * C_J)$$
$$t_R = 0.35 / f_{BW}$$

For maximum bandwidth, we recommend using a  $50\Omega$  coax cable with a  $50\Omega$  terminating resistor at the opposite end of the coax. This will also minimize ringing by matching the coax with its characteristic impedance. If bandwidth is not important, you may increase the amount of voltage for a given input light by increasing the  $R_{LOAD}$ .

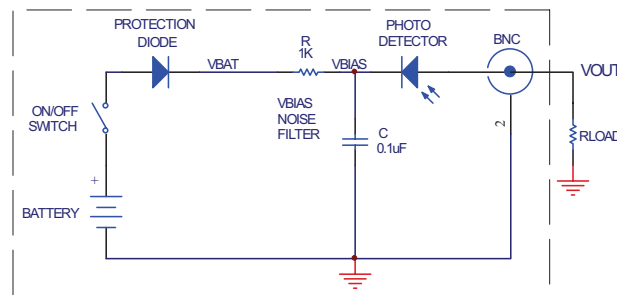


Figure 2 – Circuit Schematic

## Setup

- Unpack the optical head, install a Thorlabs TR-series  $\frac{1}{2}$ " diameter post into one of the #8-32 (M4 on /M version) tapped holes, located on the bottom and side of the sensor, and mount into a PH-series post holder.
- Attach a  $50\Omega$  coax cable (i.e. RG-58U) to the output of the DET. Select and install a terminating resistor to the remaining end of the cable and connect to a voltage measurement device. See the 'Operation' Section to determine resistor values. Thorlabs sells a  $50\Omega$  terminator (T4119) for best frequency performance and a variable terminator (VT1) for output voltage flexibility. Note the input impedance of your measurement device since this will act as a terminating resistor. A load resistor is not necessary when using current measurement devices.
- Power the DET on using the power switch. To check battery voltage, see 'Battery Check' below.
- Install any desired filters, optics, adapters, or fiber adapters to the input aperture. **Caution:** The DET100A was designed to allow maximum accessibility to the photodetector by having the front surface of the diode flush with the outside of the DET housing. When using fiber adapters, make sure that the fiber ferrule does not crash into the detector. Failure to do so may cause damage to the diode and / or the fiber. An easy way to accomplish this is to install a SM1RR retaining ring (included with the DET100A) inside the 1" threaded coupler *before* installing the fiber adapter
- Apply a light source to the detector.

## Battery Check and Replacement

### Battery Check

Thorlabs new DET series includes a battery check feature that will allow the user to monitor the bias voltage on the output BNC. Simply hold down the "VBIAS OUT" bottom located on the bottom edge of the unit. The bias voltage will be output to the BNC. If a high impedance load is used ( $>10k\Omega$ ), the output will be equal to the bias voltage. This feature includes a  $1.05k\Omega$  current limiting resistor ( $R_{CL}$ ) to prevent excessive loading of the battery if using small terminating resistors. For example, a  $50\Omega$  load resistor with a 10V bias will produce a 200mA current without this resistor. This will significantly decrease lifetime of the battery. The output bias voltage will be dependent on the load resistor as described below. The A23 battery voltage characteristics show that the charge level is almost depleted as

the voltage drops below 10V. For this calculation we assume 9.6V since  $V_{BAT} = \text{low battery voltage} - \text{one diode drop} (0.6V) = \sim 9V$ . The detector will continue to operate until the battery charge is completely drained, however these numbers provide a reference point at which the battery should be replaced.

$$V_{OUT} = V_{BAT} [R_{LOAD} / (R_{LOAD} + R_{CL})]$$

For  $V_{BAT} (\text{min}) = 9V$ ,  $R_{LOAD} = 50\Omega$ , and  $R_{CL} = 1050\Omega$   
 $V_{OUT} = 410mV$

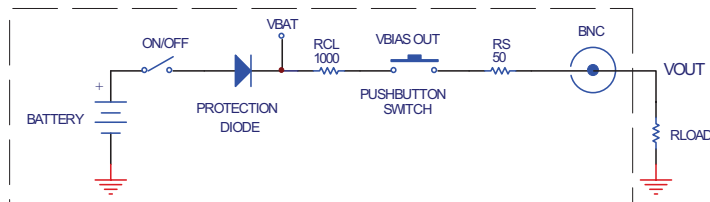


Figure 3 – Battery Check Schematic

### Battery Replacement

Thorlabs delivers each DET with an A23 12V battery installed. This battery is readily available at most retail stores, as well as through Thorlabs. The battery supplied will deliver about 40 hours with a 1mA load, roughly equivalent to a continuous 1.5mW light source at peak wavelength. The supply current when the unit is on and no light is applied is very small and should not significantly degrade the battery.

Locate the battery cap directly above the output BNC. Unthread the cap and remove the battery. Install the new battery into the cap, negative side in, and thread back into the DET. Be careful not to cross thread the cap into the housing. The DET includes a protection diode to prevent damage if the battery is installed backwards. The battery direction is located on the housing.

## Troubleshooting

### There is no signal response.

- Verify that the power is switched on and all connections are secure.
- Verify the proper terminating resistor is installed if using a Voltage measurement device.
- Verify that the optical signal wavelength is within the specified wavelength range.
- Verify that the optical signal is hitting the detector active area.
- Connect the DET to an oscilloscope without a terminating resistor installed. Most general purpose oscilloscopes will have a 10MΩ input impedance. Point the detector toward a fluorescent light and verify that a 60Hz (50Hz outside the US) signal appears on the scope. If so the device should be operating properly and the problem may be with the light source or alignment.

### There is an AC signal present when the unit is turned off.

The detector has an AC path to ground even with the switch in the OFF position. It is normal to see an output response to an AC signal with the switch in this state. However, because the detector is unbiased, operation in this mode is not recommended.

### The output appears AC coupled with long rise times and the power switch ON.

This is usually an indication that the battery level is low and needs to be changed. See the Battery Check and Replacement Section.

## Maintaining the DET100A

There are no serviceable parts in the DET100A optical sensor. The housing may be cleaned by wiping with a soft damp cloth. The window of the detector should only be cleaned using isopropyl alcohol and optical grade wipes. If you suspect a problem with your DET100A please call Thorlabs and an engineer will be happy to assist you.

## Contact

**Americas**  
 Thorlabs Inc.  
 435 Route 206 North  
 Newton NJ 07860  
 USA  
 Ph: (973) 579-7227  
 Fax: (973) 300-3600  
[www.thorlabs.com](http://www.thorlabs.com)  
 Email:  
[techsupport@thorlabs.com](mailto:techsupport@thorlabs.com)

**Europe**  
 Thorlabs GmbH  
 Gaußstr. 11  
 85757 Karlsfeld  
 Germany  
 Ph: +49 (0) 8131-59-56-0  
 Fax: +49 (0) 8131-59-56-99  
[www.thorlabs.com](http://www.thorlabs.com)  
 Email:  
[Europe@thorlabs.com](mailto:Europe@thorlabs.com)

**UK and Ireland**  
 Thorlabs, LTD.  
 1 Saint Thomas Place, Ely  
 Cambridgeshire CB7 4EX  
 Great Britain  
 Ph: +44 (0) 1353-654440  
 Fax: +44 (0) 1353-654444  
[www.thorlabs.com](http://www.thorlabs.com)  
 Email:  
[sales.uk@thorlabs.com](mailto:sales.uk@thorlabs.com)

**Scandinavia**  
 Thorlabs Sweden AB  
 Box 141 94  
 400 20 Göteborg  
 Sweden  
 Ph: +46-31-733-30-00  
 Fax: +46-31-703-40-45  
[www.thorlabs.com](http://www.thorlabs.com)  
 Email:  
[Scandinavia@thorlabs.com](mailto:Scandinavia@thorlabs.com)

**Japan**  
 Thorlabs Japan, Inc  
 5-17-1, Ohtsuka  
 Bunkyo-ku, Tokyo 112-0012  
 Japan  
 Ph: +81-3-5977-8401  
 Fax: +81-3-5977-8402  
[www.thorlabs.jp](http://www.thorlabs.jp)  
 Email:  
[sales@thorlabs.jp](mailto:sales@thorlabs.jp)

## WEEE

As required by the WEEE (Waste Electrical and Electronic Equipment Directive) of the European Community and the corresponding national laws, Thorlabs offers all end users in the EC the possibility to return “end of life” units without incurring disposal charges.

This offer is valid for Thorlabs electrical and electronic equipment

- sold after August 13<sup>th</sup> 2005
- marked correspondingly with the crossed out “wheelie bin” logo (see fig. 1)
- sold to a company or institute within the EC
- currently owned by a company or institute within the EC
- still complete, not disassembled and not contaminated

As the WEEE directive applies to self contained operational electrical and electronic products, this “end of life” take back service does not refer to other Thorlabs products, such as

- pure OEM products, that means assemblies to be built into a unit by the user (e. g. OEM laser driver cards)
- components
- mechanics and optics
- left over parts of units disassembled by the user (PCB’s, housings etc.).

If you wish to return a Thorlabs unit for waste recovery, please contact Thorlabs or your nearest dealer for further information.

### Waste treatment on your own responsibility

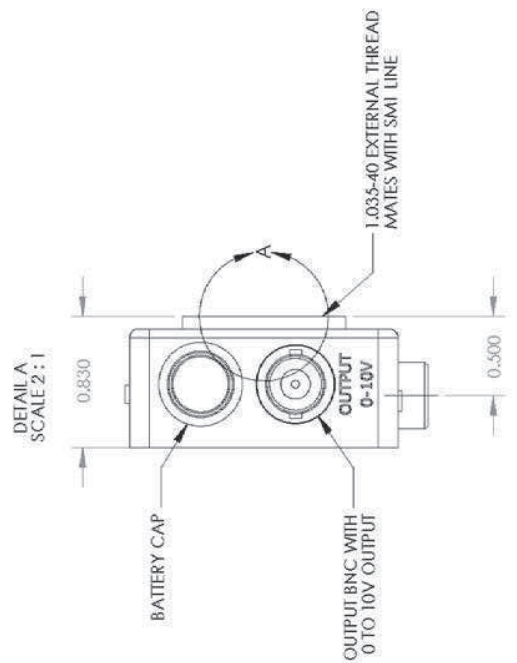
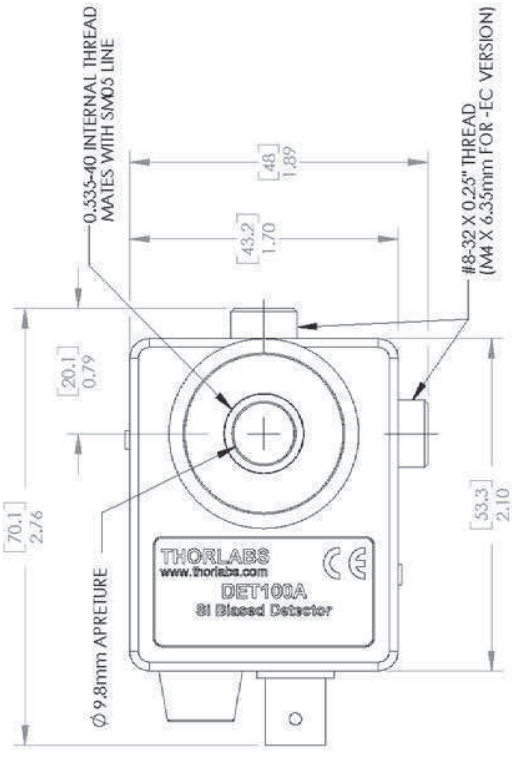
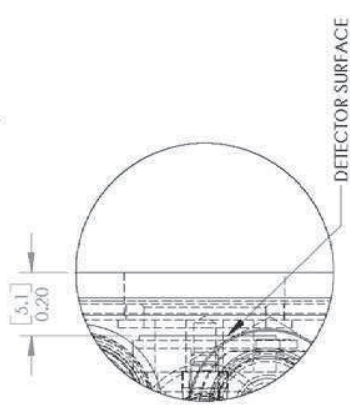
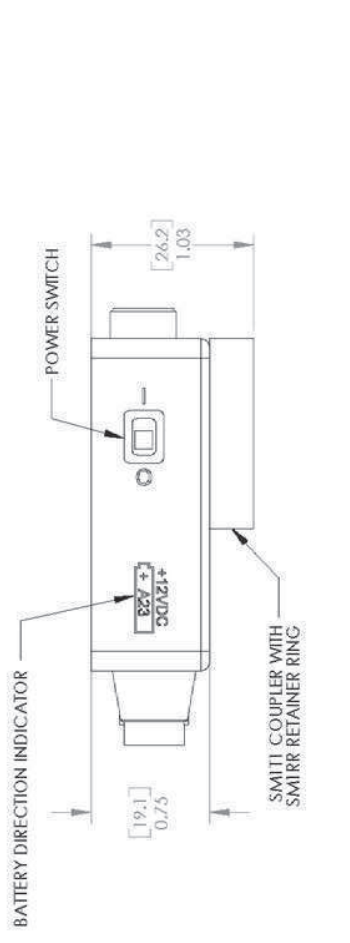
If you do not return an “end of life” unit to Thorlabs, you must hand it to a company specialized in waste recovery. Do not dispose of the unit in a litter bin or at a public waste disposal site.

### Ecological background

It is well known that WEEE pollutes the environment by releasing toxic products during decomposition. The aim of the European RoHS directive is to reduce the content of toxic substances in electronic products in the future. The intent of the WEEE directive is to enforce the recycling of WEEE. A controlled recycling of end of live products will thereby avoid negative impacts on the environment.



Crossed out “wheelie bin” symbol



DETAIL A  
SCALE 2:1

THORLABS INC. PO BOX 366 NEWTON NJ

TITLE:  $\varnothing$  9.8mm Si BIASED DETECTOR

MATERIAL: DET100A

SCALE: 1:1

SHEET 1 OF 1

DWG. NO. 13056-E01

PART NO. DET100A

TOLERANCES	NAME	DATE
UNLESS OTHERWISE SPECIFIED:	DRAWN EC	2/22/06
DIMENSIONS ARE IN INCHES	ENG. APPR. EC	2/22/06
LINEAR TOLERANCES:	MFG APPR. EC	2/22/06
THREE PLACE DECIMAL: ±0.010	<b>PROPRIETARY AND CONFIDENTIAL</b>	
TWO PLACE DECIMAL: ±0.005	THE INFORMATION CONTAINED IN THIS	
ONE PLACE DECIMAL: ±0.002	DRAWING IS THE SOLE PROPERTY OF	
PARALLELISM: 0.002	THORLABS, INC. ANY REPRODUCTION	
PERPENDICULARITY: 0.002	IN PART OR AS A WHOLE WITHOUT	
CONCENTRICITY: 0.002	THE WRITTEN PERMISSION OF	
SYMMETRY: 0.002	THORLABS, INC. IS PROHIBITED.	
THREAD CLASS 2 FIT		

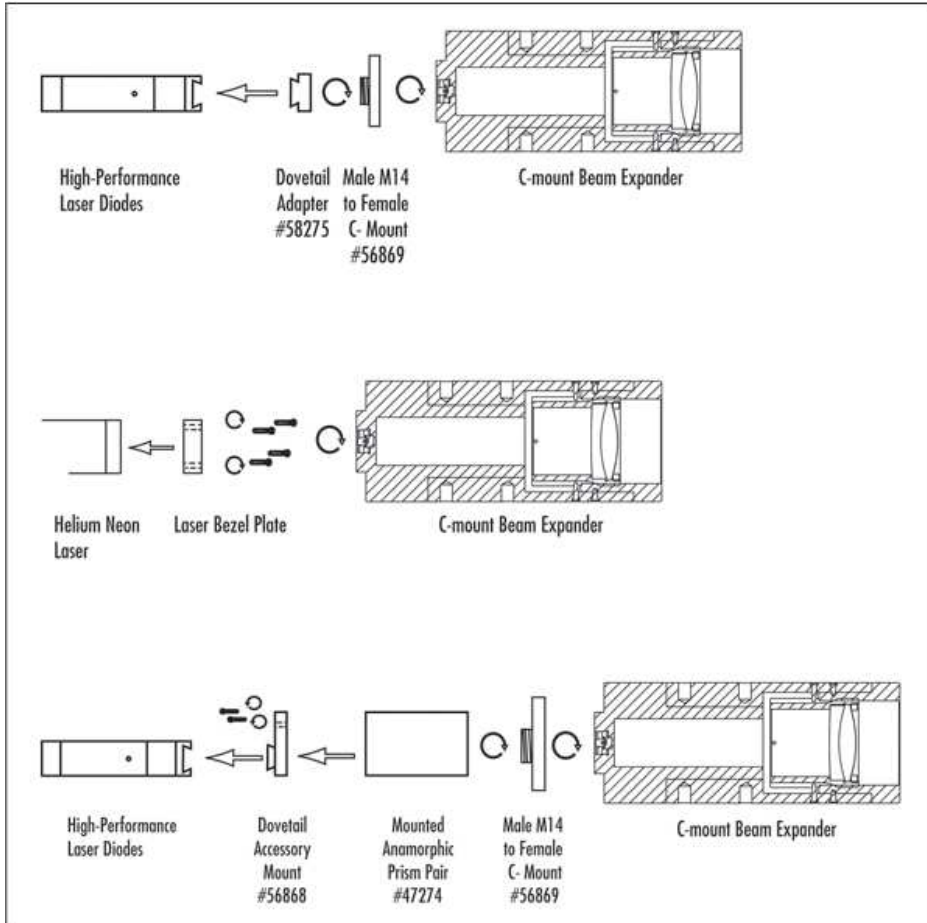
1 2 3 4 5

## D.5 Datasheet for the beam expander

### Specifications

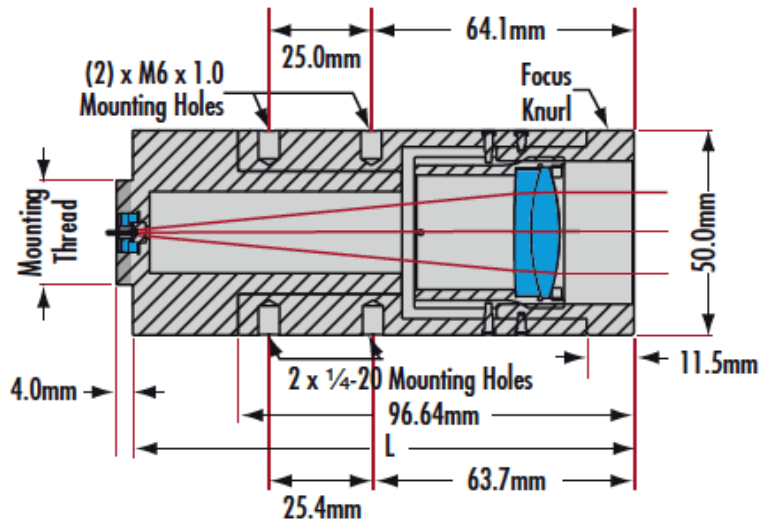
Beam Expansion Power	3X, 5X, 10X, 15X, or 20X
Entrance Aperture	2.0mm maximum [Optimized for 1.0mm (1/e <sup>2</sup> )]
Exit Aperture	Entrance Beam × Magnification (27mm Max)
Focus Range	1.2m to ∞
Optics Coating	1/4 λ MgF <sub>2</sub> @ 632.8nm
Design Wavefront Error	1/4 λ @ 632.8nm
System Length (L) of Complete Assembly	
3X	114.95mm
5X	107.5mm
10X	118.0mm
15X	120.5mm
20X	122.5mm
Diameter	50.0mm
Mount	C-Thread (1"-32 TPI)
Housing	Black Anodized Aluminum

## Beam Expander Mounting Configurations

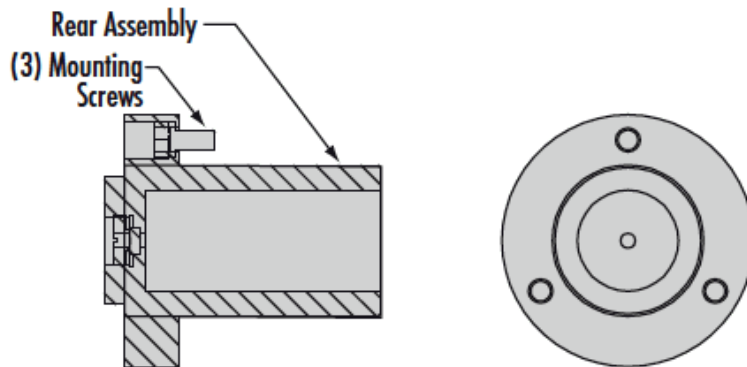


Technical Image

### Complete Beam Expander



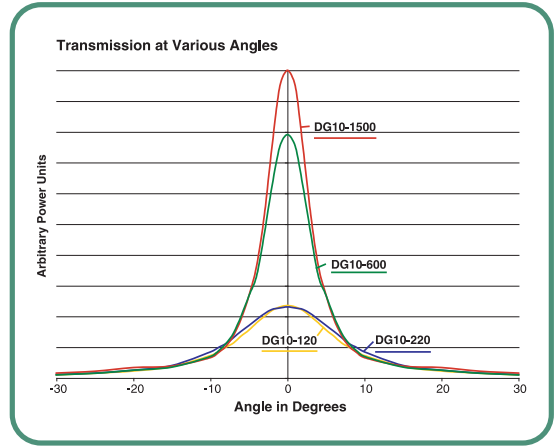
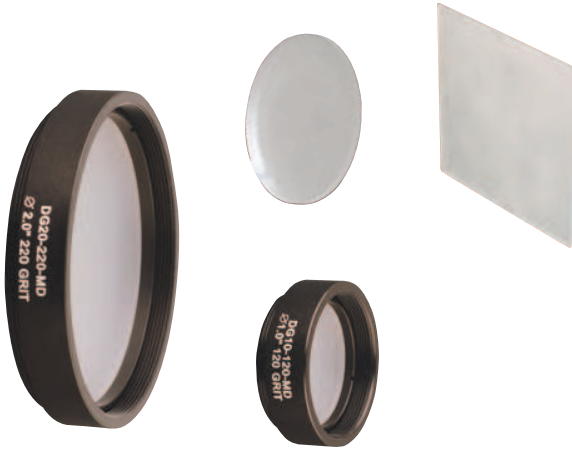
### Rear Accessory Attachments





## **D.6 Datasheet for the diffusers**

## Ground Glass Diffusers



Ground glass diffusers are the most economical diffusers and are useful for a variety of applications. Four grades of grit/grind are offered providing fine, medium, and coarse scattering. A finer grind provides a higher transmittance, while a more coarse grind creates a greater amount of diffusion at the expense of transmission. Mounted versions are set in an engraved SM1 (Ø1") or SM2 (Ø2") lens tube.

- Offered in 120, 220, 600, and 1500 Grit Polishes
- Polished for Greater Uniformity than Sand Blasting



### Round, Unmounted Ground Glass Diffusers

ITEM#	\$	£	€	RMB	DESCRIPTION
DG10-120	\$ 12.90	£ 8.95	€ 11,50	¥ 109.00	Ø1.0" Ground Glass Diffuser, 120 GRIT
DG10-220	\$ 12.90	£ 8.95	€ 11,50	¥ 109.00	Ø1.0" Ground Glass Diffuser, 220 GRIT
DG10-600	\$ 12.90	£ 8.95	€ 11,50	¥ 109.00	Ø1.0" Ground Glass Diffuser, 600 GRIT
DG10-1500	\$ 12.90	£ 8.95	€ 11,50	¥ 109.00	Ø1.0" Ground Glass Diffuser, 1500 GRIT
DG20-120	\$ 15.00	£ 10.40	€ 13,40	¥ 126.70	Ø2.0" Ground Glass Diffuser, 120 GRIT
DG20-220	\$ 15.00	£ 10.40	€ 13,40	¥ 126.70	Ø2.0" Ground Glass Diffuser, 220 GRIT
DG20-600	\$ 15.00	£ 10.40	€ 13,40	¥ 126.70	Ø2.0" Ground Glass Diffuser, 600 GRIT
DG20-1500	\$ 15.00	£ 10.40	€ 13,40	¥ 126.70	Ø2.0" Ground Glass Diffuser, 1500 GRIT



### Round, Mounted Ground Glass Diffusers

**NEW**  
versions

ITEM#	\$	£	€	RMB	DESCRIPTION
DG10-120-MD	\$ 26.50	£ 18.40	€ 23,60	¥ 223.80	SM1-Mounted Ground Glass Diffusers, 120 GRIT
DG10-220-MD	\$ 26.50	£ 18.40	€ 23,60	¥ 223.80	SM1-Mounted Ground Glass Diffusers, 220 GRIT
DG10-600-MD	\$ 26.50	£ 18.40	€ 23,60	¥ 223.80	SM1-Mounted Ground Glass Diffusers, 600 GRIT
DG10-1500-MD	\$ 26.50	£ 18.40	€ 23,60	¥ 223.80	SM1-Mounted Ground Glass Diffusers, 1500 GRIT
DG20-120-MD	\$ 34.70	£ 24.10	€ 30,90	¥ 293.10	SM2-Mounted Ground Glass Diffusers, 120 GRIT
DG20-220-MD	\$ 34.70	£ 24.10	€ 30,90	¥ 293.10	SM2-Mounted Ground Glass Diffusers, 220 GRIT
DG20-600-MD	\$ 34.70	£ 24.10	€ 30,90	¥ 293.10	SM2-Mounted Ground Glass Diffusers, 600 GRIT
DG20-1500-MD	\$ 34.70	£ 24.10	€ 30,90	¥ 293.10	SM2-Mounted Ground Glass Diffusers, 1500 GRIT



### 100 mm x 100 mm, Square, Unmounted Ground Glass Diffusers

ITEM#	\$	£	€	RMB	DESCRIPTION
DG100X100-120	\$ 42.80	£ 29.70	€ 38,00	¥ 361.50	100 mm x 100 mm, Ground Glass Diffuser, 120 GRIT
DG100X100-220	\$ 42.80	£ 29.70	€ 38,00	¥ 361.50	100 mm x 100 mm, Ground Glass Diffuser, 220 GRIT
DG100X100-600	\$ 42.80	£ 29.70	€ 38,00	¥ 361.50	100 mm x 100 mm, Ground Glass Diffuser, 600 GRIT
DG100X100-1500	\$ 42.80	£ 29.70	€ 38,00	¥ 361.50	100 mm x 100 mm, Ground Glass Diffuser, 1500 GRIT

## D.7 Datasheet for the lenses

### Lens equations

The focal length of a thick spherical lens can be calculated using the thick lens equation below. In this expression,  $n_l$  is the index of refraction of the lens,  $R_1$  and  $R_2$  are the radii of curvature for surfaces 1 and 2, respectively, and  $d$  is the center thickness of the lens.

$$\frac{1}{f} = (n_l - 1) \left[ \frac{1}{R_1} - \frac{1}{R_2} + \frac{(n_l - 1)d}{n_l R_1 R_2} \right]$$

When using the thick lens equation to calculate the focal length of a plano-convex lens,  $R_2 = \infty$  and  $R_2 = -R$ . Note that the minus sign in front of  $R$  is due to the sign convention used when deriving the thick lens equations and values of  $R$  are reported in the Specs tab as well as on the mechanical drawing for each lens. Therefore, via substitution, the thick lens equation becomes

$$\frac{1}{f} = (n_l - 1) \left[ \frac{1}{R} \right]$$

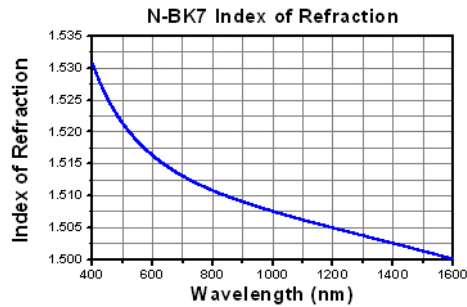
The focal length of the lens calculated using the simplified thick lens equation directly above is the distance between the second (back) principle plane ( $H''$ ) and the position at which a collimated beam incident on the curved surface of the plano-convex is focused. The principle plane positions of a thick lens can be calculated with the following equations:

$$H' = \frac{f(n_l - 1)d}{R_2 n_l} \quad \text{and} \quad H'' = \frac{f(n_l - 1)d}{R_1 n_l}$$

However, as with the thick lens equation,  $H'$  simplifies to zero and  $H''$  simplifies to

$$H'' = \frac{d}{n_l} = f - f_b$$

when used to calculate the principle plane locations of plano-convex lenses.  $f_b$  is the back focal length of the lens, which is often referred to as the working distance of the lens.



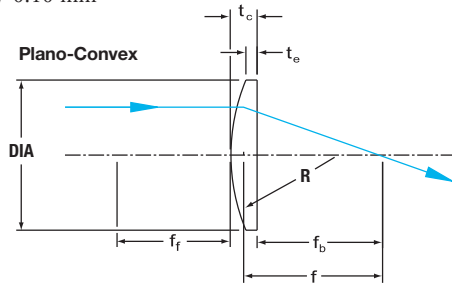
Click on the image to download the raw data. In the thick lens equation, use the index of refraction for N-BK7 at the wavelength of interest to approximate the wavelength-dependent focal length of any of the plano-convex lenses.

**AR Coating Plot on Page 589**

# N-BK7: Plano-Convex Lenses (Page 1 of 2)

## Specifications

- **Material:** N-BK7
- **Wavelength Range:** 350 nm – 2.0 μm
- **Design Wavelength:** 633 nm (n = 1.515)
- **Diameter Tolerance:** +0.00/-0.10 mm
- **Focal Length Tolerance:** ±1%
- **Surface Quality:** 40-20 Scratch-Dig
- **Centration:** ≤3 arcmin
- **Clear Aperture:** >90%



Please refer to our website for complete models and drawings.

Plano-Convex optics are best used where one conjugate point (object distance S or image distance S') is more than five times the other. The performance of this lens shape is near best-form for either focusing collimated light or for collimating a point source.

## Standard Broadband AR Coatings

To order the lens with a standard broadband AR Coating, add the coating code to the Item#, and then add the coating cost to the lens price. Example: LA1116 Coated with a 350-700 nm Broadband AR Coating is LA1116-A, and the cost is \$18.00 + \$9.20 = \$27.20.

COATING*	WAVELENGTH	\$	£	€	RMB
-A	350 - 700 nm	\$ 9.20	£ 6.40	€ 8.20	¥ 77.70
-B	650 - 1050 nm	\$ 9.20	£ 6.40	€ 8.20	¥ 77.70
-C	1050 - 1620 nm	\$12.20	£ 8.45	€ 10.90	¥ 103.10

\*Contact Tech Support for custom coatings.

## N-BK7 Plano-Convex Lenses: Diameter < 25.0 mm

ITEM#	DIA (mm)	f (mm)	PRICE UNCOATED (For Coated Lens Add Suffix)				R (mm)	t <sub>c</sub> (mm)	t <sub>c</sub> * (mm)	f <sub>b</sub> (mm)	SUGGESTED MOUNT**
			\$	£	€	RMB					
LA1116	6.0	10.0	\$ 18.00	£ 12.50	€ 16.00	¥ 152.00	5.2	2.5	1.5	8.4	LMRA6 and LMR05 See Page 238
LA1470	6.0	12.0	\$ 16.80	£ 11.70	€ 15.00	¥ 141.90	6.2	2.3	1.5	10.5	
LA1222	6.0	15.0	\$ 16.80	£ 11.70	€ 15.00	¥ 141.90	7.7	2.1	1.5	13.6	
LA1700	6.0	30.0	\$ 16.50	£ 11.50	€ 14.70	¥ 139.40	15.5	1.8	1.5	28.8	
LA1576	9.0	12.0	\$ 18.70	£ 13.00	€ 16.70	¥ 158.00	6.2	3.0	1.5	9.7	LMRA9 and LMR05 See Page 238
LA1472	9.0	20.0	\$ 16.80	£ 11.70	€ 15.00	¥ 141.90	10.3	2.5	1.5	18.3	
LA1540	12.7	15.0	\$ 18.70	£ 13.00	€ 16.70	¥ 158.00	7.7	5.1	1.8	11.6	
LA1074	12.7	20.0	\$ 18.40	£ 12.80	€ 16.40	¥ 155.40	10.3	4.0	1.8	17.4	
LA1560	12.7	25.0	\$ 17.10	£ 11.90	€ 15.20	¥ 144.40	12.9	3.5	1.8	22.7	LMR05 See Page 238
LA1289	12.7	30.0	\$ 16.80	£ 11.70	€ 15.00	¥ 141.90	15.5	3.2	1.8	27.9	
LA1304	12.7	40.0	\$ 16.40	£ 11.40	€ 14.60	¥ 138.50	20.6	2.8	1.8	38.1	
LA1213	12.7	50.0	\$ 16.30	£ 11.30	€ 14.50	¥ 137.70	25.8	2.6	1.8	48.3	
LA1207	12.7	100.0	\$ 16.30	£ 11.30	€ 14.50	¥ 137.70	51.5	2.2	1.8	98.6	LH1 See Page 242
LA1859	18.0	20.0	\$ 19.60	£ 13.60	€ 17.50	¥ 165.60	10.3	7.1	1.8	15.3	
LA1270	18.0	25.0	\$ 18.70	£ 13.00	€ 16.70	¥ 158.00	12.9	5.5	1.8	21.4	
LA1085	18.0	30.0	\$ 18.20	£ 12.70	€ 16.20	¥ 153.70	15.5	4.7	1.8	26.9	
LA1119	18.0	50.0	\$ 18.20	£ 12.70	€ 16.20	¥ 153.70	25.8	3.4	1.8	47.7	

\* Edge thickness given before 0.20 mm at 45° typical chamfer.

\*\* See the Lens Mount Section, Starting on Page 237.

**NEW versions**

## N-BK7 Plano-Convex Lenses: Diameter = 25.0 mm

ITEM#	DIA (mm)	f (mm)	PRICE UNCOATED (For Coated Lens Add Suffix)				R (mm)	t <sub>c</sub> (mm)	t <sub>c</sub> * (mm)	f <sub>b</sub> (mm)	SUGGESTED MOUNT**
			\$	£	€	RMB					
LA1252	25.0	25.4	\$ 22.00	£ 15.30	€ 19.60	¥ 185.80	51.50	3.60	2.06	97.60	LMR1 See Page 238
LA1255	25.0	50.0	\$ 20.00	£ 13.90	€ 17.80	¥ 168.90	25.80	5.30	2.07	46.50	
LA1257	25.0	75.0	\$ 19.00	£ 13.20	€ 16.90	¥ 160.50	38.60	4.10	2.02	72.30	
LA1251	25.0	100.0	\$ 19.00	£ 13.20	€ 16.90	¥ 160.50	51.50	3.60	2.06	97.60	
LA1253	25.0	200.0	\$ 18.00	£ 12.50	€ 16.00	¥ 152.00	103.00	2.80	2.04	198.20	

\* Edge thickness given before 0.20 mm at 45° typical chamfer.

\*\* See the Lens Mount Section, Starting on Page 237.

Selection continues on the next page

**AR Coating Plot on Page 589**

## N-BK7: Plano-Convex Lenses (Page 2 of 2)

### N-BK7 Plano-Convex Lenses: Diameter = 25.4 mm (1")

ITEM#	DIA (mm)	f (mm)	PRICE UNCOATED (For Coated Lens Add Suffix)				R (mm)	t <sub>c</sub> (mm)	t <sub>c</sub> * (mm)	f <sub>b</sub> (mm)	SUGGESTED MOUNT**
			\$	£	€	RMB					
LA1951	25.4	25.4	\$ 21.50	£ 15.00	€ 19,10	¥ 181.60	13.1	11.7	1.8	17.7	LMR1 See Page 238
LA1805	25.4	30.0	\$ 21.00	£ 14.60	€ 18,70	¥ 177.40	15.5	8.6	2.0	24.3	
LA1027	25.4	35.0	\$ 20.40	£ 14.20	€ 18,20	¥ 172.30	18.0	7.2	2.0	30.2	
LA1422	25.4	40.0	\$ 20.10	£ 14.00	€ 17,90	¥ 169.80	20.6	6.4	2.0	35.8	
LA1131	25.4	50.0	\$ 19.60	£ 13.60	€ 17,50	¥ 165.60	25.8	5.3	2.0	46.5	
LA1134	25.4	60.0	\$ 19.40	£ 13.50	€ 17,30	¥ 163.90	30.9	4.7	2.0	56.9	
LA1608	25.4	75.0	\$ 19.20	£ 13.40	€ 17,10	¥ 162.20	38.6	4.1	2.0	72.3	
LA1509	25.4	100.0	\$ 18.50	£ 12.90	€ 16,50	¥ 156.30	51.5	3.6	2.0	97.6	
LA1986	25.4	125.0	\$ 18.50	£ 12.90	€ 16,50	¥ 156.30	64.4	3.3	2.0	122.9	
LA1433	25.4	150.0	\$ 18.00	£ 12.50	€ 16,00	¥ 152.00	77.3	3.1	2.0	148.0	
LA1229	25.4	175.0	\$ 17.90	£ 12.50	€ 15,90	¥ 151.20	90.1	2.9	2.0	173.1	
LA1708	25.4	200.0	\$ 17.80	£ 12.40	€ 15,90	¥ 150.40	103.0	2.8	2.0	198.2	
LA1461	25.4	250.0	\$ 17.60	£ 12.30	€ 15,70	¥ 148.70	128.8	2.6	2.0	248.3	
LA1484	25.4	300.0	\$ 17.60	£ 12.30	€ 15,70	¥ 148.70	154.5	2.5	2.0	298.3	
LA1172	25.4	400.0	\$ 17.60	£ 12.30	€ 15,70	¥ 148.70	206.0	2.4	2.0	398.4	
LA1908	25.4	500.0	\$ 17.60	£ 12.30	€ 15,70	¥ 148.70	257.6	2.3	2.0	498.5	
LA1978	25.4	750.0	\$ 17.60	£ 12.30	€ 15,70	¥ 148.70	386.3	2.2	2.0	748.5	
LA1464	25.4	1000.0	\$ 17.30	£ 12.00	€ 15,40	¥ 146.10	515.1	2.2	2.0	998.6	

\* Edge thickness given before 0.20 mm at 45° typical chamfer.

\*\* See the Lens Mount Section, Starting on Page 237.

### Expanded Selection

### N-BK7 Plano-Convex Lenses: Diameter = 30 mm

ITEM#	DIA (mm)	f (mm)	PRICE UNCOATED (For Coated Lens Add Suffix)				R (mm)	t <sub>c</sub> (mm)	t <sub>c</sub> * (mm)	f <sub>b</sub> (mm)	SUGGESTED MOUNT**
			\$	£	€	RMB					
LA1274	30.0	40.0	\$ 25.30	£ 17.60	€ 22,50	¥ 213.70	20.6	9.0	2.5	34.1	LMR30 See Page 238
LA1102	30.0	50.0	\$ 22.00	£ 15.30	€ 19,60	¥ 185.80	25.8	7.3	2.5	45.2	
LA1765	30.0	75.0	\$ 22.00	£ 15.30	€ 19,60	¥ 185.80	38.6	5.5	2.5	71.3	
LA1031	30.0	100.0	\$ 21.80	£ 15.20	€ 19,40	¥ 184.10	51.5	4.7	2.5	96.9	
LA1907	30.0	150.0	\$ 22.00	£ 15.30	€ 19,60	¥ 185.80	77.3	3.1	1.6	147.0	
LA1541	30.0	200.0	\$ 22.00	£ 15.30	€ 19,60	¥ 185.80	102.8	2.8	1.7	196.8	
LA1832	30.0	250.0	\$ 22.00	£ 15.30	€ 19,60	¥ 185.80	128.3	2.6	1.7	246.6	
LA1419	30.0	300.0	\$ 22.00	£ 15.30	€ 19,60	¥ 185.80	156.6	2.5	1.8	296.3	
LA1237	30.0	500.0	\$ 22.00	£ 15.30	€ 19,60	¥ 185.80	255.9	2.3	1.8	495.2	

\* Edge thickness given before 0.20 mm at 45° typical chamfer.

\*\* See the Lens Mount Section, Starting on Page 237.

### N-BK7 Plano-Convex Lenses: Diameter = 50.8 mm (2")

ITEM#	DIA (mm)	f (mm)	PRICE UNCOATED (For Coated Lens Add Suffix)				R (mm)	t <sub>c</sub> (mm)	t <sub>c</sub> * (mm)	f <sub>b</sub> (mm)	SUGGESTED MOUNT**
			\$	£	€	RMB					
LA1401	50.8	60.0	\$ 31.50	£ 21.90	€ 28,00	¥ 266.00	30.9	16.3	3.0	49.2	LMR2 See Page 238
LA1145	50.8	75.0	\$ 29.10	£ 20.20	€ 25,90	¥ 245.80	38.6	12.5	3.0	66.7	
LA1050	50.8	100.0	\$ 25.80	£ 17.90	€ 23,00	¥ 217.90	51.5	9.7	3.0	93.6	
LA1384	50.8	125.0	\$ 25.70	£ 17.90	€ 22,90	¥ 217.10	64.4	8.2	3.0	119.6	
LA1417	50.8	150.0	\$ 25.30	£ 17.60	€ 22,50	¥ 213.70	77.3	7.3	3.0	145.2	
LA1399	50.8	175.0	\$ 25.30	£ 17.60	€ 22,50	¥ 213.70	90.1	6.7	3.0	170.6	
LA1979	50.8	200.0	\$ 25.30	£ 17.60	€ 22,50	¥ 213.70	103.0	6.2	3.0	195.9	
LA1301	50.8	250.0	\$ 25.20	£ 17.50	€ 22,40	¥ 212.80	128.8	5.5	3.0	246.4	
LA1256	50.8	300.0	\$ 26.90	£ 18.70	€ 23,90	¥ 227.20	154.5	5.1	3.0	296.6	
LA1725	50.8	400.0	\$ 27.10	£ 18.80	€ 24,10	¥ 228.90	206.0	4.6	3.0	397.0	
LA1380	50.8	500.0	\$ 27.10	£ 18.80	€ 24,10	¥ 228.90	257.3	4.3	3.0	497.2	
LA1727	50.8	750.0	\$ 27.10	£ 18.80	€ 24,10	¥ 228.90	386.3	3.8	3.0	747.5	
LA1779	50.8	1000.0	\$ 27.10	£ 18.80	€ 24,10	¥ 228.90	515.1	3.6	3.0	997.6	

\* Edge thickness given before 0.20 mm at 45° typical chamfer.

\*\* See the Lens Mount Section, Starting on Page 237.

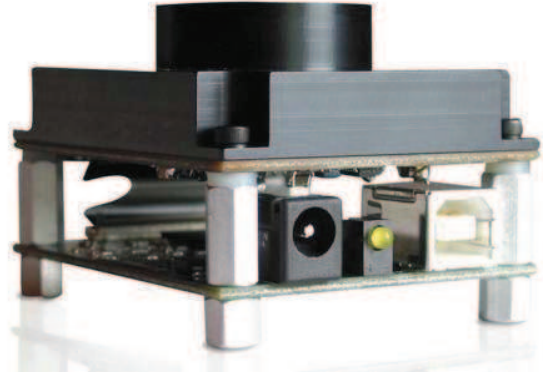
### N-BK7 Plano-Convex Lenses: Diameter = 75 mm

ITEM#	DIA (mm)	f (mm)	PRICE UNCOATED (For Coated Lens Add Suffix)				R (mm)	t <sub>c</sub> (mm)	t <sub>c</sub> * (mm)	f <sub>b</sub> (mm)	SUGGESTED MOUNT**
			\$	£	€	RMB					
LA1740	75.0	85.0	\$ 38.20	£ 26.50	€ 34,00	¥ 322.60	43.8	24.2	3.0	69.0	LMR75 See Page 238
LA1238	75.0	100.0	\$ 38.20	£ 26.50	€ 34,00	¥ 322.60	51.5	19.2	3.0	87.3	
LA1002	75.0	150.0	\$ 36.60	£ 25.40	€ 32,50	¥ 309.10	77.3	12.7	3.0	141.6	
LA1353	75.0	200.0	\$ 34.30	£ 23.80	€ 30,50	¥ 289.70	103.0	10.1	3.0	193.4	

\* Edge thickness given before 0.20 mm at 45° typical chamfer.

\*\* See the Lens Mount Section, Starting on Page 237.

## **D.8 Datasheet for the camera**



## Outline

Lumenera's Lu070 series of cameras are designed to be used in a wide variety of industrial applications, particularly in low light conditions. Color and monochrome product models are available.

With 640x480 resolution and on-board processing these cameras deliver outstanding image quality and value for industrial and scientific imaging applications.

Electronic Global Shutter provides capabilities similar to a mechanical shutter, allowing simultaneous integration of the entire pixel array, and then stopping exposure while image data is read out. Ideal for capturing objects in high speed motion.

Uncompressed images in live streaming video and still-image capture are provided across a USB2.0 digital interface. No frame-grabber is required. Advanced camera control is available through a complete Software Developer's Kit, with sample code available to quickly integrate camera functions into OEM applications.

Hardware and software based synchronization trigger is provided standard. On-board memory is available for frame buffering. Lu070 series cameras are offered in both enclosed and board-level form. Custom form factor (sizes) can be provided.

All Lumenera products are supported by an experienced team of software developers and application engineers. We understand your imaging needs and are here to help you with your integration and development. Products come with a full one (1) year warranty.

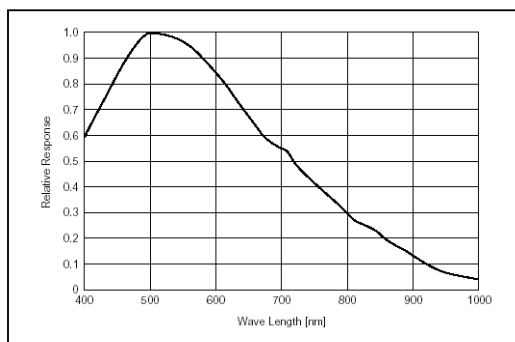
## Features

- Global electronic shutter
- Excellent sensitivity
- High speed USB2.0 (480Mbits/sec)
- Color or monochrome, interline, progressive scan, 640 x 480 resolution
- 60 fps at full 640 x 480  
100+ fps 320x240 (binning mode)
- Auto white balance & s/w adjustable exposure
- On-board image buffer
- GPIOs for control of peripherals and synchronization of lighting (4in/4out)
- FCC Class B, CE Ready
- Select 8 or 10-bit pixel data
- Simplified cabling - video, power and full camera control over a single USB cable
- Direct Show compatible
- C-Mount provided
- USB cameras are software compatible with Windows™ 98 SE, Windows Me, Windows 2K and Windows XP operating systems.
- Complete SDK available.

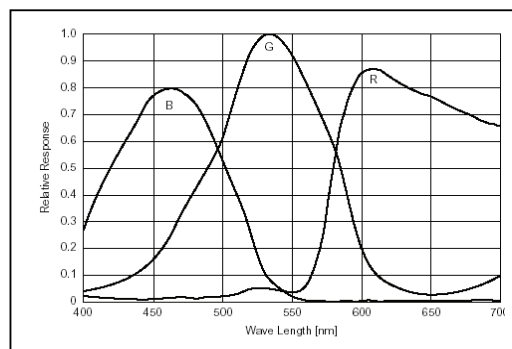
# Specifications

# Lu070

Image Sensor	<b>1/3" format, 5.8mm x 4.9mm array</b>
Effective Pixels	<b>640 x 480, 7.4um square pixels</b>
Frame Rate	<b>60 fps at 640x480, 100+ fps 320x240 (binning)</b>
Sensitivity	<b>High</b>
Exposure	<b>Auto / Manual</b>
White Balance	<b>Auto / Manual</b>
Dimensions (W x H x D)	<b>2.00 x 2.50 x 1.63 inches (board level) 2.25 x 3.85 x 1.56 inches (enclosed)</b>
Mass	<b>~150g / 300g</b>
Power Requirement	<b>USB bus power, or external 6VDC, 500mA</b>
Power Consumption	<b>~2.5Watts</b>
Operating Temperature	<b>-10° C to +50° C</b>
Operating Humidity	<b>20%-80%, Non-condensing</b>
Interface Connector	<b>Standard USB cable</b>
Lens Mount	<b>C-Mount (CS-mount option)</b>
Frame Buffer	<b>10 frame buffer (optional expansion to 50 frames)</b>



Monochrome Response



Color Response

***Full customization  
available to meet your  
exact needs!***

### Ordering Information

Lu070M	– Monochrome Camera Module
Lu070C	– Color Camera Module
Lu075M	– Enclosed Monochrome Camera
Lu075C	– Enclosed Color Camera
LuSDK	– Software Developer's Kit

Lumenera Corporation • 2470 Don Reid Dr. Ottawa Ontario K1H 1E1 • [www.lumenera.com](http://www.lumenera.com) • 613-736-4077

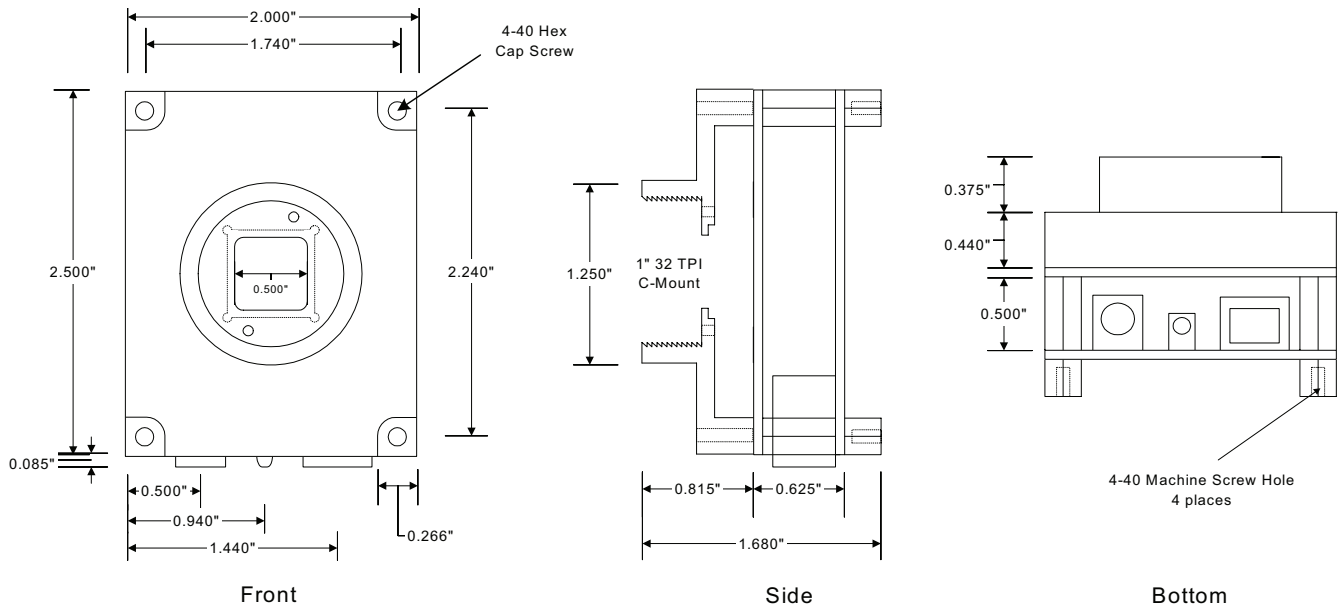
©2004 Lumenera Corporation, all rights reserved.  
Design, features, and specifications are subject to change without notice.



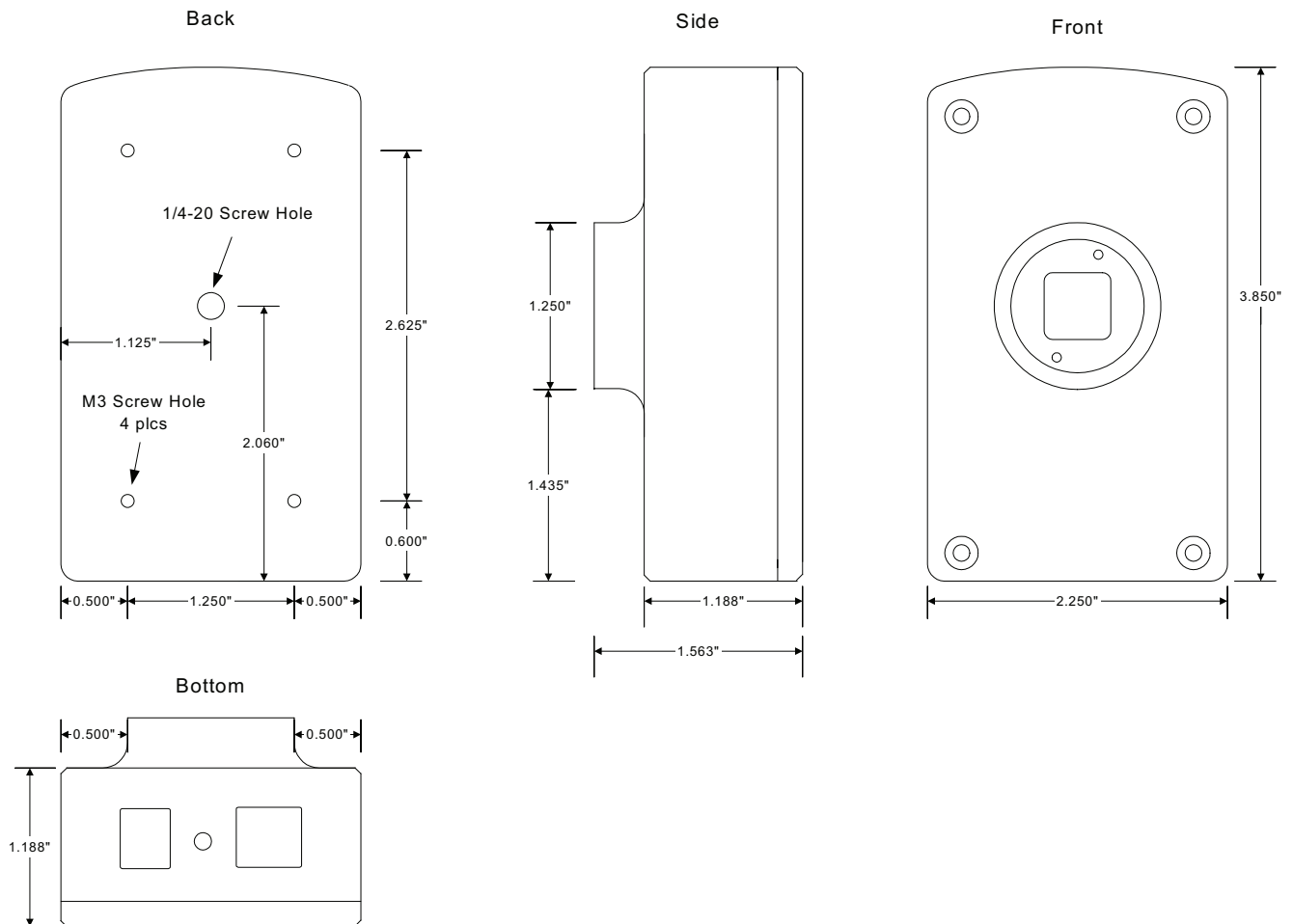
# Mechanicals

# Lu070

## OEM Board-Level Camera



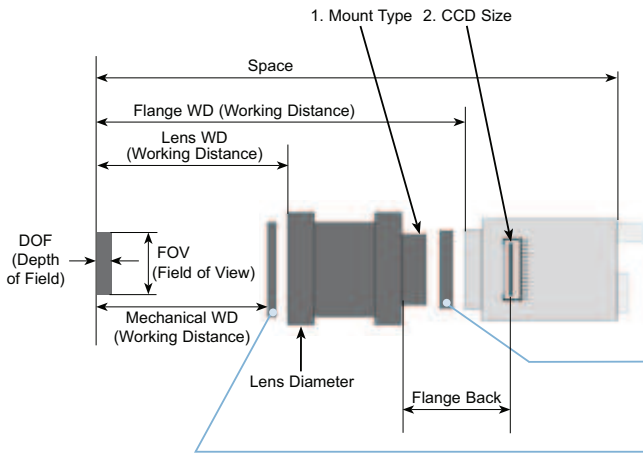
## Enclosed Camera



## **D.9 Datasheet for the camera lens**

# General Informations

## Terms and Definitions



Most industrial CCD cameras and lenses use C-mount. But there are some different mounts still used in machine vision application such as CS-mount, NF-mount, F-mount, etc.

Some remote head CCD cameras use special mount with small diameter (12 to 17mm).

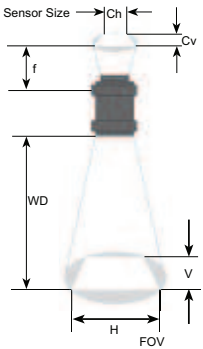
Three chip CCD cameras have a prism in front of the sensor, for this reason mechanical back is shorter (max. 4mm) than single chip CCD cameras.

**Rear End Accessories**  
Extension tubes  
Converters

**Front End Accessories**  
Filters (protector, IR cut filter, bandpass, polarizer etc.), prism or mirror

## Calculations of Optical Parameters

Optical magnification is "work" done by the lens. Defined as the ratio between the sensor size and the FOV.



### Calculation of field of view (FOV)

$$FOV = \frac{\text{Sensor size (V or H)}}{\text{Optical Mag.}}$$

### Calculation of optical magnification

$$\text{Optical Mag.} = \frac{\text{Sensor size (V or H)}}{\text{Required FOV (V or H)}}$$

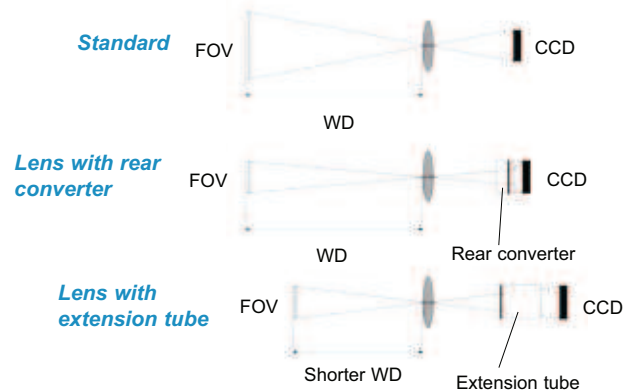
### Calculation of focal length (f)

$$f = \frac{WD \times Cv \text{ or } Ch}{FOV (V \text{ or } H)}$$

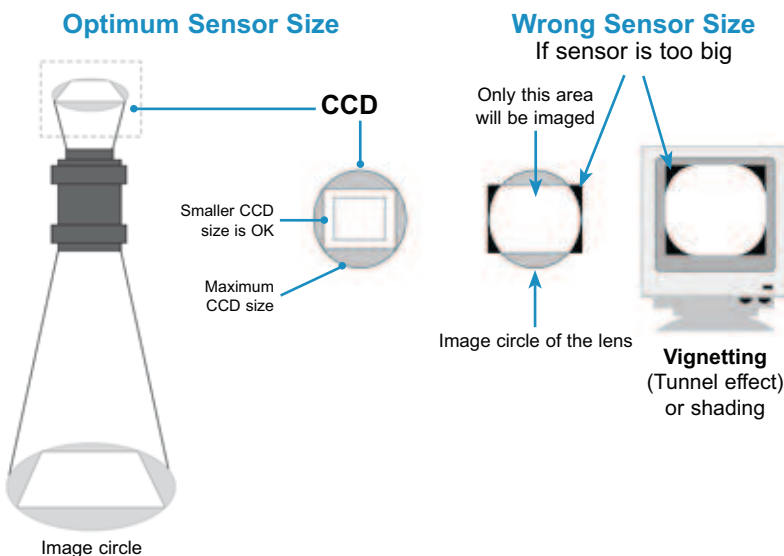
## Converters and Extension Tubes

Rear Converter (Extender) is used to obtain smaller FOV without changing WD from the lens original specification. Rear converters are placed between lens and camera.

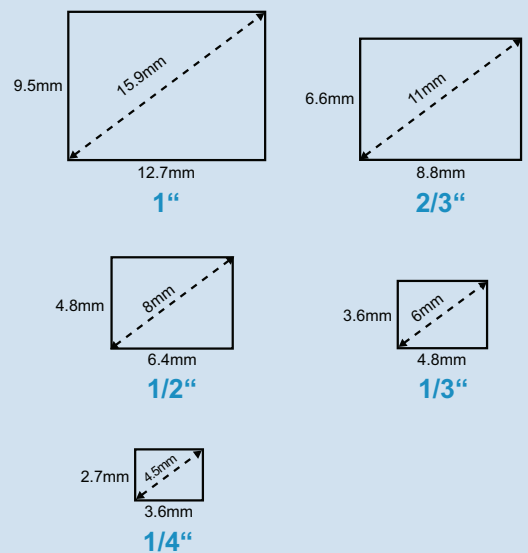
Extension tubes (Spacer) are used for fixed focal length lenses such as CCTV lenses to allow WD shorter than MOD (Minimum Object Distance). Result: A smaller FOV can be obtained by introducing extension tubes between the lens and camera.



## Ability of the Lens to Support Sensor Size



## Area Sensor



# Lenses for Large Sensors / Distortionless Lenses



## SV-L-Series for 1" CCD's

- especially designed for large sensors
- small F-number, large aperture
- usable for low-light situations

## L-Series for 1" Sensor with Lock-Screws for Focus and Iris

P. O. No.	Max. Sensor Size	Mount	Focal Length	F-Stop	MOD in mm	Dimension in mm (ØDxL)	Filter Threat
L-SV-L12513	1"	C	f=12.5mm	F:1.3-C	300	47.0 x 59.0	M43 P=0.75
L-SV-L2514	1"	C	f=25mm	F:1.4-C	500	45.0 x 28.0	M43 P=0.75
L-SV-L5013	1"	C	f=50mm	F:1.3-C	1.000	52.0 x 52.0	M49 P=0.75
L-SV-L5018	1"	C	f=50mm	F:1.8-C	1.000	42.0 x 48.5	M40.5 P=0.5
L-SV-L7513	1"	C	f=75mm	F:1.3-C	1.000	60.0 x 71.3	M58 P=0.75



## VS-LD-Series – Distortionless Macro Lenses

- especially designed for macro applications
- changeable magnification, working distance brightness
- iris with click balls
- nearly no tv-distortion
- compact size, little shading

## Megapixel Distortionless Macro Lenses

P. O. No.	Max. Sensor Size	Mount	Focal Length	F-Stop	MOD in mm	Dimension in mm (ØDxL)	Filter Threat	TV Distortion
L-VS-LD10	1/2"	C	f=10mm	F:2.2-C	89.3-500.1	32.0 x 25.8	M27 P=0.5	< -0.05%
L-VS-LD25	2/3"	C	f=25mm	F:1.9-C	90.8-190.5	32.0 x 26.35-30.5	M27 P=0.5	< +0.02%
L-VS-LD35	2/3"	C	f=35mm	F:1.8-C	95.7-142.4	32.0 x 36.5-43.5	M27 P=0.5	< -0.03%
L-VS-LD50	2/3"	C	f=50mm	F:2.5-C	213-503.7	32.0 x 46.4-53.7	M27 P=0.5	< +0.05%
L-VS-LD75	2/3"	C	f=75mm	F:3.5-C	245.9-527.7	32.0 x 70.8-85.5	M27 P=0.5	< -0.02%

## SV-PH Series Pinhole Lenses

P. O. No.	Max. Sensor Size	Mount	Focal Length	F-Stop	MOD in mm	Dimension in mm (ØDxL)
L-SV-PH085	2/3"	C	f=8.5mm	F:2.8	0.9	20.5 x 86.7
L-SV-PH04	1/2"	C	f=4mm	F:2.5	0.2	23 x 121.6



## VS-MC-Series – Machine Vision Macro Lenses

- especially designed housings for machine vision use
- vibration resistant, less shading, high resolution very small distortions
- UV and IR lenses available

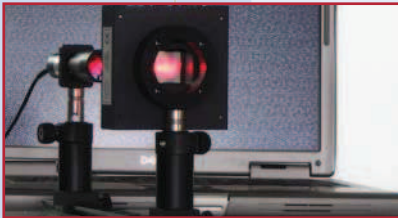
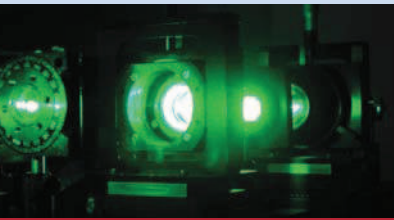
## Vibration-Resistant Macro Lens (Megapixel Distortionless)

P. O. No.	Max. Sensor Size	Mount	Optical Magnification	WD in mm	TV Distortion	Dimension in mm (ØDxL)
L-VS-MC0510 *1	2/3"	C	x0.5 – x1.0	75.2 – 121.2	0%	Length 49.4 – 72.5
L-VS-MC0510S *2	2/3"	C	x0.5 – x1.0	72.3 – 118.3	0%	31 x 64.5 – 87.6
L-VS-MC024	2/3"	C	x0.24 – x0.8	121.2 – 213.3	< 0.1%	Length 49.3 – 65.9
L-VS-MC024S *2	2/3"	C	x0.24 – x0.8	118.3 – 210.4	< 0.1%	31 x 52.2 – 68.8
L-VS-MC0103	1/2"	C	x0.1 – x0.3	182.7 – 489.7	< 0.1%	Length 42.9 – 52.1
L-VS-MC0510-“x” *3	2/3"	C	x0.5 – x1.0	75.2 – 121.2	0%	Length 49.4 – 72.5

## **D.10 Datasheet for the spatial light modulator**

# LC 2002

## >> Spatial Light Modulators



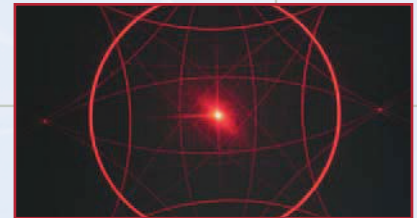
### Spatial Light Modulators

HOLOEYES Spatial Light Modulator (SLM) systems are based on liquid crystal microdisplays. These devices can modulate light spatially in amplitude and phase, so they act as a dynamic optical element. The optical function or information to be displayed can be taken directly from the optic design or an image source and can be transferred by a computer interface.

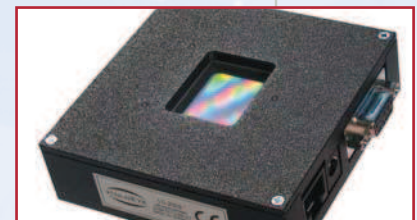
Implementation is very easy due to the smart system architecture and by an easy addressing using VGA or DVI signals directly from a computer graphics card.

### LC 2002

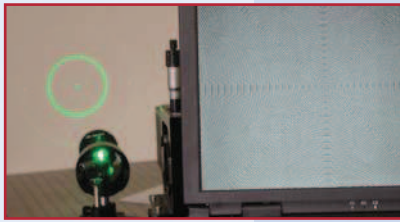
The LC 2002 is an easy-to-use spatial light modulator system based on an translucent LC microdisplay designed for prototyping in industrial development and research. It can be used to modulate light spatially, where the modulation function can be electrically addressed by a computer using a MS Windows software. Also strong laser pulses can be shaped by applied phase functions. The LC 2002 supports several display formats with a max. resolution of 832 x 624 pixels. High transmission efficiency and optimal contrast properties guarantee excellent optical quality. Minimized dimensions of the device enable easy integration into optical systems.



The highest potential of SLMs is the use as a dynamic phase modulating device, which acts as an addressable diffractive element. Besides display applications particular laser applications, such as beam splitting and beam shaping, diffractive optics, digital holography and biological laser applications are the main applications and challenges for SLMs. Even though the realization of a zoom lens without moving parts is one of the goals for a SLM implementation.



**Pioneers in Photonic Technology**



### Applications

- + Display Applications
- + Beam Splitting
- + Laser Beam Shaping
- + Coherent Wavefront Modulation
- + Phase Shifting
- + Optical Tweezers
- + Digital Holography
- + Laser Pulse Modulation

The spatial light modulator LC 2002 can be plugged directly to the VGA graphic card of your PC or notebook and behaves like an external monitor. Live addressing with the frame rate of the graphic card and the function as a MS Windows desktop is one reason why this spatial light modulator is so comfortable to use. The device is driven by a HOLOEYE driver software that runs on all MS Windows platforms. This convenient software for controlling all relevant parameters (e.g. contrast, image geometry) is delivered with the kit. Besides that, a simple programming interface allows the frequently required flexibility for incorporating the device in industrial systems. Furthermore a tailored SLM application software allows the simple generation of diverse dynamic optical functions like gratings, lenses, axicons and apertures as well as the calculation of diffractive optical elements (DOE) from user defined images. The complete kit contains the modulator, a video splitter and all relevant cables for monitoring the addressed image data. Due to its small size and the transmittive display, the LC 2002 can easily be applied into optical systems by using the mounting ring which is also supplied with the kit. To guarantee the best performance, individual configuration measurements for each device are performed by HOLOEYE in advance.

### Main Features:

Liquid Crystal Microdisplay (Transmission)  
 SVGA Resolution (800 x 600 Pixels)  
 60 Hz Image Frame Rate  
 Full Developers Kit (easy to run using a standard PC)  
 Microsoft Windows Driver Software  
 Application Software



### Display Features:

Pixels: 800 x 600  
 Pixel Pitch: 32  $\mu\text{m}$   
 Fill Factor: 55%  
 Panel Size: 21 x 26 mm  
 Addressing: 8 Bit (256 Pixel Values)  
 Signal Format: VGA, SVGA



### Special Optical Features:

Amplitude or Phase Modulation  
 $2\pi$  Phase Shift @ 532 nm  
 Intensity Ratio of 1000:1 @ 633 nm Coherent Light Source



### Software Features:

Driver: Brightness / Contrast / Geometry / Gamma Control  
 Application: Basic DOE computations; Generation of optical functions (Circular Aperture, Fresnel Zone Lens, Axicon, Single and Double Slit ...); Gratings (incl. Blazed and Sinusoidal)



**Pioneers in Photonic Technology**

**HOLOEYE Photonics AG**  
 Albert-Einstein-Str. 14  
 12489 Berlin, Germany  
 Phone +49 (0)30 63 92 36 60  
 Fax +49 (0)30 63 92 36 62  
 contact@holoeeye.com  
 www.holoeye.com